

# Hiding a Light Vector Boson from Terrestrial Experiments: A Chargephobic Dark Photon

Haidar Esseili<sup>1</sup> and Graham D. Kribs<sup>1,2</sup>

<sup>1</sup>*Department of Physics and Institute for Fundamental Science,  
University of Oregon, Eugene, Oregon 97403, USA*

<sup>2</sup>*Theoretical Physics Department, CERN, 1211 Geneva 23, Switzerland*

## Abstract

We calculate the terrestrial, astrophysical and cosmological constraints on a light vector boson that couples to an arbitrary combination of the electromagnetic and  $B - L$  currents of the Standard Model. The dark photon and a vector boson coupling to  $B - L$  are special cases of our generalized flavor-universal anomaly-free vector boson, requiring just one additional parameter (the “dark mixing angle” corresponding to the linear combination of the electromagnetic and  $B - L$  currents) beyond that of the overall coupling strength and the vector boson mass, where we focus on the range 1 MeV to 60 GeV. We perform a detailed investigation of a unique combination where the vector boson couplings to electrically charged leptons and protons are highly suppressed: the “chargephobic dark photon”. A chargephobic vector boson is very weakly constrained by current terrestrial experiments including beam dumps and collider experiments, since they rely on couplings to electrons and protons. Instead, neutrino scattering experiments (such as COHERENT), astrophysical sources (supernova emission), and cosmology ( $\Delta N_{\text{eff}}$ ) provide the strongest constraints due to the nonzero couplings of the chargephobic vector boson to neutrinos and neutrons. Indeed, we find that supernova emission and  $\Delta N_{\text{eff}}$  provide constraints throughout the space of dark mixing angles, demonstrating their importance to provide model-independent constraints. For nearly all of the parameter space, a chargephobic vector boson is the most weakly constrained anomaly-free vector boson that couples to flavor-independent or flavor-dependent combinations of Standard Model currents. Finally, we highlight the importance of future experiments, including SHiP, that *are* able to probe new regions of the chargephobic parameter space due to the significantly improved detector capabilities.

# Contents

<b>1</b>	<b>Introduction</b>	<b>2</b>
<b>2</b>	<b>Model</b>	<b>4</b>
2.1	Vector Bosons Coupling to EM and $B - L$ Currents . . . . .	4
<b>3</b>	<b>Overview of Results</b>	<b>7</b>
3.1	Dark Photon and $B - L$ Results . . . . .	7
3.2	Chargephobic Dark Photon Results . . . . .	7
3.3	Other Dark Mixing Angles . . . . .	8
<b>4</b>	<b>Production</b>	<b>10</b>
4.1	Branching Fraction . . . . .	11
<b>5</b>	<b>Constraints</b>	<b>15</b>
5.1	Cosmology: CMB & BBN . . . . .	15
5.2	Astrophysics . . . . .	20
5.2.1	Protoneutron Star Cooling: SN1987A . . . . .	20
5.2.2	Electromagnetic-Based Supernova Signals . . . . .	24
5.3	Neutrino Experiments . . . . .	25
5.3.1	Coherent elastic neutrino-nucleus scattering Experiments . . . . .	26
5.3.2	Neutrino-electron Scattering Experiments . . . . .	28
5.3.3	Invisible Searches . . . . .	29
5.3.4	Collider Neutrinos . . . . .	30
5.4	Beam Dump & Fixed Target Experiments . . . . .	30
5.5	Collider Experiments . . . . .	31
5.6	Precision Constraints . . . . .	32
<b>6</b>	<b>Discussion</b>	<b>33</b>
<b>A</b>	<b>Generating the Dark Mixing Angle</b>	<b>35</b>
<b>B</b>	<b>Renormalization Group Equations</b>	<b>35</b>
<b>C</b>	<b>Bremsstrahlung Interaction in Proto-Neutron Star</b>	<b>38</b>

## 1 Introduction

Light vector bosons are ubiquitous in dark sectors, with their utility to connect the SM with the dark sector. An essential ingredient to achieve a relic abundance of light dark matter consistent with cosmology requires a light mediator, and a light vector boson has long been considered a prime candidate for this interaction. The diversity of uses and implications of light vector boson mediators have motivated a vast range of experimental searches. Extensive reviews (see, e.g., [1–5]) have surveyed the terrestrial, astrophysical, and cosmological constraints on light vector boson couplings and masses.

The simplest model of a light vector boson mediator is the dark photon  $A'$ . The low energy effective theory of a massive dark photon is simply a vector boson with Stückelberg mass and kinetic mixing with electromagnetism<sup>1</sup>,  $\epsilon F_{A',\mu\nu} F_{em}^{\mu\nu}$ . The kinetic mixing can be rotated away resulting in the dark photon coupled

---

<sup>1</sup>Above the electroweak scale, kinetic mixing with  $U(1)_Y$ .

to the electromagnetic current,  $\epsilon e j_{\text{em}}^\mu A'_\mu$ . Electromagnetic current conservation ensures the longitudinal mode of the massive vector boson does not couple to the SM (at zero temperature). Other anomaly-free currents in the SM include  $B - L$ , the only other flavor-universal conserved current, when three right-handed neutrinos are added to the model (early discussions include [6–8] and a review of massive  $Z$ 's [9]), while a light vector boson coupled to  $B - L$  has been considered in detail in [1, 2, 10, 11]). Other anomaly-free flavor-dependent combinations of  $B$ ,  $L_e$ ,  $L_\mu$ ,  $L_\tau$  have also been considered (there is a vast literature, including [12–18] and more recently [19–26]).

In this paper we consider a single, massive vector boson  $X^\mu$ , that couples to a *linear combination* of the electromagnetic current and the  $B - L$  current of the SM. The notion that a new vector boson could couple to an arbitrary linear combination of these currents is not new, and was emphasized long ago in the context of  $Z$ 's detectable at LHC [27] as well as for light vector bosons in [11]. Indeed, Refs. [11, 27] emphasized that it is expected that a vector boson coupling purely to  $B - L$  at a high scale will automatically develop couplings to the hypercharge current (becoming a rescaled electromagnetic current below electroweak symmetry breaking) through renormalization group evolution. The size of these induced couplings depends critically on the field content and the extent of running. We will be agnostic towards the UV theory, and instead focus on the phenomenology within the low energy effective theory with no UV priors on the coupling strength, mixing angle, and vector boson mass.

A vector boson with a Stückelberg mass is a vector boson without gauge invariance [28]. Consequently, the vector boson can be directly coupled to an arbitrary vector current, i.e.,  $j_\mu X^\mu$ , within or beyond the SM. That said, not all vector currents are the same, and in particular, nonconserved currents (such as baryon number) have significant additional constraints that arise from new processes enabled by anomalous couplings [29, 30] (see also [28]). For this reason, in this paper we focus on coupling to anomaly-free conserved currents, and choose to restrict to (linear combinations of) flavor-independent currents of the SM.

Readers who are already familiar with the constraints on a dark photon and a  $B - L$  vector boson will recognize that there is a *large* overlap of the terrestrial, astrophysical, and cosmological constraints on these two distinct “pure” vector mediators. The overlap arises because just as a dark photon couples to charged leptons and protons, a  $B - L$  vector boson also couples to leptons and hadrons. The main distinction is that there are additional constraints that arise on  $B - L$  due to its couplings to neutrinos (as well as couplings to neutrons). Yet, much of the constraints that rely on couplings to electrons and/or protons broadly carry over from the case of a dark photon to the case of a  $B - L$  vector boson.

In this paper, we show that there is an anomaly-free light vector boson with *qualitatively* different flavor-independent couplings: a “chargephobic” vector boson. A chargephobic vector boson couples to a specific linear combination of the electromagnetic current and the  $B - L$  current,  $-j_{\text{em}}^\mu + j_{B-L}^\mu$ , where the couplings to charged leptons and singly positively charged baryons vanishes.<sup>2</sup> In this case, the vast majority of constraints from terrestrial experiments *disappear*. This is because most terrestrial experiments rely on the coupling of the vector boson to electrons or muons and/or the coupling to protons. At first glance, this has the potential to wipe clean the constraints in the coupling versus mass parameter space for a light vector boson mediator. However, as we will see, several constraints remain: terrestrial experiments that measure neutrino scattering off nuclei restrict much of the parameter space at larger couplings, while constraints on supernova cooling and constraints on modifications to early universe cosmology from  $\Delta N_{\text{eff}}$  restrict smaller couplings for smaller vector boson masses.<sup>3</sup>

The particular linear combination of currents that leads to chargephobic couplings is a tuned choice of

---

<sup>2</sup>Note that a vector boson with “chargephobic” couplings is *neither* “leptophobic” (since there are couplings to neutrinos) nor “protophobic” [1] (since protophobic vector bosons typically assumes there are couplings to charged leptons, while chargephobic does not couple to charged leptons). Yet another flavor-dependent current that is distinct from what we consider is  $B - 2L_\mu - L_\tau + r_{\mu\tau}(L_\mu - L_\tau)$ , where  $r_{\mu\tau}$  is arbitrary. This has been called “electrophobic” [22], since the vector boson does not couple to electrons, but does couple to muons and/or taus.

<sup>3</sup>Ref. [11] presaged several of these constraints, but did not carry out a detailed investigation.

parameters in the low energy effective theory. There is no technical obstacle to achieving this tuning from a UV theory. Indeed, for larger couplings, Ref. [27] suggested that  $g_Y \sim -g_{B-L}$  could be an attractor of the renormalization group evolution that is close (but not identical) to achieving chargephobic couplings. Our interest will generally be much smaller couplings, and so we do not anticipate RG fixed points with SM couplings. We briefly discuss how linear combinations of electromagnetism and  $B-L$  could arise by renormalization group evolution from a high scale in Appendix A.

What is more relevant for phenomenology is that there is renormalization group evolution of the dark mixing angle, and hence the couplings to SM fields. As we show, this effect is smaller than one might think, leaving a substantial range of energies where chargephobic couplings are present; see Appendix B. Nevertheless, we take into account this coupling evolution in our analysis, and show the constraints from experiments that operate at larger energies (such as LHCb and CMS searches for vector boson resonances to  $e^+e^-$  or  $\mu^+\mu^-$ ), where the small regenerated coupling to charged leptons and protons is relevant.

Finally, in the course of calculating the constraints on a vector boson with chargephobic couplings, we also revisit the constraints on dark photons,  $B-L$ , and other linear combinations (that are not chargephobic). While we have employed recasting for a handful of constraints such as collider searches, we have also performed independent calculations of the major constraints that apply to a chargephobic gauge boson and other mixing angles  $\varphi$ . This includes a full out-of-equilibrium evolution of early universe dynamics of  $X$  including finite temperature effects to determine the cosmological implications. For supernova, we have carefully considered the production processes that arise as a function of  $\varphi$ , and used the Garching simulations [31] to model the detailed proto-neutron star properties that are essential to determine the cooling constraint. This has not only allowed us to determine the constraint on the chargephobic case, but it has also allowed us to obtain an accurate cooling constraint on a  $B-L$  vector boson (clearing up some tension in past literature). Finally, we have performed a thorough analysis of the constraints from neutrino scattering off nucleons, using the data releases from the experiments, to determine the constraints that arise for  $\varphi \neq 0$ . These constraints are the most powerful when couplings to electrons and protons are suppressed.

## 2 Model

### 2.1 Vector Bosons Coupling to EM and $B-L$ Currents

We now provide an overview of the extension to the SM that we consider in the paper, specifying the parameters and couplings relevant to our analysis. Consider a vector boson  $X^\mu$  with Proca Lagrangian

$$\mathcal{L}_X = -\frac{1}{4}F_{X,\mu\nu}F_X^{\mu\nu} + \frac{1}{2}m_X^2 X_\mu X^\mu, \quad (1)$$

where we are interested broadly in the mass range  $1 \text{ MeV} \lesssim m_X \lesssim 60 \text{ GeV}$ . For the purposes of this paper, the vector boson mass could arise from a spontaneously broken theory with suitable Higgs sector, where we assume the Higgs states are heavy enough to be neglected in our analysis, or simply it could be simply a Stückelberg mass. We will adopt the latter point of view, i.e., the vector field has a Stückelberg mass, and hence  $X^\mu$  has no gauge invariance [28]. This immediately implies that we are free to write interactions of  $X^\mu$  to arbitrary currents of the SM. In this paper we further restrict the interactions of  $X^\mu$ :

- Couplings to the SM are flavor-independent;
- Couplings only to conserved currents<sup>4</sup> of the SM; and,

<sup>4</sup>More precisely, only linear interactions of  $X^\mu$  with SM conserved currents. We do not include a Higgs portal interaction  $H^\dagger H X^\mu X_\mu$ .

- Dark sector interactions, if present, do not affect the couplings to the SM nor the decay width of  $X^\mu$ .

While there are rather stealthy anomaly-free combinations of baryon number and one or more specific flavors of lepton number (for example,  $B - 3L_\tau$ ), these interactions have strong constraints from non-standard neutrino interactions (NSI), for example [21, 22, 24–26]. Couplings to non-conserved currents have also been considered in [28–30, 32–34], where non-trivial phenomenology arises because longitudinal mode of  $X^\mu$  also can couple to the SM. This can result in amplitudes involving  $X^\mu$  that diverge at large  $\sqrt{s}/m_X$ , leading to a host of other strong experimental constraints. Finally, interactions between a light vector boson and the dark sector have been considered in a variety of contexts. For our purposes, if  $X^\mu$  couples to other dark sector fields, we assume these interactions do not affect the couplings the SM, nor do they change the decay width of  $X^\mu$ .

The interactions of  $X^\mu$  to the SM that we consider are thus

$$\mathcal{L}_{\text{int}} = (\varepsilon e j_\mu^{\text{EM}} + g_{B-L} j_\mu^{B-L}) X^\mu, \quad (2)$$

where

$$j_\mu^{\text{EM}} = \sum_f Q_f \bar{f} \gamma_\mu f \quad (3)$$

$$j_\mu^{B-L} = \sum_f q_f \bar{f} \gamma_\mu f \quad (4)$$

and  $Q_f = (-1, 0, 2/3, -1/3)$  are the usual electric charges of the SM fermions ( $e, \nu, u, d$ ) while

$$q_f = (B-L)_f = \begin{cases} +1/3 & u, d \\ -1 & e, \nu_L, \nu_R, \end{cases} \quad (5)$$

are also the usual  $B-L$  charges of the SM fermions. We have normalized the relative strength of  $X^\mu$  couplings to the  $B-L$  current with  $g_{B-L}$  and the EM current with  $\varepsilon e$  which is familiar from dark photon literature. We have included right-handed neutrinos to ensure  $B-L$  is anomaly-free, however we take the right-handed neutrinos to be heavy, above at least the weak scale, so that they do not directly affect the phenomenology of  $X^\mu$ . A detailed discussion of the role of right-handed neutrinos, and the effects of taking them heavy can be found in our previous work [35].

We can rewrite the interactions of  $X^\mu$  as

$$\mathcal{L}_X = g_X j_\mu^X X^\mu \quad (6)$$

$$j_\mu^X = \cos \varphi j_\mu^{\text{EM}} + \sin \varphi j_\mu^{B-L} = \sum_f x_f \bar{f} \gamma_\mu f, \quad (7)$$

where we define the overall coupling strength and dark mixing angle as

$$g_X \equiv \sqrt{(\varepsilon e)^2 + g_{B-L}^2} \quad (8)$$

$$\varphi \equiv \tan^{-1} \frac{g_{B-L}}{\varepsilon e}, \quad (9)$$

such that the “charges” (or couplings) for an arbitrary fermion to the  $j_\mu^X$  current are

$$x_f = Q_f \cos \varphi + q_f \sin \varphi \quad (10)$$

and for the SM fermions,

$$x_e = -\cos \varphi - \sin \varphi, \quad x_\nu = -\sin \varphi, \quad x_u = \frac{2 \cos \varphi}{3} + \frac{\sin \varphi}{3}, \quad x_d = -\frac{\cos \varphi}{3} + \frac{\sin \varphi}{3}, \quad (11)$$

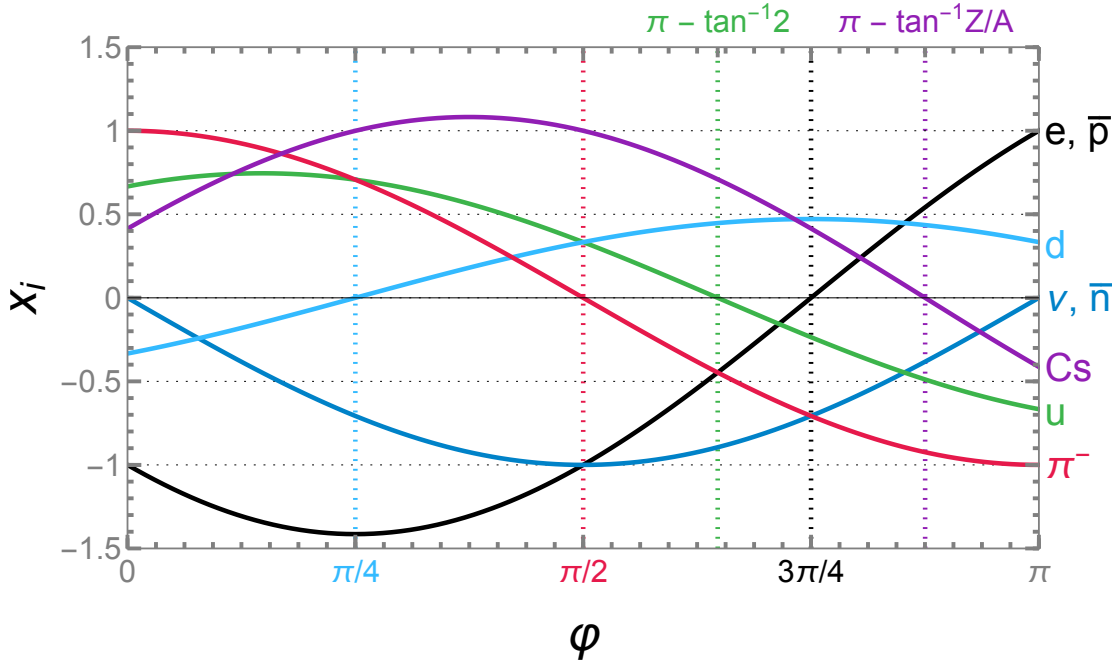


Figure 1: Charges  $x_i$  defined in Eq. (11). The proton, neutron, and  $\pi^+$  charges are equal and opposite to the electron, neutrino, and  $\pi^-$  respectively. We also show the scaled Cesium charge  $x_{Cs}/A_{Cs}$  which is relevant for CE $\nu$ NS experiments. The vertical dotted lines correspond to specific combinations of the electromagnetic and  $B - L$  currents that are of interest, as shown in Fig. 2.

that we illustrate in Fig. 1. Note that under  $X^\mu \rightarrow -X^\mu$ ,  $\varphi \rightarrow \varphi + \pi$ , and so without loss of generality we can restrict  $0 \leq \varphi < \pi$ .

Mesons obviously do not carry  $B - L$  number, and so their couplings to  $X^\mu$  are determined just by their couplings to the electromagnetic current. For example, the pions

$$x_{\pi^\pm} = \pm \cos \varphi \quad (12)$$

$$x_{\pi^0} = 0. \quad (13)$$

Similarly, neutral baryons obviously do not carry electric charge, with their coupling to  $X^\mu$  being the same as their coupling to a  $B - L$  vector boson. Positive electrically charged baryons have a  $\varphi$ -dependent coupling to  $X^\mu$ , which is easy to see is identical to the coupling of an electrically charged anti-lepton. For example, for the proton,  $x_p = -x_e$  (and  $x_{\bar{p}} = x_e$ ). Similarly, the neutron and neutrino have equal and opposite couplings,  $x_n = -x_\nu$  (and  $x_{\bar{n}} = x_\nu$ ). The couplings to baryons with different electrical charges differ from one another, for example for the  $\Delta$  multiplet:

$$x_{\Delta^{++}} = 2 \cos \varphi + \sin \varphi \quad (14)$$

$$x_{\Delta^+} = x_p = \cos \varphi + \sin \varphi \quad (15)$$

$$x_{\Delta^0} = x_n = \sin \varphi \quad (16)$$

$$x_{\Delta^-} = -\cos \varphi + \sin \varphi. \quad (17)$$

## 3 Overview of Results

### 3.1 Dark Photon and $B - L$ Results

In general, small deviations in  $\varphi$  result in small modifications to observables, and thus unsurprisingly small modifications to the constraints for a given  $\varphi$ . This general result does *not* hold when the charge of a particle or set of particles is close to or exactly zero, i.e.,  $x_i = 0$ . In these special cases, unique and nontrivial phenomenology arises. The best known example is the dark photon, corresponding to  $\varphi = 0$ , and thus  $x_\nu = 0$ : the dark photon has no coupling to neutrinos. The next best known example is the  $B - L$  vector boson, corresponding to  $\varphi = \pi/2$ . In this case, the couplings to mesons vanish, while the proton and neutron couplings are identical.

Anticipating the many various constraints arising from terrestrial experiments, astrophysics, and cosmology, we first show the bounds we obtain on the well-known cases of the dark photon and  $B - L$  in Fig. 3. Besides some minor differences in constraint shapes, the main difference between the dark photon and the  $B - L$  vector boson cases is the additional set of constraints from neutrino-dependent observables that arise with  $B - L$ . Our results are broadly consistent with prior equivalent results that can be found in [1, 2, 5]. The primary purpose of showing our calculated constraints is to demonstrate that our analysis pipeline for general  $\varphi$  broadly reproduces existing results in the specific  $\varphi = 0$  (dark photon) and  $\varphi = \pi/2$  ( $B - L$  vector boson) limits. In later sections, we highlight a few specific distinctions between our results and those in past literature.

In order to orient the reader to which results correspond to which mixing angle, we provide a mixing angle “compass” defined in Fig. 2. This shows the cases of interest in the paper (dark photon,  $B - L$ , chargephobic) as well as several additional angles with their own unique properties.

### 3.2 Chargephobic Dark Photon Results

Our main purpose is to explore the chargephobic case,  $\varphi = 3\pi/4$ . The tree-level couplings to quarks, leptons, the proton, neutron, and charged pions are:

$$\left. \begin{aligned} x_u &= -\frac{1}{3\sqrt{2}} \\ x_d &= \frac{\sqrt{2}}{3} \end{aligned} \right\} \longrightarrow \begin{cases} x_p &= 0 \\ x_n &= \frac{1}{\sqrt{2}} \\ x_{\pi^\pm} &= \mp \frac{1}{\sqrt{2}} \end{cases} \quad (18)$$

$$\begin{aligned} x_e &= 0 \\ x_\nu &= -\frac{1}{\sqrt{2}} \end{aligned}$$

A chargephobic  $X^\mu$  couples to quarks, and therefore baryons, in a very specific way:  $X^\mu$  is “phobic” only to singly positively charged baryons (and singly negatively charged anti-baryons). Moreover, while  $X^\mu$  couples to charged mesons, there is no coupling to neutral mesons. The couplings to neutrons and neutrinos implies important astrophysical and cosmological consequences. For astrophysics, the constraint from excessive cooling of SN1987A by  $X^\mu$  emission remains strongly constrained in a way broadly comparable to the dark photon and  $B - L$ . This occurs dominantly because of  $X^\mu$  bremsstrahlung and other emission processes from neutrons in the supernova. Differences are present, however, since once  $X^\mu$  is emitted from a supernova, it decays nearly 100% of the time into neutrinos, whereas both a dark photon and  $B - L$  vector boson have a large branching fraction to charged leptons. Similarly, for cosmology,  $X^\mu$  can be produced from its interactions with neutrinos, modifying  $\Delta N_{\text{eff}}$ , again broadly comparable to  $B - L$  (where production of  $X$  can occur from all leptons) or the dark photon (production of  $X$  restricted to just charged leptons).

Our results for the chargephobic case are shown in Fig. 4. The majority of constraints from beam dump experiments, fixed target experiments, colliders, precision constraints, neutrino-electron scattering experiments, and searches to invisible decays are either *absent* or *suppressed*. What remains are constraints from coherent neutrino nuclear scattering experiments, a small region related to hadron beam fixed target experiments that are specifically sensitive to neutrinos (DONuT and FASER $\nu$ ), early universe modification to  $\Delta N_{\text{eff}}$ , and excessive cooling of proton-neutron star after supernova (SN1987A), and all of which are resilient to a vanishing charged lepton coupling.

The astute reader will observe that Fig. 4 still contains weakened “stalactite” bounds in green from collider experiments, despite the fact that these constraints rely on couplings to muons. The re-appearance of these bounds arises because the mixing angle  $\varphi$  has a loop-induced energy dependence due to the renormalization group evolution of the underlying couplings. In Fig. 4, we made the particular choice  $\varphi(\mu = m_e) = 3\pi/4$ , and evolved the angle using the renormalization of the couplings detailed in App. B. While the electromagnetic coupling evolves with renormalization scale above  $\mu = m_e$  as usual, the dark mixing angle  $\varphi$  does not actually start to deviate from its low energy value until  $\mu \gtrsim m_\pi$ ; see Appendix B. This explains why the collider experiment bounds appear only above about 200 MeV, and get slightly stronger with increasing mass up to  $m_X = 60$  GeV at the upper right-edge of the plot.

Fig. 4 is the main result of our paper, with the subsequent sections of the paper detailing how the individual terrestrial, astrophysical, and cosmological constraints are obtained. What should be clear from Fig. 4 is that current terrestrial experiments are highly insensitive to a chargephobic vector boson.

### 3.3 Other Dark Mixing Angles

There are several other dark mixing angles (beyond  $\varphi = 0, \pi/2$ ) that have their own interesting properties. In particular, consider  $\varphi = \pi - \tan^{-1}(Z_{\mathcal{N}}/A_{\mathcal{N}})$ , where the coupling to an entire nucleus with charge number  $Z_{\mathcal{N}}$  and mass number  $A_{\mathcal{N}}$  can vanish. (The vanishing of the coupling assumes that  $X^\mu$  couples *coherently* to the nucleus, i.e., the momentum transfer is small compared with inverse size of the nucleus.) We will call this angle *nucleophobic*, and consider the implications in the context of the CE $\nu$ NS analysis. (A related idea, “xenophobic”, tunes the proton and neutron couplings so that the coherent response of xenon nuclei is strongly suppressed for the purposes of suppressing dark matter direct detection signals in [36].) Of particular interest to our analysis are the nuclei of cesium, iodine, and germanium. For example,  $\varphi = \pi - \tan^{-1}(55/133)$  results in a model with vanishing tree level coupling to Cesium; here  $x_p/x_n \approx -1.42$  which leads to  $x_p Z_{\text{Cs}} + x_n N_{\text{Cs}} = 0$ . The angle has the added consequence of suppressing the coupling to other intermediate mass stable nuclei which share a similar number ratio of proton to neutrons; for example,  $N_{\text{Cs}}/Z_{\text{Cs}} \approx N_{\text{I}}/Z_{\text{I}} \approx 1.4$ . This is evident in the valley of stability relation as derived from the semi-empirical mass formula  $A/2Z \approx 1 + 0.007A^{2/3}$ . The suppression is still in effect but less severe for lighter nuclei such as germanium and argon where  $N/Z \approx 1.2$ . Explicitly, the nuclear coupling to  $X$  are  $\{x_{\text{Cs}}, x_{\text{I}}, x_{\text{Ge}}, x_{\text{Ar}}\}_{B-L} = \{133, 127, 72, 40\}$  for  $B-L$  and are suppressed to  $\{x_{\text{Cs}}, x_{\text{I}}, x_{\text{Ge}}, x_{\text{Ar}}\}_{\cancel{B-L}} = \{0, -0.4, -2, -1.3\}$  in the nucleophobic case with vanishing Cesium coupling.<sup>5</sup>

---

<sup>5</sup>Note that  $\varphi = \pi - \tan^{-1} Z/A$  is quite close to  $\varphi = \pi - \tan^{-1} 1/2$ , which is the angle where  $\omega$  mixing vanishes in Fig. 2. In the former case,  $x_p = -x_n(A-Z)/Z$  and the coupling to the nucleus vanishes. As for the latter case  $x_p = -x_n$  and  $X$  effectively couples to the difference  $A-2Z$  rather than the full nucleus  $A$  as it would occur for  $B-L$ . The two angles converge for light nuclei with  $A = 2Z$ .

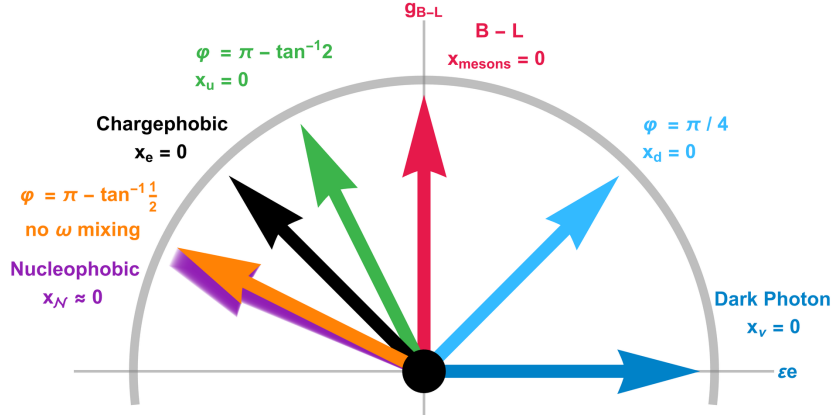


Figure 2: The dark mixing angle “compass”. Each arrow corresponds to a dark mixing angle  $\varphi$  that has a vanishing tree-level coupling to at least one SM state. The compass is used in subsequent plots to easily illustrate which dark mixing angles are being considered.

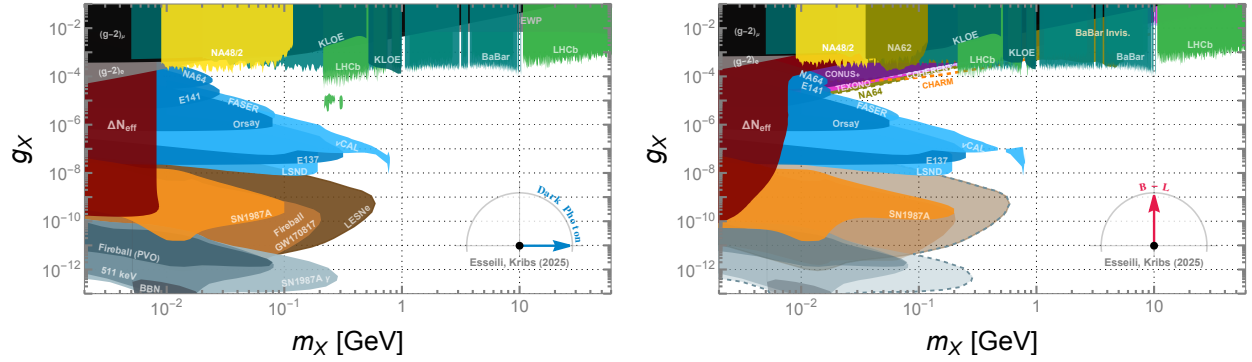


Figure 3: Terrestrial experiment constraints, astrophysical constraints, and cosmological constraints on the dark photon ( $\varphi = 0$ ) and  $B-L$  case ( $\varphi = \pi/2$ ), see text for full details. For  $B-L$ , there are additional constraints that arise due to non-zero couplings to neutrinos, in particular those labeled CHARM, COHERENT, CONUS, NA64, and TEXONO. For the dark photon case, the constraints labeled BBN, LESNe, SN1987A  $\gamma$ , 511 keV line, Fireball PVO/GW170817 were taken directly from Ref. [5]. Since the branching fraction to charged leptons in the  $B-L$  case is comparable to the dark photon case, we anticipate the same processes that led to the bounds [5] to also apply to  $B-L$ . We have taken the liberty to overlay these dark photon bounds from [5] as unlabeled light-shaded regions with dashed-lines in the  $B-L$  case. This is illustrative of where one might expect these constraints to appear, however, a detailed calculation for  $B-L$  is beyond the scope of the paper.

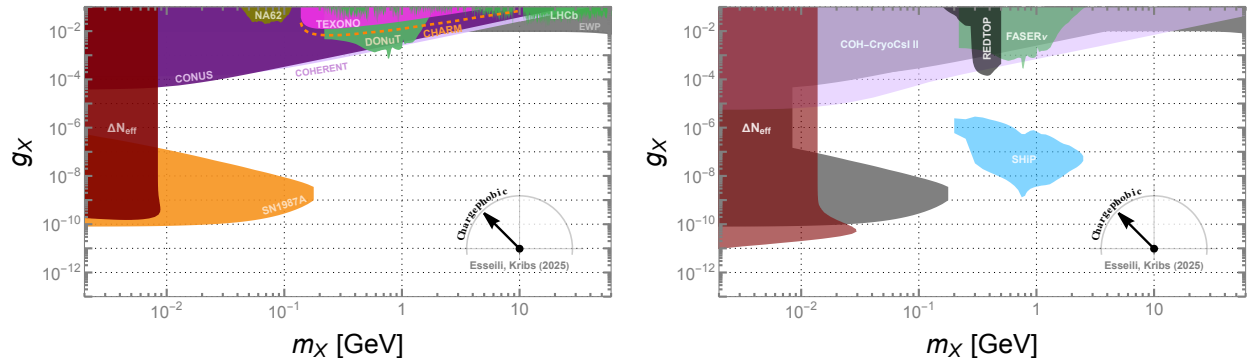


Figure 4: The central results of our paper: the current constraints (left) and anticipated future sensitivity (right) on a chargephobic dark photon ( $\varphi = 3\pi/4$ ). The absence of the vast majority of terrestrial experiments (compare with Fig. 3) arises due to the specific couplings that vanish for chargephobic dark photon: charged leptons and protons. See text for full details.

## 4 Production

In constraining our parameter space, we encounter a variety of production mechanisms that depend non-trivially on  $\{m_X, g_X, \varphi\}$ . These production mechanisms are well cataloged in the literature for some vector bosons, such as the dark photon, denoted by  $A'$ . In this section, we generalize these production mechanisms to include dependence on the dark mixing angle,  $\varphi$ , and compare the rates to their respective counterparts in dark photon case. Doing so will reveal the regions in the parameter space where we expect significant deviations from the dark photon constraints, to be distinguished from other regions where the change is expected to be modest.

The experiments/probes that will be used to set constraints on the generalized vector boson  $X$  (with arbitrary  $\varphi$ ) can be broadly classified into five production mechanism categories:

- i)  $X$  bremsstrahlung – emission in nucleon-nucleon scattering,  $NN \rightarrow NNX$ , in the dense nuclear medium of a proto-neutron star, as well as in the production processes  $eZ \rightarrow eZX$  and  $pZ \rightarrow pZX$  in electron and proton beam dumps, with  $Z$  the nucleus of the target material.
- ii) Drell-Yan processes  $f\bar{f} \rightarrow X$  with  $f$  being a charged fermion – an important production mode in the early universe evolution of  $X$ , and a key production mechanism in collider experiments.
- iii) Meson decay – for example:  $\pi^0 \rightarrow X\gamma$  and  $\eta \rightarrow X\gamma$  in FASER [37,38] and  $\phi \rightarrow X\eta$  in the KLOE [39].
- iv) QCD vector meson  $V = \omega, \rho, \phi$  mixing  $V \rightarrow X$  using the vector meson dominance framework (VMD) [1, 40, 41].
- v) Enhancement of electron-neutrino scattering  $\nu e \rightarrow \nu e$ , such as TEXONO [42, 43], or coherent elastic neutrino-nucleus scattering (CE $\nu$ NS)  $\nu N \rightarrow \nu N$  such as COHERENT [44], both occurring through  $X$ -exchange.

In order to most easily see the changes resulting from varying  $\varphi$ , we consider the production ratio  $\mathbb{P}_X$ , defined by the cross section ratio  $\sigma_X/\sigma_{A'}$ , and the decay width ratio  $\Gamma_X/\Gamma_{A'}$  for a given process. This ratio is summarized for various production mechanisms in Table 5 and Fig. 5. Importantly, the production ratio vanishes for special values of  $\varphi$  as detailed in the previous section. Thus, when an experiment relies on one such production mechanism, it can lose sensitivity to  $X$  for some values of  $\varphi$ .

Next we discuss four relevant decay width ratios processes by adapting the VMD framework developed in [1, 41] to our case. These decay ratios are

$$\mathbb{P}_{\omega \rightarrow \pi^0 X} = \cos^2 \varphi \tag{19}$$

$$\mathbb{P}_{\phi \rightarrow X\eta} = (\cos \varphi - \sin \varphi)^2 \tag{20}$$

$$\mathbb{P}_{\pi^0 \rightarrow X\gamma} = \frac{|\text{BW}_\rho \cos \varphi + \text{BW}_\omega (\cos \varphi + 2 \sin \varphi)|^2}{|\text{BW}_\rho + \text{BW}_\omega|^2} \tag{21}$$

$$\mathbb{P}_{\eta \rightarrow X\gamma} = \frac{|9 \text{BW}_\rho \cos \varphi - 2 \text{BW}_\phi (\cos \varphi - \sin \varphi) + \text{BW}_\omega (\cos \varphi + 2 \sin \varphi)|^2}{|9 \text{BW}_\rho - 2 \text{BW}_\phi + \text{BW}_\omega|^2} \tag{22}$$

$$\mathbb{P}_{\eta' \rightarrow X\gamma} = \frac{|9 \text{BW}_\rho \cos \varphi + 4 \text{BW}_\phi (\cos \varphi - \sin \varphi) + \text{BW}_\omega (\cos \varphi + 2 \sin \varphi)|^2}{|9 \text{BW}_\rho + 4 \text{BW}_\phi + \text{BW}_\omega|^2}. \tag{23}$$

Here,

$$\text{BW}_V(m_X) = \frac{m_V^2}{m_V^2 + m_X^2 - im_X \Gamma_V(m_X)}, \tag{24}$$

Process	$\mathbb{P}_X \equiv \sigma_X/\sigma_{A'}$
$\omega \rightarrow X$	$(\cos \varphi + 2 \sin \varphi)^2$
$eZ \rightarrow eZX$	$(\cos \varphi + \sin \varphi)^2$
$pZ \rightarrow pZX$	$(\cos \varphi + \sin \varphi)^2$
$u\bar{u} \rightarrow X$	$\frac{1}{4}(2 \cos \varphi + \sin \varphi)^2$
$\rho \rightarrow X$	$\cos^2 \varphi$
$d\bar{d} \rightarrow X$	$(\cos \varphi - \sin \varphi)^2$
$\phi \rightarrow X$	$(\cos \varphi - \sin \varphi)^2$

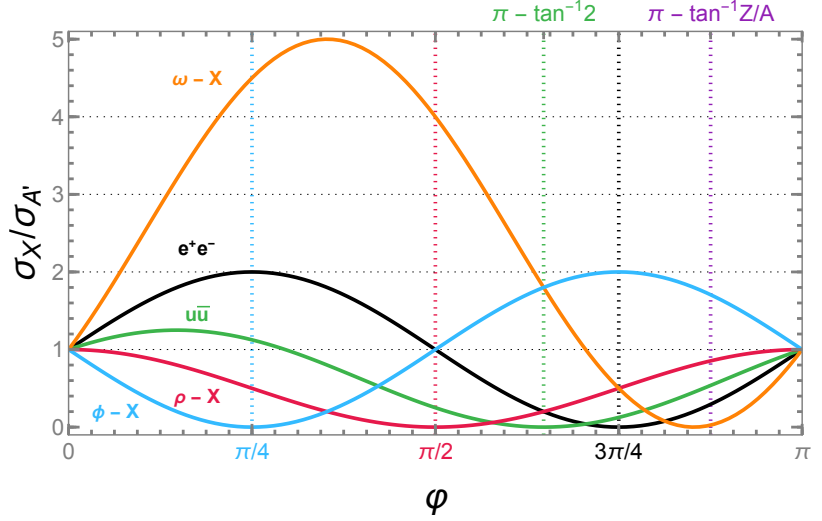


Figure 5: Tree level cross section ratio of  $X$  to  $A'$  production rate. All values in the table are multiplied by a factor of  $g_X^2/(\varepsilon e)^2$ ; we set this extra term to one in the plot. The ratio also sets energies in both models equal when necessary.

is the Breit-Wigner expression for vector meson  $V$  and  $\Gamma_V(m_X)$  is the total decay width. The  $\pi^0$  and  $\eta$  decays ratios are shown in Fig. 6 for some critical values of  $\varphi$ . In Eqs. (21–23), the  $\rho$ ,  $\phi$ , and  $\omega$  contributions to the decay width vanishes for  $\varphi = \pi/2, \pi/4$ , and  $\pi - \tan^{-1}(1/2)$  respectively.<sup>6</sup> Furthermore,  $m_\rho \approx m_\omega$  leads to an partial cancellation between the two Breit-Wigner terms in the chargephobic limit at  $\varphi = 3\pi/4$ . These limits correspond to dips in Fig. 6 near the resonance of the relevant meson.

The production mechanisms discussed in this section have important implications to collider, fixed target, and beam dump experiments and their associated constraints. Production in the early universe, proto-neutron star cooling, and neutrino scattering experiments require a more careful analysis and will be the subject of later sections.

## 4.1 Branching Fraction

We assume  $X$  decays entirely to SM final states, and so the partial decay widths and branching ratios of  $X$  are completely determined by  $\{g_X, m_X, \varphi\}$ . For fermions, the decay width is

$$\Gamma_{X \rightarrow f\bar{f}} = \frac{C_f g_X^2 x_f^2}{12\pi} m_X \left( 1 + 2 \frac{m_f^2}{m_X^2} \right) \sqrt{1 - 4 \frac{m_f^2}{m_X^2}} \quad (25)$$

where  $x_f$  are the couplings in Eq. (11) and  $C_f$  is 1 for charged leptons, 3 for quarks, and 1/2 for neutrinos. Decay into hadrons is considered separately in two regimes on either side of  $m_X = 2$  GeV. The simpler of the two is  $m_X > 2$  GeV where the decay is given by

$$\Gamma_{X \rightarrow \text{hadrons}} = \frac{\sum_q \Gamma_{X \rightarrow q\bar{q}}}{\sum_q \Gamma_{\gamma^* \rightarrow q\bar{q}}} \Gamma_{\gamma^* \rightarrow \mu^+\mu^-} \mathcal{R}(m_X), \quad (26)$$

<sup>6</sup>For  $\varphi = \pi - \tan^{-1}(1/2)$ , the charges are given by  $x_e = x_d = x_n = -x_\nu = -x_u = -x_p = 1/\sqrt{5}$  and pion charges  $m_{\pi^\pm} = \mp 2/\sqrt{5}$ .

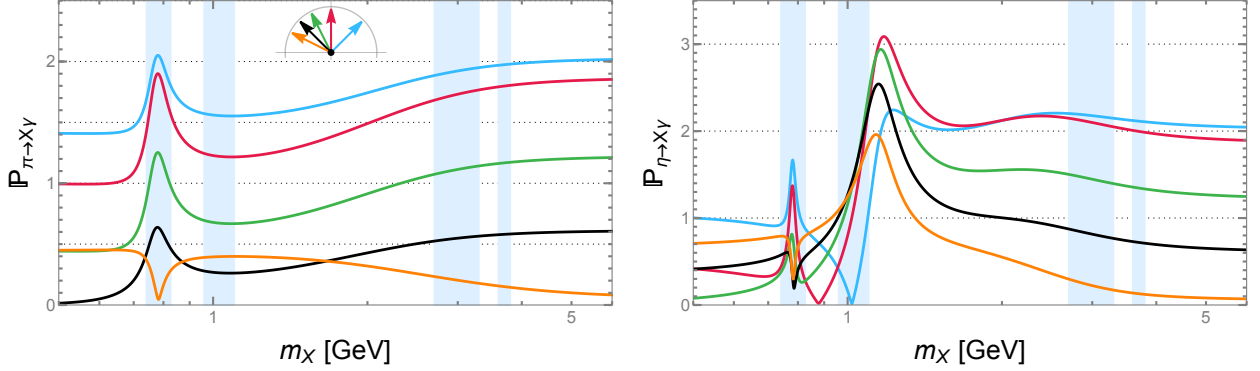


Figure 6: Decay widths for  $\pi^0 \rightarrow X\gamma$  (left) and  $\eta \rightarrow X\gamma$  (right), each normalized to the corresponding dark photon widths  $\pi^0 \rightarrow A'\gamma$  and  $\eta \rightarrow A'\gamma$  as given in Eqs. (21) and (22). The mixing angles are represented with colors indicated by the inset compass:  $\varphi = \pi/4$  (blue),  $B - L$  (red),  $\varphi = \pi - \tan^{-1} 2$  (green), chargephobic (black), and  $\varphi = \pi - \tan^{-1} (1/2)$  (orange).

with the sum ranging over all kinematically accessible quarks, and  $\mathcal{R}(m_X)$  is the experimentally determined cross section ratio given by  $\mathcal{R}(m_X) = \sigma_{e^+e^- \rightarrow \text{hadrons}} / \sigma_{e^+e^- \rightarrow \mu^+\mu^-}$  [45, 46]. For  $m_X \lesssim 2$  GeV, QCD becomes non-perturbative and the decay into hadrons can no longer be estimated by summing the contribution of  $q\bar{q}$  decays. In this range, we are also interested in decays into specific hadronic final states, i.e.,  $\pi^+\pi^-$ , rather than the total sum of all hadronic decays. Accordingly, we employ the data driven analysis in [1] based in the vector meson dominance (VMD) framework [41]. In this approach, the data from the most important hadronic contributions  $\mathcal{F}$  [47–54] at low mass are fit to

$$\mathcal{R}_\mu^{\mathcal{F}}(m) = \frac{\sigma_{e^+e^- \rightarrow \mathcal{F}}}{\sigma_{e^+e^- \rightarrow \mu^+\mu^-}} = \frac{9}{\alpha_{\text{EM}}^2} |\mathcal{A}_{\mathcal{F}}|^2, \quad (27)$$

where  $\mathcal{A}_{\mathcal{F}}$  is the sum of a real function and functions of a Breit-Wigner form accounting for the contributions of the three vector mesons  $\rho, \omega, \phi$ . The fits are then used to decompose the decay into hadrons to  $\rho$ -like  $\mathcal{R}_\mu^\rho$ ,  $\omega$ -like  $\mathcal{R}_\mu^\omega$ , and  $\phi$ -like  $\mathcal{R}_\mu^\phi$  contributions giving

$$\Gamma_{X \rightarrow \text{hadrons}} = \frac{g_X^2 m_X}{12\pi} \left( \sum_V \mathcal{R}_X^V + \mathcal{R}_X^{\omega-\phi} \right) \quad (28)$$

with

$$\begin{aligned} \mathcal{R}_X^\rho(m) &= \cos^2 \varphi \mathcal{R}_\mu^\rho(m) \\ \mathcal{R}_X^\omega(m) &= (\cos \varphi + 2 \sin \varphi)^2 \mathcal{R}_\mu^\omega(m) \\ \mathcal{R}_X^\phi(m) &= (\cos \varphi - \sin \varphi)^2 \mathcal{R}_\mu^\phi(m) \\ \mathcal{R}_X^{\omega-\phi}(m) &= [1 - 3 \cos 2\varphi - 2 \sin 2\varphi] \mathcal{R}_\mu^{\omega-\phi}(m) \end{aligned} \quad (29)$$

and  $\mathcal{R}_X^{\omega-\phi}$  is the only non-negligible interference term between  $\omega$ -like and  $\phi$ -like to the  $\pi^+\pi^-\pi^0$  final hadronic decay state.

The branching ratios for four mixing angles  $\varphi = \{0, \frac{\pi}{4}, \frac{\pi}{2}, \frac{3\pi}{4}\}$  are shown in Fig. 7; of those, the branching ratio to individual hadronic modes for  $\sqrt{s} < 2$  GeV are shown in Fig. 8. The  $\varphi = 0$  and  $\varphi = \pi/2$  correspond to the dark photon and  $B - L$  cases respectively and have been discussed thoroughly in the literature. The  $\varphi = \pi/4$  figure shows the transition between the two aforementioned models with a nonzero neutrino branching fraction, where the absence of  $\phi - X$  mixing, as in Eq. (29), leads to the disappearance of the  $\phi$  resonance and the subsequent  $KK$  and  $KK\pi$  decay modes. The case  $\varphi = \pi/2$  ( $B - L$ ) does not have

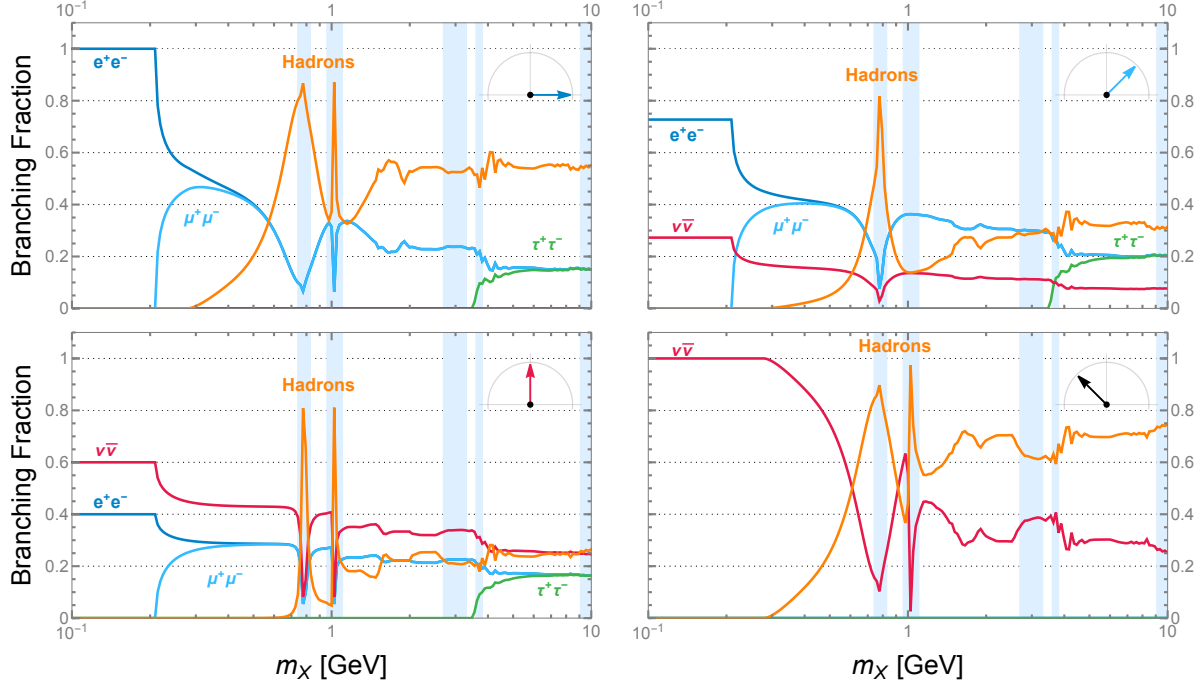


Figure 7: Branching fraction of  $X$  with  $\varphi = \{0, \frac{\pi}{4}, \frac{\pi}{2}, \frac{3\pi}{4}\}$  as indicated by the inset compass. The blue shaded regions correspond to meson resonances.

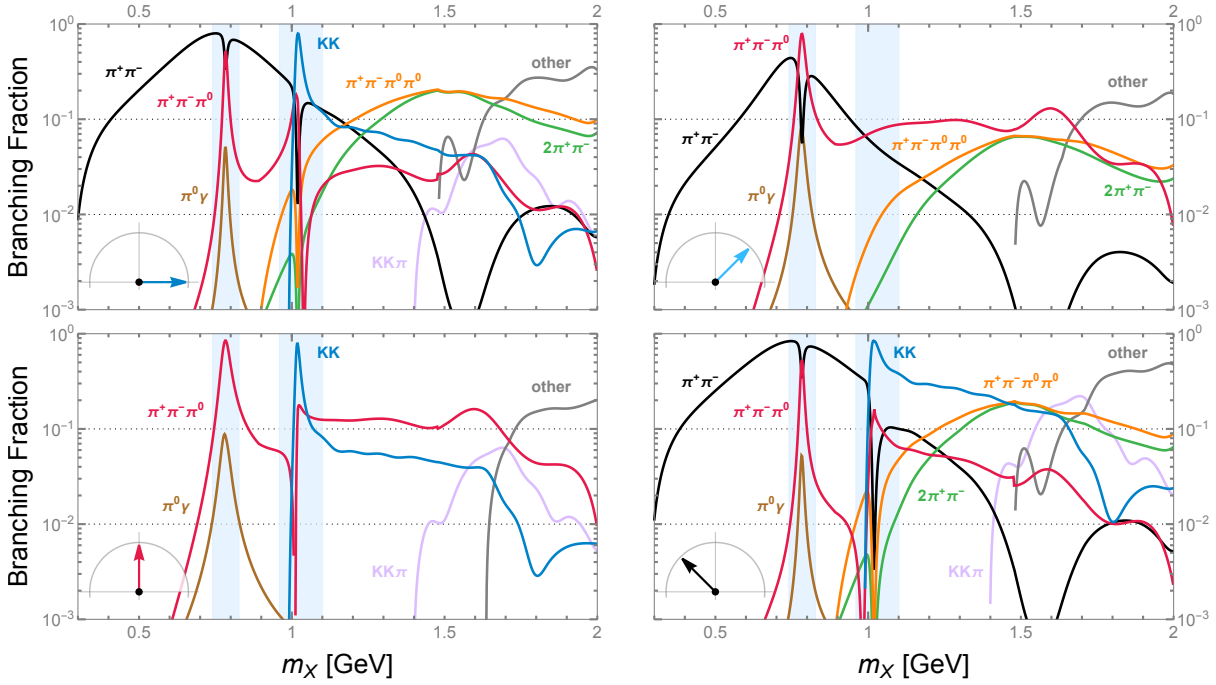


Figure 8: Branching fraction of  $X$  to individual hadronic that compose the results in Fig. 7 for  $\varphi = \{0, \frac{\pi}{4}, \frac{\pi}{2}, \frac{3\pi}{4}\}$  as indicated by the inset compass.

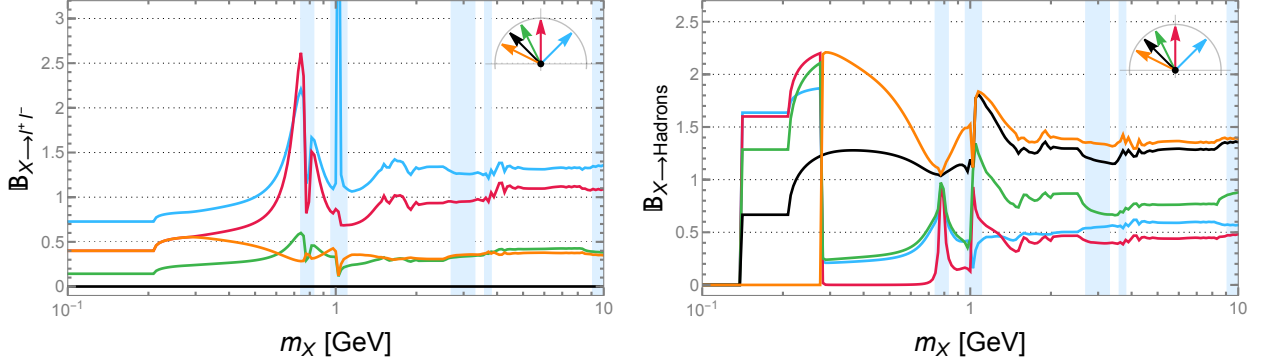


Figure 9: Ratio of the branching fractions of  $X$  to those of the dark photon  $A'$  into charged leptons (left) and hadrons (right). The mixing angles are represented with colors indicated by the inset compass:  $\varphi = \pi/4$  (blue),  $B - L$  (red),  $\varphi = \pi - \tan^{-1} 2$  (green), chargephobic (black), and  $\varphi = \pi - \tan^{-1}(1/2)$  (orange).

$\rho - X$  mixing, leading to the disappearance of  $\pi^+\pi^-$ ,  $\pi^+\pi^-\pi^0\pi^0$ , and  $\pi^+\pi^-\pi^+\pi^-$  decay modes. This distinction means that  $X$  decay to hadronic modes for  $B - L$  (and related flavor-dependent currents such as  $B - 3L_\tau$ ) remain suppressed up to  $m_X \simeq 700$  MeV, whereas for all of the mixing angles, including the chargephobic case, there are hadronic decay channels ( $X$  mixing  $\rho$  decaying to  $\pi^+\pi^-$ ) that start appearing once  $m_X \gtrsim 300$  MeV.<sup>7</sup> Fig. 7 demonstrates that the chargephobic case  $\varphi = 3\pi/4$  has the most striking differences in branching fraction with the other angles given the absence of a tree-level coupling to charged leptons. The plots include the RGE evolution of  $x_e$  as discussed in App. B, although the branching ratio to charged leptons is at most  $\mathcal{O}(10^{-4})$ .

The blue shaded regions in Fig. 7 correspond to the following meson resonances in mass ranges [MeV]:  $\rho$  and  $\omega$  at (741, 827),  $\phi$  at (960, 1100),  $J/\psi$  at (2700, 3300),  $\psi(2S)$  &  $\psi(3770)$  at (3600, 3800), and  $\Upsilon(1S) - \Upsilon(4S)$  at (9100, 10600). These bands are obtained from [55] where prompt-like  $A'$  searches are vetoed due to the large resonance contribution, and are meant only to illustrate an example of experimental veto window rather than a theoretical limitation. In our analysis, we have not explicitly included the  $J/\psi, \psi(2S), \psi(3770)$ , and  $\Upsilon(1S) - \Upsilon(4S)$  resonances in hadronic decays, but their effects are consistently considered in the constraints.

Experiments search for the decay products of  $X$ , or lack thereof, as a signal to set constraints on the  $\{m_X, g_X\}$  parameter space. The branching fraction is a guide for experiments as to which SM particles can be suitably employed as a signal for a given mass  $m_X$ . The ratio of branching fraction of  $X$  to  $A'$  provides a quantitative guide to how the sensitivity of a given search to  $X$  differs from the corresponding dark photon case. For some experiments, a constraint on  $A'$  can be recast to a constraint on  $X$  via  $\sigma_X \text{Br}_{X \rightarrow \mathcal{F}} \text{Eff}(\tau_X) = \sigma_{A'} \text{Br}_{A' \rightarrow \mathcal{F}} \text{Eff}(\tau_{A'})$ , where  $\text{Br}$  is the branching ratio and  $\text{Eff}(\tau_X)$  is the experimental efficiency with explicit dependence on  $X$  lifetime. Equivalently, when applicable, constraints can be recast using

$$\mathbb{P}_X \mathbb{B}_{X \rightarrow \mathcal{F}} \mathbb{E}(\tau_X) = 1, \quad (30)$$

where  $\mathbb{P}_X$  is shown in Fig. 5 and Fig. 6,  $\mathbb{B}_{X \rightarrow \mathcal{F}}$  is the ratio of branching fractions and  $\mathbb{E}(\tau_X)$  is the efficiency ratio. The ratio of branching fractions  $\mathbb{B}_{X \rightarrow \mathcal{F}}$  for charged leptons and hadrons for  $\varphi = \{\frac{\pi}{4}, \frac{\pi}{2}, \pi - \tan^{-1} 2, \frac{3\pi}{4}, \pi - \tan^{-1}(1/2)\}$  are shown in Fig. 9.

The recasting equation, Eq. (30), is powerful and can be applied to a variety of constraints set by fixed target experiments, colliders, beam dumps, and searches to invisible final states. For these experiment categories, we use the methodology developed in [1]<sup>8</sup> to recast the constraints. Otherwise, we rederive

<sup>7</sup>For the case  $\varphi = \pi - \tan^{-1} 1/2$  (not shown), the absence of  $\omega - X$  mixing leads to the disappearance of  $\pi^+\pi^-\pi^0$  and  $\pi^0\gamma$ .

<sup>8</sup>The reference [1] also provides a publicly available code `Darkcast` <https://gitlab.com/philten/darkcast> which we have

the constraints set on beam dump experiments<sup>9</sup>, neutrino experiments, SNe cooling, early universe  $\Delta N_{\text{eff}}$  modification and some precision experiments. In the following sections, we summarize the derivation of all aforementioned constraints.

## 5 Constraints

We now detail the derivation of the constraints in Figs. 3,4 that span a rich set of cosmological, astrophysical and terrestrial experiment observables. As we have seen, cosmology and astrophysics provide constraints throughout the range of dark mixing angles  $\varphi$ . Consequently, we present these constraints first, since we have carried out independent calculations of the contribution of  $X$  production and decay to  $\Delta N_{\text{eff}}$  during the early universe as well as our own  $X$  emission from SN1987A. Next, we derive constraints on neutrino experiments, since they provide some of the strongest constraints on the chargephobic case. We then consider beam dump experiments and colliders, and detail the effects of  $X$  production and decay with the critically important  $\varphi$  dependence. Finally, we consider constraints from precision tests of the Standard Model, which provide leading bounds on the large  $m_X$  in the chargephobic model.

### 5.1 Cosmology: CMB & BBN

The precision determination of the effective number of relativistic species in the early universe,  $N_{\text{eff}}$ , from CMB power spectra [56–58] and primordial element abundances [59–62] is in good agreement with the SM prediction [63–77]. Hence, BSM physics that alters  $N_{\text{eff}}$  before recombination is strongly constrained [23, 78–101]. In our case, a well known effect is that an  $X$  boson can “freeze in” [102], become nonrelativistic, redshift as matter, and then decay back into SM states, modifying  $\Delta N_{\text{eff}}$ . This constraint was derived for a dark photon [94],  $U(1)_{\mu-\tau}$  [23], and  $U(1)_{B-L}$  [35, 103]<sup>10</sup>.

In this paper, we utilize the formalism and approximations outlined in [23, 35, 92, 95] to derive constraints on  $X$ . Specifically, our previous work in [35] can be fully adapted to this case by modifying the couplings

---

recreated in `Mathematica` and used to recast constraints from some experiments as discussed in the text.

<sup>9</sup>We rederive constraints from electron beam dump experiments and the bremsstrahlung process in proton beam dump experiments even though those can be recast. Constraints set from meson decay in proton beam dumps are recast from dark photon constraints.

<sup>10</sup>The constraint in our previous work [35] is stronger than that in Ref. [103] as the latter neglected including the coupling to charged leptons (electrons) and finite temperature effects in their  $B-L$  constraint calculation. These effects play a crucial role in determining the constraint in a large portion of the parameter space.

appropriately. For each given  $\{m_X, g_X, \varphi\}$ , we solve the five Boltzmann equations

$$\begin{aligned}
\frac{dT_X}{dt} &= \mathbb{D}(T_X, \mu_X) \left[ -3H \left( (\rho_X + P_X) \frac{\partial n_X}{\partial \mu_X} - n_X \frac{\partial \rho_X}{\partial \mu_X} \right) + \frac{\partial n_X}{\partial \mu_X} \frac{\delta \rho_X}{\delta t} - \frac{\partial \rho_X}{\partial \mu_X} \frac{\delta n_X}{\delta t} \right], \\
\frac{dT_\nu}{dt} &= \mathbb{D}(T_\nu, \mu_\nu) \left[ -3H \left( (\rho_\nu + P_\nu) \frac{\partial n_\nu}{\partial \mu_\nu} - n_\nu \frac{\partial \rho_\nu}{\partial \mu_\nu} \right) + \frac{\partial n_\nu}{\partial \mu_\nu} \frac{\delta \rho_\nu}{\delta t} - \frac{\partial \rho_\nu}{\partial \mu_\nu} \frac{\delta n_\nu}{\delta t} \right], \\
\frac{dT_\gamma}{dt} &= \left( \frac{\partial \rho_\gamma}{\partial T_\gamma} + \frac{\partial \rho_e}{\partial T_\gamma} \right)^{-1} \left[ 4H \rho_\gamma + 3H(\rho_e + P_e) + \frac{\delta \rho_e}{\delta t} \right], \\
\frac{d\mu_X}{dt} &= -\mathbb{D}(T_X, \mu_X) \left[ -3H \left( (\rho_X + P_X) \frac{\partial n_X}{\partial T_X} - n_X \frac{\partial \rho_X}{\partial T_X} \right) + \frac{\partial n_X}{\partial T_X} \frac{\delta \rho_X}{\delta t} - \frac{\partial \rho_X}{\partial T_X} \frac{\delta n_X}{\delta t} \right], \\
\frac{d\mu_\nu}{dt} &= -\mathbb{D}(T_\nu, \mu_\nu) \left[ -3H \left( (\rho_\nu + P_\nu) \frac{\partial n_\nu}{\partial T_\nu} - n_\nu \frac{\partial \rho_\nu}{\partial T_\nu} \right) + \frac{\partial n_\nu}{\partial T_\nu} \frac{\delta \rho_\nu}{\delta t} - \frac{\partial \rho_\nu}{\partial T_\nu} \frac{\delta n_\nu}{\delta t} \right] \\
\mathbb{D}(T, \mu) &= \left( \frac{\partial n}{\partial \mu} \frac{\partial \rho}{\partial T} - \frac{\partial n}{\partial T} \frac{\partial \rho}{\partial \mu} \right)^{-1},
\end{aligned} \tag{31}$$

numerically from  $T \sim \mathcal{O}(100)$  MeV all the way down to recombination at  $T \simeq 0.3$  eV.

In writing these equations, we made the implicit assumption that fermions and bosons follow Fermi-Dirac (FD, positive) and Bose-Einstein (BE, negative),  $f(E) = [e^{(E-\mu)/T} \pm 1]^{-1}$  distributions respectively. Here  $n, \rho, P$  are the number, energy, and pressure densities for a particle  $i$  with  $d_i$  degrees of freedom obtained by integrating the particle distribution  $f$  over  $d_i d^3p/(2\pi)^3$ ,  $d_i E d^3p/(2\pi)^3$ , and  $d_i \frac{p^2}{3E} d^3p/(2\pi)^3$  respectively.  $\delta n/\delta t$  and  $\delta \rho/\delta t$  are the number and energy transfer rates between particle species obtained by integrating collision terms over the same measures. Finally,  $H = \sqrt{\rho_{\text{tot}}/(3M_{\text{Pl}}^2)}$  is the Hubble expansion rate and  $M_{\text{Pl}} = 2.4 \times 10^{18}$  GeV. The formulae for these thermodynamic quantities and their derivatives can be found in Appendix A.6 of [95].

The  $\delta n/\delta t$  and  $\delta \rho/\delta t$  terms account for all relevant interactions driving the dynamics. At the temperature range of interest,  $e^+e^- \leftrightarrow \bar{\nu}_\alpha \nu_\alpha$ ,  $e^\pm \nu_\alpha \leftrightarrow e^\pm \nu_\alpha$ , and  $e^\pm \bar{\nu}_\alpha \leftrightarrow e^\pm \bar{\nu}_\alpha$  are the only SM interactions needed. These interactions, mediated by  $W$  and  $Z$  exchange, drive the neutrino and electron population to equilibrium for temperatures above neutrino decoupling  $T \sim 2$  MeV. If  $X$  couples to neutrinos and electrons, these interactions can also be mediated by  $X$ . We also include the interactions  $X \leftrightarrow \nu \bar{\nu}$ ,  $X \leftrightarrow e^+e^-$ ,  $\gamma X \leftrightarrow e^+e^-$ , and  $e^\pm X \leftrightarrow e^\pm \gamma$  when applicable. Interactions such as  $e^+e^- \leftrightarrow \gamma X$ ,  $\nu \bar{\nu} \leftrightarrow X X$ ,  $X e^\pm \leftrightarrow X e^\pm$ , and  $X \nu \leftrightarrow X \nu$  are subdominant to the aforementioned interactions and can be neglected. The rates, along with a detailed discussion of the dynamics, can be found in [35]. These rates are trivially adapted to our case with the appropriate coupling substitutions.

Following the discussion in [35, 61] and based on the datasets in [56, 57, 104–117], constraints in Fig. 4 are set on modifications to  $N_{\text{eff}}$  of  $|\Delta N_{\text{eff}}| \geq 0.4$  and/or helium mass fraction  $Y_p$  of  $\Delta Y_p > 0.008$ ; we also show future projected sensitivity at  $|\Delta N_{\text{eff}}| \geq 0.05$ . The first constraint is set from  $X$  modifying the effective number of relativistic species in the early universe defined as

$$N_{\text{eff}} = \frac{8}{7} \left( \frac{11}{4} \right)^{4/3} \left( \frac{\rho_{\text{rad}} - \rho_\gamma}{\rho_\gamma} \right), \tag{32}$$

which is the ratio of non-photon to photon radiation density. The state-of-the-art calculation in the SM gives  $N_{\text{eff}}^{\text{SM}} = 3.045\text{--}3.046$ , that takes into higher order corrections, non-thermal neutrino distribution functions, neutrino oscillations, etc. [63, 64]. Using the method outlined above without  $X$ , we obtain the photon-to-neutrino temperature ratio, the neutrino chemical potential, and  $N_{\text{eff}}$  in the SM

$$T_\gamma/T_\nu = 1.3945, \quad \mu_\nu/T_\nu = -4.82 \times 10^{-3}, \quad N_{\text{eff}}^{\text{SM}} = 3.042. \tag{33}$$

This demonstrates that our calculation is able to reproduce the non-instantaneous decoupling of neutrinos in the SM to an accuracy of order  $\Delta N_{\text{eff}} \sim 0.01$ . The value of  $N_{\text{eff}}$  in Eq. (33) will be modified when solving

the Boltzmann equations in Eq. (31) including  $X$  and a constraint is set if  $\Delta N_{\text{eff}} \geq 0.4$ . The constraint from  $\Delta Y_p$  can be also be derived as in [35]; however, this constraint is weaker than that derived from  $\Delta N_{\text{eff}}$  everywhere in our parameter space.

The normalized density evolution for two representative points in the parameter space is shown in Fig. 10. Here,  $T_\xi$  is a reference temperature as in [35] that can be thought of as the evolution of a fictitious massless particle with a temperature that is initially set to the SM temperature but is actually decoupled from all other particles. Using  $T_\xi$  makes it simple to compare different values of  $\varphi$  where  $X$  couples differentially to neutrinos and electron photon bath.

When the mass of  $X$  is of order a few MeV, the majority of the production and decay dynamics occur after neutrino decoupling as can be seen in the representative example  $m_X = 1.5$  MeV in Fig. 10. For this mass and in the chargephobic limit (dashed),  $X$  is slowly populated at the expensive of the  $\nu$  population through  $\nu\bar{\nu} \rightarrow X$ . The rates are maximal around  $T_\xi \sim m_X/3$  where the  $X$  population becomes non-relativistic and starts decaying back into neutrinos. Importantly, the  $X$  distribution evolves as matter  $\rho_X \propto a^{-3}$  before dumping its entropy back into neutrinos, that themselves have been evolving as radiation  $\rho_\nu \propto a^{-4}$ . Hence, this back and forth exchange in energy heats up the neutrino plasma. The result is a neutrino energy density that is larger than it would have been in the SM as compared to the photon energy density. This effect *increases* the value of  $N_{\text{eff}}$  in Eq. (32) and gives  $\Delta N_{\text{eff}} = 0.27$  for  $m_X = 1.5$  MeV and  $g_X = 10^{-10}$ . The small shift in the electron and photon densities here is due to the dynamics commencing slightly before neutrinos are fully decoupled.

The dark photon limit (dotted) for  $m_X = 1.5$  MeV proceeds similarly with the dynamics now occurring between  $X$  and the electron-photon bath instead of neutrinos. The result is a photon energy density that is larger than it would have been in the SM as compared to neutrino density and a *decrease* in  $N_{\text{eff}}$ ; in this case  $\Delta N_{\text{eff}} = -0.27$ . In the  $B-L$  case (dot-dashed),  $X$  couples to  $e$  and  $\nu$  and has access to a larger energy density bath. This leads to a larger  $X$  population produced at a slightly earlier time as compared to the previous two cases. The  $X$  population then decays back into both  $e$  and  $\nu$ . However, this decay occurs around the time that electrons also become non-relativistic and the dynamics become highly nontrivial as discussed in [35]. The upshot is a preferential heating of the neutrinos and an increase in  $N_{\text{eff}}$  giving  $\Delta N_{\text{eff}} = 0.86$  for  $m_X = 1.5$  MeV and  $g_X = 10^{-10}$ .

For  $m_X = 15$  MeV and  $g_X = 4 \times 10^{-10}$ , the majority of  $X$  production occurs before the neutrinos are fully decoupled. This means that regardless of the charge assignment,  $X$  has access to the entire SM thermal bath. For example, in the chargephobic limit,  $X$  is produced via  $\nu\bar{\nu} \rightarrow X$  which effectively cools the neutrino population. However, in this case, processes such as  $e^+e^- \leftrightarrow \bar{\nu}_\alpha\nu_\alpha$ , which have previously kept neutrinos and the electron-photon bath in equilibrium, are still active. These processes transfer energy from the electron-photon bath to neutrinos driving the system to a new equilibrium at a lower temperature. These two effects occur simultaneously and proceed until the neutrinos decouple from SM. After  $X$  decays and heats up the neutrino plasma, some of this energy is transferred into the electron-photon bath through  $e^+e^- \leftrightarrow \bar{\nu}_\alpha\nu_\alpha$  interactions which are still partially active. This leads to an attenuated increase in  $N_{\text{eff}}$  giving  $\Delta N_{\text{eff}} = 0.03$  for  $m_X = 15$  MeV and  $g_X = 4 \times 10^{-10}$ . A similar effect is seen in dark photon case where  $\Delta N_{\text{eff}} = -0.1$ . Lastly, in the  $B-L$  case,  $X$  decays and heats up both neutrinos and electron-photon bath with comparable amounts leading to a weaker increase in  $N_{\text{eff}}$ ; in this case  $\Delta N_{\text{eff}} = -0.02$ . For larger values of  $m_X$ , the production and decay of  $X$  terminates completely before neutrino decoupling. This gives the SM enough time to return to thermal equilibrium leading to no change in  $N_{\text{eff}}$ .

Fig. 11 contains a summary of the  $\Delta N_{\text{eff}}$  constraints on a dark photon, a  $B-L$  vector boson, and on a chargephobic vector boson. Given the discussion above, we find that  $\Delta N_{\text{eff}}$  receives positive contributions in the  $B-L$  and chargephobic cases, and negative contributions in the dark photon case. This last result is potentially interesting in the context of some CMB results that find a best fit to  $\Delta N_{\text{eff}} < 0$  [58].

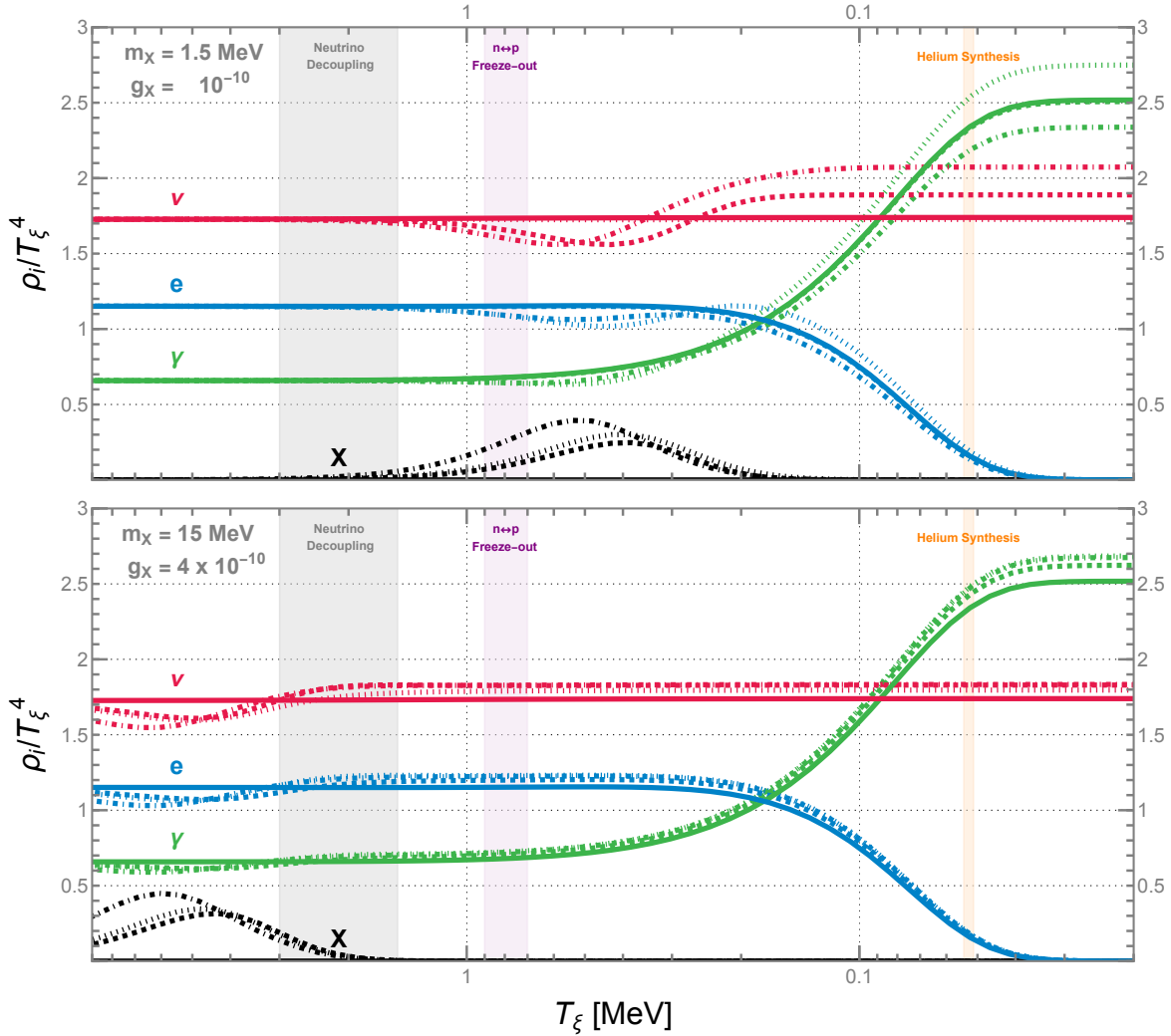


Figure 10: The normalized energy density evolution  $\rho/T_\xi^4$  of the neutrino (red), electron (blue), photon (green), and  $X$  (black) around the BBN era as a function of a reference temperature  $T_\xi$  explained in the text. (Top)  $m_X = 1.5$  MeV with  $g_X = 10^{-10}$  and (bottom)  $m_X = 15$  MeV with  $g_X = 4 \times 10^{-10}$ . In both plots, (solid) lines are SM evolution with no  $X$  included, (dotted) dark photon ( $\varphi = 0$ ), (dot-dashed)  $B-L$  ( $\varphi = \pi/2$ ) and (dashed) chargephobic case ( $\varphi = 3\pi/4$ ).

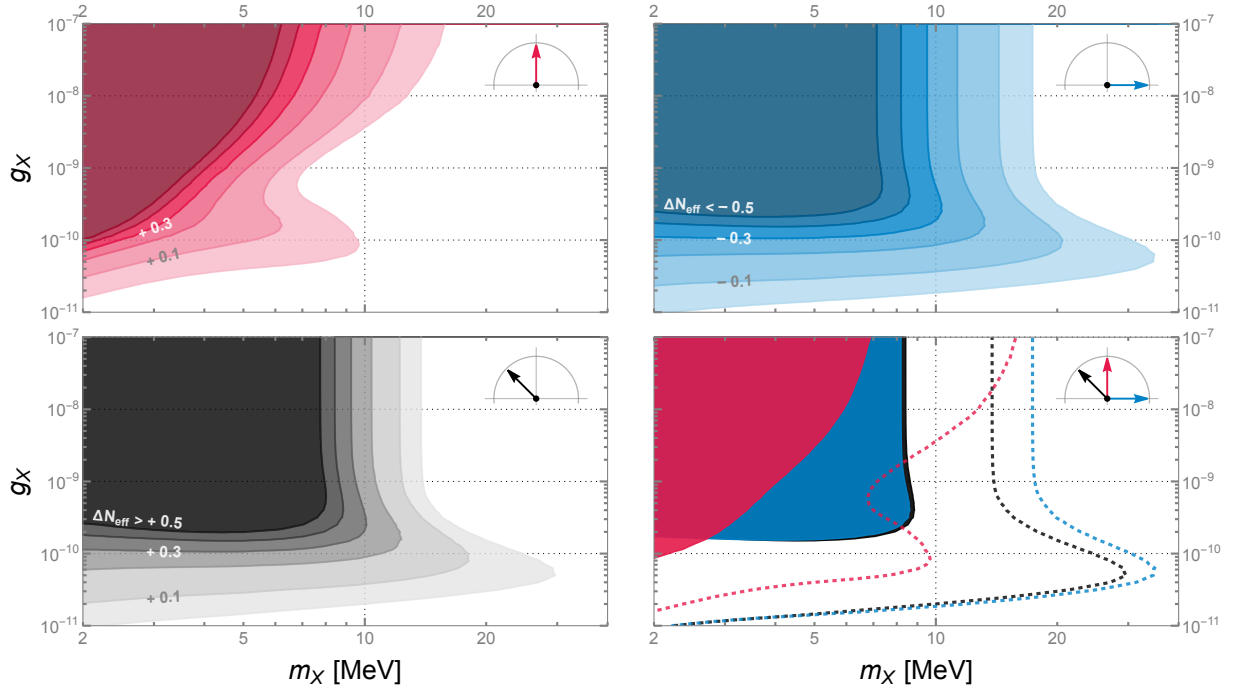


Figure 11:  $\Delta N_{\text{eff}}$  contours for the  $B-L$ , dark photon, and chargephobic cases as indicated by compass inset plot. The color shading from lighter to darker corresponds to  $\Delta N_{\text{eff}} = \{0.05, 0.1, 0.2, 0.3, 0.4, 0.5\}$  and contours greater than 0.5 are not shown. Note that the dark photon limit drags  $N_{\text{eff}}$  below its SM value (negative  $\Delta N_{\text{eff}}$ ) as opposed to  $B-L$  and chargephobic limits with positive  $\Delta N_{\text{eff}}$  values. The fourth plot shows the (solid) current constraint corresponding to  $\Delta N_{\text{eff}} = 0.4$  and (dashed) future CMB experiment sensitivity projection corresponding  $\Delta N_{\text{eff}} = 0.05$  for the three models.

## 5.2 Astrophysics

### 5.2.1 Protoneutron Star Cooling: SN1987A

The explosion of the blue supergiant Sanduleak –69 202 in the Large Magellanic Cloud and its subsequent detection is known as supernova 1987A (SN1987A). The supernova is estimated to have released  $\approx 3 \times 10^{53}$  erg in the form of neutrinos. The Kamiokande II [118] and IMB collaboration [119] detection of  $\sim 20$  neutrino events within  $\sim 10$  seconds of the explosion agrees with the predictions of the standard model for total energy, average neutrino energy, and burst duration based on simulation of neutrino emission from stellar core collapse for SN1987A [120–122]. For reviews of supernova core collapse theory see [123–126].

This agreement allows constraints to be established on BSM models that provide an additional cooling mechanism to the proto-neutron star (PNS) after collapse [124]. For dark photons, the PNS cooling constraint was determined by Refs. [5, 127, 128], which improved on previous constraints [129–132] by including finite temperature and density effects. For a  $B - L$  vector boson, calculations were carried out in Refs. [133, 134], however the resulting constraint differs between the two references in certain regions of parameter space by up to an order of magnitude in the values of  $g_{B-L}$ . As discussed below, we rederive the constraints from PNS cooling in our parameter space. In the dark photon case, our results are in good agreement with the previous results [5, 127, 128]. In the  $B - L$  case, our results resolve the discrepancy between the constraints in [133] and [134], by including effects neglected in both analyses. Finally, we derive PNS cooling constraints in the chargephobic case; this is an important result since PNS cooling is one of the few ways the chargephobic vector boson couplings can be constrained. Aside from the cooling constraint, there are several supernova based constraints arising from the production and decay to visible modes (especially  $e^+e^-$ ); these bounds were most recently derived on a dark photon in [5] and will be discussed in Sec. 5.2.2.

The PNS cooling constraint is traditionally set by demanding the instantaneous luminosity of the new particles  $L_X(m_X, g_X)$  not exceed the ‘‘Raffelt Criterion’’,  $L_\nu = 3 \times 10^{52}$  erg/s [124]. Specifically, this limit is applied around  $t = 1$  s post-bounce where the PNS core reaches peak density. The duration of SN1987A neutrino burst is reduced by half if the luminosity exceeds this limit which is inconsistent with observations. The instantaneous luminosity of  $X$  is

$$L_X(m_X, g_X, R_\nu, R_{\text{far}}) = \int_{r=0}^{R_\nu} \int_{\omega=m_X}^{\infty} \exp[-a(r)\tau(m_X, g_X, \omega, r, R_{\text{far}})] \frac{dP(m_X, g_X, \omega, r)}{dV d\omega} d\omega dV, \quad (34)$$

with differential power

$$\frac{dP}{dV} = \int d\omega \frac{\omega^3 v}{2\pi^2} \sum \Gamma_{\text{prod}}(\omega, r), \quad (35)$$

$$(36)$$

and optical depth of  $X$  traveling radially outwards

$$\tau = \int_r^{R_{\text{far}}} \Gamma'_{\text{abs}}(m_X, g_X, \omega, r') dr'. \quad (37)$$

The geometric factor  $a(r) = 1 - r(r - R_c)/(2R_\nu^2)$  is an approximation that allows for a radial treatment on the optical depth [127].<sup>11</sup> The three radii that appear in these equations are: the radius of peak temperature,  $R_c$ ; the radius at which neutrinos transition from diffusion to free streaming,  $R_\nu$ ; and, the radius

<sup>11</sup>The full angular treatment [135] leads to larger values of optical depth and consequently a  $\sim 10\%$  weaker bound in the trapping regime. This effect, however, is washed out by our treatment of  $R_{\text{far}}$  which weakens the bound by an order of magnitude in the trapping regime.

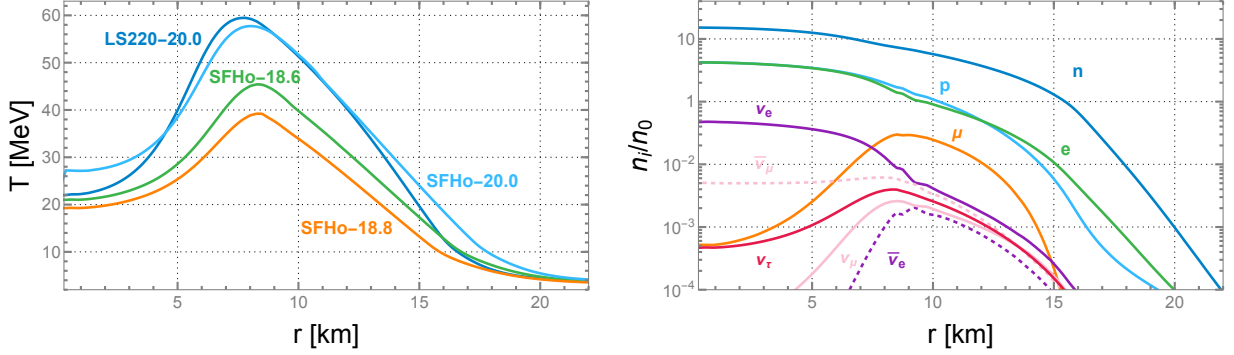


Figure 12: (Left) temperature profile of the 4 models used, and (right) particle number density profile in the SFHo-18.8 model normalized to  $n_0 = 0.181 \text{ fm}^{-3}$  corresponding to nuclear density of  $3 \times 10^{14} \text{ g cm}^{-3}$ .

at which neutrinos are no longer efficiently produced,  $R_{\text{far}}$ . This luminosity describes energy that escapes the neutrinosphere and thus cannot be reprocessed as neutrino energy. The value of these radii along with various PNS property profiles depend on the theoretical modeling of the core collapse process.

To ensure our bounds are robust with respect to SN modeling, we use four representative models to derive the constraints. The models are SFHo-18.6, SFHo-18.8, SFHo-20.0, and LS220-20.0, where SFHo [136] and LS220 [137] are the equations of states used at supernuclear densities, and 18.6 [138], 18.8 [139], and 20.0 [140] are the progenitor masses. More information of these models can be found in [141]. The temperature profiles and normalized number densities of particles in the PNS at 1 s after core collapse are shown in Fig. 12.<sup>12</sup> For all  $\varphi$ , we find that the SFHo-18.8 model leads to the most conservative bounds, and so we adopt this model when presenting our results.

In medium, the SM photon acquires nonzero effective plasma mass [142, 143] which is characterized by the real part of the photon polarization tensor

$$\text{Re } \Pi_{\mathbf{L}} = \frac{3\omega_p^2}{v^2}(1-v^2) \left[ \frac{1}{2v} \ln \left( \frac{1+v}{1-v} \right) - 1 \right] \quad \text{Re } \Pi_{\mathbf{T}} = \frac{2\omega_p^2}{2v^2} \left[ 1 - \frac{1-v^2}{2v} \ln \left( \frac{1+v}{1-v} \right) \right]. \quad (38)$$

Here  $\omega_p^2 = 4\pi\alpha_{\text{EM}}n_e/\sqrt{m_e^2 + (3\pi^2n_e)^{2/3}}$  is the plasma frequency,  $v$  is the photon velocity, and  $\mathbf{T}$ ,  $\mathbf{L}$  are the transverse and longitudinal polarizations of the photon each with a different in-medium dispersion relation. The polarization tensor also dynamically changes the coupling of  $X$  with the SM particles charged under  $U(1)_{\text{EM}}$ . Explicitly,

$$g_X \longrightarrow g_{X,m} = \frac{m_X^2}{m_X^2 - \Pi} g_X \equiv \xi_m g_X \quad (e, q, p) \quad (39)$$

$$g_X \longrightarrow g_X \quad (\nu, n), \quad (40)$$

where

$$\xi_m^2 = \frac{1}{(1 - \text{Re } \Pi/m_X^2)^2 + (\text{Im } \Pi/m_X^2)^2}. \quad (41)$$

The imaginary part of the polarization tensor is  $\text{Im } \Pi_{\mathbf{L},\mathbf{T}} = -\omega(\Gamma_{\text{abs}|\mathbf{L},\mathbf{T}} - \Gamma_{\text{prod}|\mathbf{L},\mathbf{T}})$ , where  $\Gamma_{\text{abs}}$  and  $\Gamma_{\text{prod}}$  are the absorption width and production rate of SM photon at energy  $\omega$  [144]. In local thermal equilibrium at temperature  $T$ , these rates are related through detailed balance  $\Gamma_{\text{prod}} = e^{-\omega/T}\Gamma_{\text{abs}}$ . The absorption rates of interest in a proto-neutron star are inverse bremsstrahlung, semi-Compton scattering, and  $X$  decays into  $e^+e^-$  and  $\nu\bar{\nu}$ .

<sup>12</sup>The full profile data can be found at the Garching Core Collapse Supernova Archive [31].

The bremsstrahlung rate is composed of  $pn$ ,  $pp$ , and  $nn$  collisions and is derived in App. C using the soft radiation approximation,

$$\Gamma_{\text{ibr}|\mathbf{L},\mathbf{T}}^{ij} = \frac{8n_i n_j}{15\pi^2 \omega^3 S_{\mathbf{L},\mathbf{T}}} \left( \frac{\pi T}{m_N} \right)^{3/2} \left\{ \begin{aligned} & \left[ 10q_-^2 \langle \sigma_{ij}^{(2)} \rangle + 9q_+^2 \frac{Tv^2}{m_N} \langle \sigma_{ij}^{(4)} \rangle \right] & (\mathbf{T}) \\ & \left[ 5q_-^2 \langle \sigma_{ij}^{(2)} \rangle + 6q_+^2 \frac{Tv^2}{m_N} \langle \sigma_{ij}^{(4)} \rangle \right] (1 - v^2) & (\mathbf{L}). \end{aligned} \right. \quad (42)$$

Here  $q_{\pm} = q_1 \pm q_2$  with  $q_1, q_2$  the charges of the two nucleons,  $\langle \sigma_{ij}^{(2)}(T) \rangle = \frac{1}{2} \int_0^\infty dx e^{-x} x^2 \sigma_{ij}^{(2)}(xT)$  and  $\langle \sigma_{ij}^{(4)}(T) \rangle = \frac{1}{6} \int_0^\infty dx e^{-x} x^3 \sigma_{ij}^{(4)}(xT)$  are the energy and angle-averaged nucleon-nucleon scattering cross section found in [132]. The production rate is identical with the restriction that the energy of  $X$  must not exceed the energy of the collision. This takes  $\int_0^\infty \rightarrow \int_{\omega/T}^\infty$ ; for example  $\langle \sigma_{ij}^{(2)}(T) \rangle \rightarrow \langle \sigma_{ij}^{(2)}(T, \omega) \rangle = \frac{1}{2} \int_{\omega/T}^\infty dx e^{-x} x^2 \sigma_{ij}^{(2)}(xT)$ .

When calculating the imaginary part of the polarization tensor of the SM photon  $\text{Im} \Pi_{\mathbf{L},\mathbf{T}}$ , the charges in question are  $q_p = e$  for the proton and  $q_n = 0$  for the neutron. When calculating the absorption rate for  $X$ , the proton charge is  $q_{p,\text{med}} = \xi_m q_p = \xi_m g_X (\cos \varphi + \sin \varphi)$  and the neutron charge  $q_{n,\text{med}} = q_n = g_X \sin \varphi$ . In a general model, the  $pn$ ,  $pp$  and  $nn$  charges in Eq. (42) become

$$(q_p \pm q_n)_{\text{med}}^2 = q_n^2 + \xi_m^2 \left[ (q_p^2 \pm 2q_p q_n) \mp 2 \frac{\text{Re} \Pi}{m_X^2} q_p q_n \right] \quad (43)$$

$$(q_p + q_p)_{\text{med}}^2 = 4\xi_m^2 q_p^2 \quad (44)$$

$$(q_n + q_n)_{\text{med}}^2 = 4q_n^2. \quad (45)$$

When the couplings of the proton and neutron to  $X$  are the same [ $q_-^2 = 0$  in Eq. (42)], the bremsstrahlung rate arises only at the quadrupole order and is suppressed. When the couplings are different, the  $pn$  bremsstrahlung rate dominates. In the dark photon case, there is no coupling to neutrons and we are left with two diagrams for  $pn$  and four for  $pp$ . For  $pp$  bremsstrahlung rate,  $q_- = q_p - q_p = 0$  and first contribution is suppressed by  $T/m_N$  as compared to the  $pn$  bremsstrahlung rate. Hence only the  $pn$  bremsstrahlung rate is important in the dark photon limit. In the  $B - L$  case with  $\text{Re} \Pi \ll m_X^2$ , the couplings of  $X$  to the proton and neutron are the same, and so the leading contribution to bremsstrahlung is of order  $\mathcal{O}(T/m_N)$  requiring all of  $pn$ ,  $pp$ , and  $nn$  bremsstrahlung rates to be included [the  $q_+^2 \langle \sigma_{ij}^{(4)} \rangle$  terms]. However, when  $\text{Re} \Pi \gg m_X^2$ , only the  $pn$  bremsstrahlung rate (off of neutrons) is important since the in-medium proton charge is suppressed and is thus non-degenerate with the neutron charge. Similarly, in the chargephobic limit, only the  $pn$  bremsstrahlung rate is important, though in this case, the bremsstrahlung is  $X$  off neutrons (and not protons). Hence, the  $pp$  and  $nn$  bremsstrahlung are only important in the  $B - L$  case when  $m_X \gtrsim 10 \text{ MeV}$ .

The decay rates  $X \rightarrow e^+ e^-$  and  $X \rightarrow \nu_i \bar{\nu}_i$  provide an important contribution to the optical depth. The widths are

$$\Gamma_{f\bar{f}|\mathbf{L},\mathbf{T}} = C_f \frac{1}{4\pi} \frac{(q_f)_m^2 m_X^2}{\sqrt{\omega^2 - m_X^2}} \int_{x_-}^{x_+} \frac{\mathbf{m}_f(\omega x)_{\mathbf{L},\mathbf{T}}^2 dx}{\left[ \exp\left(\frac{\mu_f - \omega x}{T}\right) + 1 \right] \left[ \exp\left(-\frac{\mu_f + \omega(1-x)}{T}\right) + 1 \right]}, \quad (46)$$

where  $\mu_f$  is the chemical potential, and  $x_{\pm} = \frac{1}{2} \left[ 1 \pm \sqrt{(1 - 4(m_f^{\text{eff}})^2/m_X^2)(1 - m_X^2/\omega^2)} \right]$  are the limits of integration, and  $C_f = 1$  ( $1/2$ ) for  $e^+ e^-$  ( $\nu_i \bar{\nu}_i$ ). We also have the dimensionless squared matrix elements  $\mathbf{m}_f(E_1)_{\mathbf{T}}^2 = (m_f^{\text{eff}})^2/m_X^2 + z(E_1)$  and  $\mathbf{m}(E_1)_{\mathbf{L}}^2 = 1 - 2z(E_1)$  where

$$z(E_1) = \frac{E_1 E_2}{m_X^2} - \frac{(E_1 \omega - m_X^2/2)(E_2 \omega - m_X^2/2)}{\omega^2 - m_X^2}, \quad (47)$$

and  $E_2 = \omega - E_1$  [127]. The two factors in the denominator of Eq. (46) are due to Pauli blocking of  $f$  and  $\bar{f}$  respectively. In particular,  $\mu_e/T \gg 1$  and so the second term reduces to unity, since the positron abundance

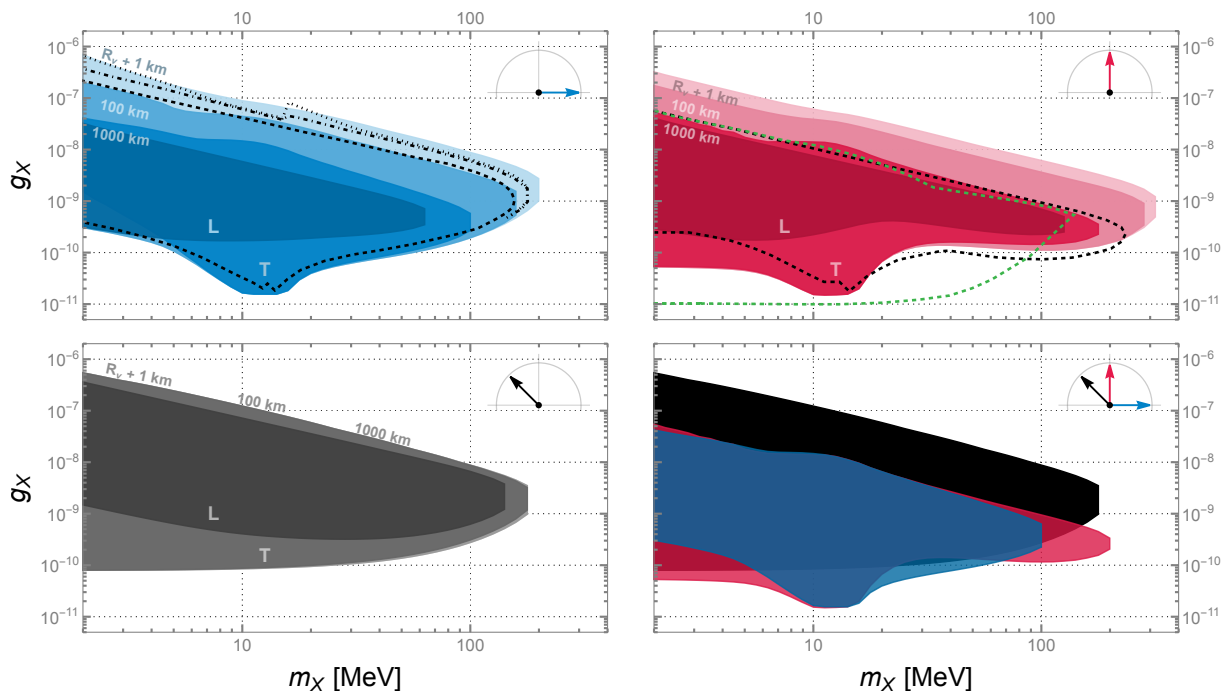


Figure 13: SN1987a constraints on (top left) dark photon limit  $\varphi = 0$ , (top right)  $B - L$  limit  $\varphi = \pi/2$ , (bottom left) chargephobic limit  $\varphi = 3\pi/4$ , and (bottom right) comparison between the aforementioned models for  $R_{\text{far}} = 1000$  km. The colors are chosen to match the compass inset. The shaded regions are excessive cooling constraints for three values of  $R_{\text{far}}$  derived on the SN model SFHo-18.8 which sets the most conservative constraints. For  $R_{\text{far}} = R_\nu + 1$  km and  $R_{\text{far}} = 100$  km we show the total constraint, whereas for  $R_{\text{far}} = 1000$  km we show the constraint set from the transverse and longitudinal polarizations individually to highlight their unique dynamics. The black dotted, dot-dashed, and dashed lines in the DP limit are constraints taken from [127] for the same values of  $R_{\text{far}}$ . The black dashed line in  $B - L$  limit is the constraint taken from [133] ( $R_{\text{far}} = 100$  km, and using a similar analysis to [127]) and is in tension with the constraint in [134] ( $R_{\text{far}} = 1000$  km) shown as a green dashed line.

is negligible in the PNS. On the other hand,  $\mu_{\nu_\tau} = 0$ , and so both terms contribute to blocking. In medium, the electrons also acquire an effective mass [145]

$$m_e^{\text{eff}} = \frac{m_{e,0}}{2} + \sqrt{\frac{m_{e,0}^2}{4} + \frac{\alpha}{2\pi} (\pi^2 T^2 + \mu_e^2)}. \quad (48)$$

This electron effective mass ranges between 0.6 – 11.3 MeV within  $R_\nu$  and the electron-positron decay channel is accessible only when  $m_X \geq 2m_e^{\text{eff}}$ . As a consequence, this channel can never be resonant since  $m_X < 2m_e^{\text{eff}}$  is always true when  $m_X^2 = \text{Re} \Pi_{\mathbf{L},\mathbf{T}}$ . It is unclear if previous results in the literature have considered this effect. Furthermore, electron-positron coalescence can be safely ignored everywhere since positrons are so rare in the PNS. On the other hand, neutrino-antineutrino coalescence is only important in the high mass region of the  $B - L$  case where the bremsstrahlung rate is suppressed. The PNS cooling constraints on the dark photon,  $B - L$ , and chargephobic cases are shown in Fig. 13.

In the dark photon limit, we compare our result to those in Ref. [127]. Here, we find excellent agreement in the lower bound where trapping dynamics are negligible and the produced  $X$  free streams out of the PNS. As for the upper bound, we find that our constraint is more sensitive to the  $R_{\text{far}}$  parameter than is

presented in Ref. [127]. Our result can be understood through the following simple argument. Beyond the neutrinosphere  $R_\nu \sim 25$  km, decays to  $e^+e^-$  are the main mode of absorption for a dark photon. Here, finite temperature effects are negligible and the decay rate in Eq. (46), at rest, simplifies to vacuum width in Eq. (25) or simply  $\Gamma_{e^+e^-} = g_X^2 m_X / 12\pi$ . A dark photon with energy  $\omega$  has a decay length of

$$\begin{aligned} 3L_{\text{dec}} &\approx (100 \text{ km}) \left( \frac{2.5 \times 10^{-9}}{g_X} \right)^2 \left( \frac{100 \text{ MeV}}{m_X} \right)^2 \left( \frac{\omega}{300 \text{ MeV}} \right) \\ &\approx (1000 \text{ km}) \left( \frac{8 \times 10^{-10}}{g_X} \right)^2 \left( \frac{100 \text{ MeV}}{m_X} \right)^2 \left( \frac{\omega}{300 \text{ MeV}} \right). \end{aligned} \quad (49)$$

These upper bound couplings  $g_X = 2.5 \times 10^{-9}$  ( $8 \times 10^{-10}$ ) at  $m_X = 100$  MeV are roughly what we get from the full numerical calculation for  $R_{\text{far}} = 100$  km (1000 km) in Fig. 13. Despite this discrepancy, our results and the ones presented in Ref. [127] share very similar qualitative features, especially for lower values of  $R_{\text{far}}$ .

In the  $B - L$  case and for  $m_X \gtrsim 20$  MeV, in-medium effects are negligible and the proton/neutron charges are degenerate resulting in quadrupole suppressed bremsstrahlung production and absorption rates. In this regime, neutrino coalescence is an important production mode. For  $m_X \lesssim 10$  MeV, finite temperature effects alter the proton effective charge but not for the neutron. This alleviates the quadrupole suppression in  $pn$  bremsstrahlung and the resulting production is two fold:  $pn$  bremsstrahlung off of neutrons which is  $m_X$  independent, and resonant production off of protons when  $m_X^2 = \text{Re} \Pi_{\mathbf{L}, \mathbf{T}}$ . The resonance around  $m_X \sim 10$  MeV in the lower bound of the  $B - L$  case is the same as that in the dark photon case; this is to be expected since the resonant production can be understood as a thermal bath of photons slowly transitioning to  $X$  independent of the details of the production process [143]. The upper bound is set considering the same effects with a small subtlety, the  $X \rightarrow \nu\bar{\nu}$  decays contribute to the optical depth only inside the PNS.

The lower bound in Ref. [134] (dashed green) is an order of magnitude stronger than ours. This discrepancy can be attributed to the way the bremsstrahlung rates are implemented. Ref. [134] used one-pion exchange, which is known to overestimate this rate as compared to nucleon-nucleon bremsstrahlung data. This overestimate was first shown in [132] and more recently in [146]. Following the argument in Appendix D of [146], we have used soft radiation approximation in deriving our bremsstrahlung rates Eq. (42). The lower bound in Ref. [133] (dashed black) for  $m_X \lesssim 10$  MeV was obtained by recasting the constraint on a vector boson coupling to just baryon number. However, in this process they did not take into account finite temperature effects lifting the bremsstrahlung quadrupole suppression, and hence arrived at a bound that is weaker than ours.

In the chargephobic case, the dominant production mode is  $pn$  bremsstrahlung off of neutrons which is both  $m_X$  independent and oblivious to finite temperature corrections. This rate sets the lower bound. The upper bound is set by inverse bremsstrahlung and decays into neutrinos inside the PNS. Furthermore, with the absence of the  $X \rightarrow e^+e^-$  decay channel, there are no efficient processes to facilitate the absorption of  $X$  outside the neutrinosphere. Consequently, the constraint is insensitive  $R_{\text{far}}$ . In terms of complexity, the chargephobic SN cooling constraint is the simplest of  $\varphi$  limits to derive. Nevertheless, this limit demonstrates the resilience of the SN cooling bound even when  $X$  has no couplings to electrons and protons.

### 5.2.2 Electromagnetic-Based Supernova Signals

When  $X \rightarrow e^+e^-$  is accessible, such as in the dark photon case, core collapse supernovae are capable of constraining  $X$  emission not only through cooling but also through several electromagnetic signatures labeled in Fig. 3 as LESNe, SN1987A  $\gamma$ , 511 keV line, and the fireball bounds PVO/GW170817 that were taken directly from Ref. [5].

The LESNe constraint arises by requiring that the energy deposited in the mantle, due to dark photon decays into  $e^+e^-$ , does not over-energize a sample of very low-energy Type II supernovae whose light curves imply explosion energies  $\lesssim 0.1$  Bethe [147,148]. Instead of decaying in the mantle, if the dark photons escape the progenitor and subsequently decays into  $e^+e^-$  pairs and photons outside the star, this would yield a detectable prompt MeV  $\gamma$ -ray burst signal; the absence of such signal in the Gamma-Ray Spectrometer (GRS) in SN1987A [149] sets the constraint labeled SN1987A  $\gamma$ . When these decays are frequent enough that the produced  $e^+e^-$  and photons become optically thick and thermalize, they form a fireball [150]. The Pioneer Venus Orbiter, which was sensitive to photons in the 0.2–2 MeV range consistent with the expected thermalized fireball spectrum, saw no significant  $\gamma$ -ray excess from SN1987A [151,152], thereby setting the constraint fireball (PVO). Similarly, for the compact binary merger GW170817 [153,154], X-ray observations from CALET/CGBM, Konus-Wind, and Insight-HXMT/HE place an upper limit on any GRB-like fireball emission [155], setting the constraint fireball (GW170817). The injection of positrons into the Milky Way through these decays can substantially enhance the diffuse  $\gamma$ -ray emission from the Galactic Center, which is tightly constrained by the INTEGRAL/SPI measurement of the 511 keV line [152,156].

We emphasize that we did not derive or recast these constraints, but rather simply adopted them directly from [5] for the dark photon case in Fig. 3. In the  $B-L$  case, we expect these constraints to remain but with some slight changes compared to the dark photon case. The difference can be characterized as follows: the  $X \rightarrow e^+e^-$  branching fraction in  $B-L$  is 40% smaller than in the DP case which reduces the signal from these constraints. Furthermore, important differences arise for the dominant production modes for  $X$  inside the PNS between the dark photon and  $B-L$  cases as discussed in Sec. 5.2.1. For example, an estimate of the lower bound of the LESNe constraint can be obtained by simply rescaling the lower bound of the cooling bound [5]. Hence, we expect the qualitative shape of the LESNe bound in the  $B-L$  to mimic that of the  $B-L$  cooling bound in Fig. 13. Recasting these constraints to  $B-L$ , and more general angles  $\varphi$ , requires a dedicated analysis that is beyond the scope of our work. We have taken the liberty to overlay these dark photon bounds from [5] as unlabeled light-shaded regions with dashed-lines in the  $B-L$  case shown in Fig. 3. This is merely illustrative of where one might expect these constraints to appear.

In the chargephobic vector boson case, virtually all of aforementioned constraints vanish due to the absence of  $X$  decays to charged leptons. The one potential exception to this is the LESNe constraint, since this extends up to a dark photon mass of about 500 MeV. For chargephobic masses  $m_X \gtrsim 200$  MeV, a very small branching fraction to charged leptons ( $\sim 10^{-6}$ ) develops from the renormalization-group evolution of the couplings. However, we suspect this is much too small to lead to a constraint on its own. Instead, for  $m_X > 2m_\pi$ , a chargephobic vector boson has an increasing branching fraction to  $\pi^+\pi^-$  (few to 20%), that may or may not affect the low energy supernova dynamics. While we have not shown a constraint in Fig. 4, we caution the reader that a small region of LESNe parameter space may be constrained, if the convolution of  $X$  decay and  $\pi$  decay leads to enough energy deposition. This is an interesting question, but beyond the scope of our work.

### 5.3 Neutrino Experiments

Neutrino experiments can be classified into four categories: neutrino-electron scattering (NES) experiments, coherent elastic neutrino-nucleus scattering (CE $\nu$ NS) experiments, experiments sensitive to collider neutrinos, and searches for invisible final states. The last of these relies on the assumption that the invisible final states can be treated as  $X$  decaying to neutrinos. NES and CE $\nu$ NS rates are mediated by the neutral and charged electroweak current interactions in the SM and obtain a new contribution through  $X$  exchange. The resulting enhancement in these rates can be detected in experiments sensitive to the NES and CE $\nu$ NS process, or conversely, the lack of signal can be interpreted as constraints on the  $\{m_X, g_X\}$  parameter space. In this section, we describe how  $X$  modifies each of these four classes of neutrino observables and outline the procedure used to translate them into constraints on the parameter space of a given  $\varphi$ .

In the SM, the electron-neutrino scattering amplitude consists of contributions from the charged and neutral currents. The SM differential cross section is

$$\left[ \frac{d\sigma}{dE_r}(\nu e^- \rightarrow \nu e^-) \right]_{\text{SM}} = \frac{2G_F^2 m_e}{\pi E_\nu^2} (a_1^2 E_\nu^2 + a_2^2 (E_\nu - E_r)^2 - a_1 a_2 m_e E_r), \quad (50)$$

where  $G_F$  is Fermi coupling constant,  $E_r$  is the recoil energy of the electron,  $E_\nu$  is the energy of incoming neutrino, and  $\{a_1, a_2\} = \sin^2 \theta_W \{1, 1\} + \frac{1}{2} A$  with  $A = \{1, 0\}$  for  $\nu_e e$ ,  $\{0, 1\}$  for  $\bar{\nu}_e e$ ,  $\{-1, 0\}$  for  $\nu_\alpha e$ , and  $\{0, -1\}$  for  $\bar{\nu}_\alpha e$ . The incoming neutrino must have a minimum energy of  $E_\nu^{\text{min}} = \frac{1}{2} (E_r + \sqrt{E_r^2 + 2E_r m_e})$  for a given recoil energy. The  $X$  contributions to NES and the interference between  $X$  exchange and the SM  $Z$  exchange are given by

$$\left[ \frac{d\sigma}{dE_r} \right]_X = \frac{g_X^4 m_e \sin^2 \varphi (\cos \varphi + \sin \varphi)^2}{4\pi E_\nu^2 (m_X^2 + 2m_e E_r)^2} (2E_\nu^2 + E_r^2 - 2E_\nu E_r - m_e E_r), \quad (51)$$

$$\left[ \frac{d\sigma}{dE_r} \right]_{\text{Int}} = \frac{g_X^2 G_F m_e \sin \varphi (\cos \varphi + \sin \varphi)}{2\sqrt{2}\pi E_\nu^2 (m_X^2 + 2m_e E_r)^2} (b_1(2E_\nu^2 - m_e E_r) + b_2(2E_r^2 - 4E_\nu E_r) + \beta), \quad (52)$$

where  $\beta = \sin^2 \theta_W (8E_\nu^2 - 8E_\nu E_r - 4m_e E_r + 4E_r^2)$ , and  $\{b_1, b_2\}$  are  $\{1, 0\}$  for  $\nu_e e$ ,  $\{1, 1\}$  for  $\bar{\nu}_e e$ ,  $\{-1, 0\}$  for  $\nu_\alpha e$ , and  $\{-1, -1\}$  for  $\bar{\nu}_\alpha e$  [42].

CE $\nu$ NS occurs when the momentum transfer between the neutrino and the nucleus is comparable to inverse of the nuclear radius. The differential cross section is

$$\left[ \frac{d\sigma}{dE_r} \right]_{\text{CE}\nu\text{NS}} = \frac{G_F^2 Q^2}{2\pi} M F^2(2ME_r) \left( 2 - M \frac{E_r}{E_\nu} - 2 \frac{E_r}{E_\nu} + \frac{E_r^2}{E_\nu^2} \right) \quad (53)$$

where  $M$  is the mass of the target nucleus and  $F(Q^2)$  is the nuclear form factor. In the SM, the effective charge is  $Q_{\text{SM}} = Z(\frac{1}{2} - 2\sin^2 \theta_W) - \frac{1}{2}N$  for a nucleus with  $Z$  protons and  $N$  neutrons. This charge is approximately  $Q_{\text{SM}} \sim -\frac{1}{2}N$  since the proton weak charge is quite small. When we include the contribution from  $X$ , the effective charge [157] becomes

$$Q_{\text{SM}+X}^2 = \left( Q_{\text{SM}} - [Z(\cos \varphi + \sin \varphi) + N \sin \varphi] \sin \varphi \frac{g_X^2}{2\sqrt{2}G_F(2ME_r + m_X^2)} \right)^2. \quad (54)$$

The CE $\nu$ NS related constraints are of particular interest in this paper as they are some of the few terrestrial experiment constraints that do not vanish in the chargephobic case.

### 5.3.1 Coherent elastic neutrino-nucleus scattering Experiments

The first observation of CE $\nu$ NS in 2017 by the COHERENT collaboration [158] spurred an extensive experimental program aimed at precision measurements of this process [159]. The CE $\nu$ NS rate is sensitive to modifications by BSM mediators coupled to neutrinos and nucleons and can be leveraged to set constraints on light vector mediators [157, 160–174]. In our mass range of interest, the current leading CE $\nu$ NS constraints on light vector mediators are placed by COHERENT [158, 175, 176] and CONUS+ [177]. These two constraints will be the focus of this section and will be treated as representative of the current CE $\nu$ NS constraint landscape for vector mediators of masses  $m_X > 1$  MeV.

The COHERENT collaboration has measured the CE $\nu$ NS process using two detectors, in a sodium doped CsI scintillator [158, 175] and in a liquid argon detector [176] with future plans expanding to more detector materials [178]. These detectors are exposed to the neutrino emissions from the Spallation Neutron Source (SNS) at Oak Ridge National Laboratory. In the CsI detector [175], the SM best fit prediction

models the observed data with a  $\chi^2/\text{dof} = 82.6/98$  and the observed data rejects the no-CE $\nu$ NS hypothesis at  $11.6\sigma$ . The  $X$  exchange contribution to the CE $\nu$ NS rate, Eq. (53), can spoil this agreement and lead to a constraint on the couplings of  $X$ . In this work, we focus on constraints obtained from the CsI data release only; the inclusion of argon data provides only slight improvements. We set constraints following the analysis in [44] using a Poissonian least-squares function over event counts in 9 energy and 11 timing bins.

Three neutrino flavors are produced in the SNS; prompt mono-energetic 30 MeV  $\nu_\mu$  produced via the decay of stopped  $\pi^+$ , and delayed  $\bar{\nu}_\mu$  and  $\nu_e$  produced from the decay of  $\mu^+$  which was in turn produced from pion decay. Neutrino fluxes  $d\Phi_\nu/dE_\nu$  and timing spectra  $f_T^\nu(t)$  can be found in [179]. For a given nucleus  $\mathcal{N}$ , the expected number of events per energy  $i$  and time  $j$  bin is

$$N_{i,j}^{\text{CE}\nu\text{NS}, \mathcal{N}} = \sum_{\nu=\nu_e, \nu_\mu, \bar{\nu}_\mu} N_{\text{target}} \int_{t^j}^{t^{j+1}} dt f_T^\nu(t, \alpha_6) \epsilon_T(t) \int_{E_{\text{nr}}^j}^{E_{\text{nr}}^{j+1}} dE_{\text{nr}} \epsilon_E(E_{\text{nr}}, \alpha_7) \times \int_0^{E'_{\text{nr}}^{\text{max}}} dE'_{\text{nr}} P(E_{\text{nr}}, E'_{\text{nr}}) \int_{E_\nu^{\text{min}}(E'_{\text{nr}})}^{E_\nu^{\text{max}}} dE_\nu \frac{d\Phi_\nu}{dE_\nu}(E_\nu) \frac{d\sigma_{\nu\mathcal{N}}}{dE_r}(E_\nu, E'_{\text{nr}}, \alpha_4), \quad (55)$$

where  $N_{\text{target}}$  is the number of target atoms in the detector,  $\epsilon_T(E_E)$  are the time (energy)-dependent detector efficiencies, and  $E_{\text{nr}}$  and  $E'_{\text{nr}}$  are the reconstructed and true nuclear recoil energy respectively related via the energy resolution function  $P(E_{\text{nr}}, E'_{\text{nr}})$ . The first two integrals are bounded by bin edges, the third integral by  $E_{\text{nr}}^{\text{max}} = 2(E_\nu^{\text{max}})^2/m_N$ , and the fourth by  $E_\nu^{\text{min}} \simeq \sqrt{m_N E'_{\text{nr}}/2}$  and  $E_\nu^{\text{max}} = m_\mu/2$ . The total binned number of events is given by  $N_{i,j}^{\text{CE}\nu\text{NS}} = N_{i,j}^{\text{CE}\nu\text{NS}, \text{Cs}} + N_{i,j}^{\text{CE}\nu\text{NS}, \text{I}}$ .

The analysis is then performed using a Poissonian least-squares function

$$\chi_{\text{CsI}}^2 = 2 \sum_{i=1}^9 \sum_{j=1}^{11} \left[ N_{\text{th}}^{\text{CsI}} - N_{ij}^{\text{exp}} + N_{ij}^{\text{exp}} \ln \left( \frac{N_{ij}^{\text{exp}}}{N_{\text{th}}^{\text{CsI}}} \right) \right] + \sum_{k=0}^4 \left( \frac{\alpha_k}{\sigma_k} \right)^2, \quad (56)$$

$$N_{\text{th}}^{\text{CsI}, \text{CE}\nu\text{NS}} = (1 + \alpha_0) N_{i,j}^{\text{CE}\nu\text{NS}}(\alpha_4, \alpha_6, \alpha_7) + (1 + \alpha_1) N_{i,j}^{\text{BRN}}(\alpha_6) + (1 + \alpha_2) N_{i,j}^{\text{NIN}}(\alpha_6) + (1 + \alpha_3) N_{i,j}^{\text{SSB}}. \quad (57)$$

We use the CsI unbinned data events provided by the COHERENT collaboration [175] to extract the measured binned event number  $N_{ij}^{\text{exp}}$  and to estimate the number of events  $N_{i,j}^{\text{SSB}}$  from the beam-uncorrelated steady-state background (SSB). We also include the prompt beam-related neutron (BRN) and neutrino-induced neutron (NIN) events. The nuisance parameters are as follows:  $\alpha_0$  encodes the efficiency and flux uncertainties,  $\alpha_1$  ( $\alpha_1$ ) [ $\alpha_3$ ] correspond to the BRN (NIN) [SSB] uncertainties,  $\alpha_4$  modifies the nuclear form factor  $R_A = 1.23A^{1/3}(1 + \alpha_4)$ ,  $\alpha_6$  accommodates the uncertainty in beam timing ( $\pm 250$  ns), and  $\alpha_7$  allows for deviations in the energy-dependent detector efficiency ( $\epsilon_E[x + \alpha_7]$  with  $\alpha_7$  allowed to vary in the range  $[-1, 1] \times \text{PE}$ )<sup>13</sup>. Finally, the uncertainties  $\sigma_i$  associated with nuisance parameter  $\alpha_i$  are given by  $\{\alpha_0, \dots, \alpha_4\} = \{11, 25, 35, 2.1, 5, 3.8\} \%$ .

The CONUS+ collaboration recently achieved the first clear observation of reactor neutrino CE $\nu$ NS [177], with earlier evidence from Dresden-II [180] and prior CONUS runs [168]. Furthermore, many reactor-based experiments aim to lower detection thresholds and in doing so enhance sensitivity to light mediators; such as TEXONO [181], NUCLEUS [182], RICOCHET [183], and CONNIE [184]. Reactor-based CE $\nu$ NS experiments probe neutrino energies of a few MeV, providing leading CE $\nu$ NS sensitivity to light vector mediators below roughly  $m_X \lesssim 10$  MeV. This mass range is dominated by  $\Delta N_{\text{eff}}$  constraints discussed in Section 5.1, however, the CONUS+ constraint still rules out a novel region of parameter space. Similar to the COHERENT analysis, we follow the procedure laid out in [172, 173] to place constraints from the CONUS+ data release [177]. Note, the combined analysis of CONUS+, TEXONO, and COHERENT data [185] result

<sup>13</sup>The nuisance parameter  $\alpha_5$  is associated with the quenching factor. This parameter can be neglected in the region of the parameter space ( $m_X > 1$  MeV) where electron scattering does not play an important role. We drop this parameter but keep the numbering convention to match [175].

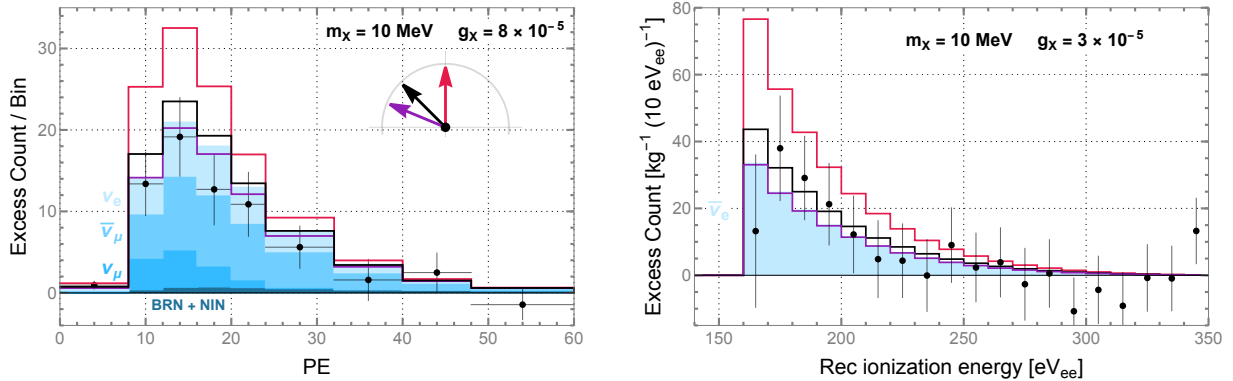


Figure 14: (Left) COHERENT CsI detector data residual over SSB background [175]. (Right) CONUS+ excess counts from three HPGGe detectors (C2, C3, C5) [177]. The axes are chosen to match those in the original plots in the data release. The shaded steps represent the  $\nu_i$  SM CE $\nu$ NS prediction and the BRN and NIN backgrounds. The lines with no filling correspond to total excess count (SM + BSM) when  $X$  with charge assignment of  $B-L$ ,  $\varphi = 3\pi/4$ , and  $\varphi = \pi - \tan^{-1}(55/133)$  are considered. In all BSM cases, we have  $m_X = 10$  MeV with (right)  $g_X = 8 \times 10^{-5}$  and (left)  $g_X = 3 \times 10^{-5}$ .

in a slightly stronger bound; this is beyond the scope of our analysis and we do not attempt to replicate these results.

An example of the excess count calculation for  $B-L$ , chargephobic, and nucleophobic cases in COHERENT and CONUS+ detectors is shown in Fig. 14. The nucleophobic case is chosen such that the effective charge of a cesium nucleus vanishes. This specific choice is arbitrary, but captures the typical extent to which CE $\nu$ NS experiment sensitivity to  $X$  is suppressed. The nucleus charge scales as  $A$  in  $B-L$ ,  $\sim N$  in the SM and the chargephobic case, and  $(N - (N_{Cs}/Z_{Cs})Z)$  in the nucleophobic case. This explains the extent to which each model contributes to the excess count as is evident in the BSM excess (BSM - SM) in both experiments. The excess count does not vanish in the nucleophobic case since there are couplings to Ge and I nuclei. These couplings are, however, suppressed:  $\{x_{Cs}, x_I, x_{Ge}\}_{\mathcal{C}_s} = \{0, -0.4, -2\}$  when compared to  $\{x_{Cs}, x_I, x_{Ge}, x_{Ar}\}_{B-L} = \{133, 127, 72, 40\}$  for  $B-L$ . Furthermore, the negative nucleus charge in the nucleophobic case interferes destructively with the SM nucleus charge in Eq. (54). This can lead to excess counts lower than those in the SM as shown in Fig. 14. Finally, the COHERENT and CONUS+ constraints are shown in Fig. 15 where we emphasize constraints from the neutrino experiments discussed in Sec. 5.3. The aforementioned interference effect can be also be seen through the unconstrained band in the COHERENT and CONUS+ nucleophobic bounds.

Finally, to illustrate the potential of next-generation CE $\nu$ NS experiments, we show the recasted COH-CryoCsI II sensitivity [186] in Fig. 4 for the chargephobic limit. Here, the combination of a larger cryogenic CsI target, a lower nuclear recoil threshold, and an increased SNS beam power allows this setup to substantially improve upon current CE $\nu$ NS bounds.

### 5.3.2 Neutrino-electron Scattering Experiments

Experiments in this category are sensitive to deviations from the SM NES rate via the  $X$  mediated NES channel. In our parameter space, the leading NES experimental constraints are set by Borexino Phase-II [187–192], TEXONO [193], and CHARM-II [194, 195]. TEXONO is a CsI(Tl) scintillating crystal array measuring  $\bar{\nu}_e e^-$  elastic scattering with the  $\bar{\nu}_e$  produced at the Kuo-Sheng Nuclear power station. The

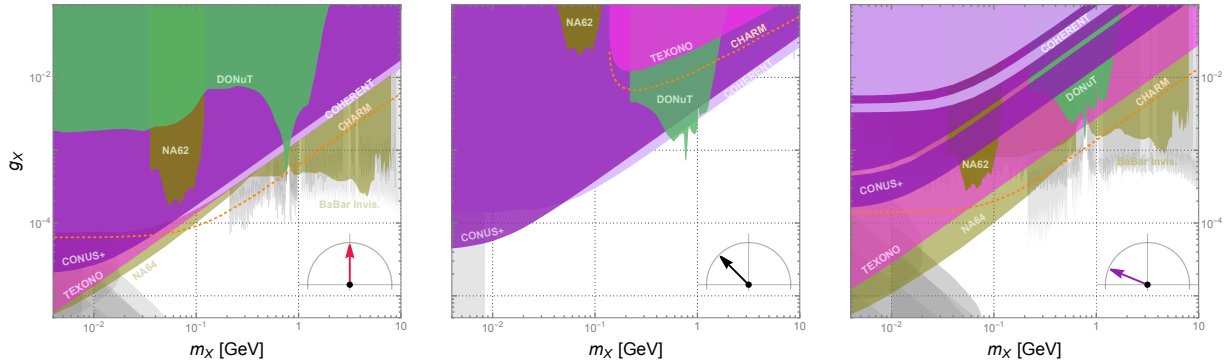


Figure 15: Constraints on (left)  $B - L$  ( $\varphi = \pi/2$ ), (middle) chargephobic ( $\varphi = 3\pi/4$ ), and (right) nucleophobic [ $\varphi = \pi - \tan^{-1}(55/133)$ ] limits with a focus on the neutrino constraints discussed in Sec. 5.3. Other constraints in Fig. 3 are displayed in gray.

detector is exposed to an average  $\bar{\nu}_e$  flux of  $6.4 \times 10^{12} \text{ cm}^{-2} \text{ s}^{-1}$  with standard reactor  $\bar{\nu}_e$  spectrum [196]. We derive the constraint from TEXONO following the analysis in [42, 43]. Borexino presents a comprehensive measurement of the solar neutrino spectrum from the pp chain in the energy range of (0.19 – 16) MeV. This data set in conjunction with standard solar model were used in [10, 42, 197] to set a constraint on the  $B - L$  case. We adopt this constraint, without reproducing it, for the  $B - L$  case and recast it using the appropriate charge scaling. For  $m_X \gtrsim 3$  MeV, TEXONO is the leading NES constraint whereas Borexino leads in the region below where the  $\Delta N_{\text{eff}}$  constraint dominates. Hence, we focus on TEXONO constraints when presenting our analysis in Fig. 15. As for CHARM-II, it was pointed out in [2] that the exact neutrino fluxes seem to be unknown in the experimental publication. This casts some doubt on the validity of neutrino rate calculation in [42, 43]. Following [2], we show the CHARM bound as a dashed line to remind the reader of this subtlety and we assume that the correct neutrino flux was used for the bound calculation.

### 5.3.3 Invisible Searches

Invisible searches assume that the dark photon decays predominantly into a dark sector state  $\chi$  via  $X \rightarrow \chi\bar{\chi}$ , which occurs when  $m_X > 2m_\chi$  and the coupling  $g_X$  is sufficiently small that visible decays are subdominant [198–205]. The experimental signature is a visible SM particle accompanied by large missing energy and momentum. The same signature arises if  $X$  instead decays mainly to neutrinos,  $X \rightarrow \nu\bar{\nu}$ . As a result, existing invisible searches can be recast using the neutrino branching fraction for a given  $\varphi$ .<sup>14</sup>

In our analysis, we consider three invisible searches to provide constraints on  $X$ . The BaBar invisible search uses  $53 \text{ fb}^{-1}$  of  $e^+e^-$  collision data to search for a single high-energy photon and a large missing momentum and energy via the process  $e^+e^- \rightarrow \gamma X$  followed by  $X$  invisible decay [200]. The invisible search in NA64 uses an electron beam dump setup to look for single electron events with large missing energy from  $eZ \rightarrow eZX$  production followed by invisible  $X$  decay [205]. The NA62 invisible search uses the process  $K^+ \rightarrow \pi^+\pi^0$ ,  $\pi^0 \rightarrow \gamma X$  followed by an invisible decay of  $X$  [202]. BaBar and NA64 set leading constraints on  $B - L$  and nucleophobic cases as shown in Fig. 15. NA62 is one of the few constraints that remain in the chargephobic case as it does not rely on a charged lepton coupling for either production or detection. The constraint is nonetheless significantly weakened due to the  $\pi^0 \rightarrow \gamma X$  suppression in the chargephobic case as seen in Fig. 6.

<sup>14</sup>At the  $J/\psi$ ,  $\psi(2S)$ ,  $\psi(3770)$ , and  $\Upsilon(1S) - \Upsilon(4S)$  resonances, the  $X \rightarrow \nu\bar{\nu}$  branching ratio can be non-trivially altered from the one reported in Fig. 7. In these narrow regions, the invisible search constraints can lose sensitivity or even vanish. We have not included this effect and report the invisible search constraints as they are traditionally displayed in the literature [1, 2].

### 5.3.4 Collider Neutrinos

Collider neutrino experiments [206–209] are sensitive to new physics that produces an additional forward flux of tau neutrinos on top of the SM  $\nu_\tau$  component from  $D_s$  and other heavy meson decays. In our model,  $X$  is produced via bremsstrahlung or meson decays and can subsequently decay as  $X \rightarrow \nu_\tau \bar{\nu}_\tau$ , thereby enhancing the flux incident on these detectors. To illustrate this, we use two representative experiments: the fixed target DONuT experiment at Fermilab as a current constraint and the forward LHC detector FASER $\nu$  for future projected sensitivity. In the  $B-L$  case, we simply adopt these constraint from [210]. We recast this constraint using Eq. (30) and the LHCb production fractions in Figure 11 from [1] for masses  $m_X > 0.2$  GeV. We do not recast or show the constraints for  $m_X < 0.2$  GeV in the chargephobic and nucleophobic cases in Fig. 15; this region of parameter space is already well covered by NES and CE $\nu$ NS experiments.

There are several qualitative differences in the shape of the DONuT constraint between the  $B-L$ , chargephobic, and nucleophobic cases. For  $B-L$ , the resonance near  $m_X \sim 0.8$  GeV is driven by  $\omega-X$  mixing, while the  $\rho-X$  production mode is absent. In the chargephobic case, the  $\rho-X$  channel is active, leading to a broader resonance, while the  $\omega-X$  mixing is reduced by a factor of 8, as shown in Fig. 5. In the nucleophobic case,  $\omega-X$  mixing is highly suppressed and so the resonance reach is reduced. The branching fraction to tau neutrinos is also affected by the width of the hadronic resonance; see the  $B-L$  and chargephobic cases in Fig. 7. The combination of these effects accounts for the shape of the DONuT constraint near the resonance. In our analysis, we used the LHCb production fractions [1] to determine the relative rates, however, they are not provided near the  $\omega$  resonance. We have used interpolations in the mass ranges where no results were shown in [1], and so our recasted DONuT resonant behavior in this mass range should be taken as approximate. A robust bound near the  $\omega$  resonance requires a dedicated reanalysis of Ref. [210] taking into account the production modes in Ref. [211], but this is beyond the scope of this work.

## 5.4 Beam Dump & Fixed Target Experiments

Electron and proton beam dump (BD) experiments direct high intensity beams onto thick targets, which can produce  $X$  via bremsstrahlung (in  $eBD$  &  $pBD$ ) or meson decay/mixing (in  $pBD$ ). A long-lived  $X$  vector boson that is produced in this collision and survives the shielding can decay in a downstream decay volume, with its decay products registered in a detector located anywhere from meters to hundreds of meters away. Decay modes of  $X$  that lead to visible signals are typically  $X \rightarrow \ell^+ \ell^-$  and in particular  $X \rightarrow e^+ e^-$ , which appears as an electromagnetic shower. Accordingly, constraints set by these beam dump experiments vanish in the chargephobic case. A notable exception is the projected sensitivity of SHiP [212–214], whose ability to fully reconstruct displaced  $X$  decay vertices extends the signal reach to the broad range of hadronic decays in Fig. 8. This makes SHiP uniquely positioned to probe the chargephobic parameter space in the future.

In electron beam dumps, the production cross section of  $X$  can be approximated using the Weizsäcker Williams approximation where the target nuclei  $\mathcal{N}$  are replaced by an effective flux of photons [215]. The bremsstrahlung process is simplified to semi-Compton scattering,  $e\gamma \rightarrow eX$ , and is given to a good approximation by

$$\frac{d\sigma_X}{dr_e} \simeq \frac{\alpha^2}{\pi} g_X^2 (1 + \sin 2\varphi) \xi \sqrt{1 - \frac{m_X^2}{E_e^2} \frac{1 - r_e + \frac{r_e^2}{3}}{m_X^2 \frac{1-r_e}{xre} + m_X^2 r_e}}, \quad (58)$$

where  $r_e \equiv E_X/E_e$  is the fraction of electron beam's energy carried by  $X$  and  $\xi(E_e, m_X, Z, A)$  is the effective photon flux [129]. The electron beam can interact with the shielding material which diminishes its energy from initial beam energy  $E_0$  to  $E_e$ . The energy distribution of the electron beam as function of penetration

depth  $t$  [216] is

$$I_e(E_0, E_e, t) = \frac{1}{E_0} \frac{\ln\left(\frac{E_0}{E_e}\right)^{\frac{4}{3}t-1}}{\Gamma\left(\frac{4}{3}t\right)}. \quad (59)$$

The expected number of  $e^+e^-$  events in the detector for an electron beam of  $N_e$  electrons and energy  $E_0$  is

$$N \simeq N_e \frac{N_0 X_0}{A} \int_{m_X}^{E_0 - m_e} dE_X \int_{E_X + m_e}^{E_0} dE_e \int_0^{T_{\text{sh}}} dt_{\text{sh}} \left[ I_e(E_0, E_e, t_{\text{sh}}) \frac{1}{E_e} \frac{d\sigma_X}{dr_e} e^{-L_{\text{sh}}/l_X} \left(1 - e^{-L_{\text{dec}}/l_X}\right) \right] \text{Br}_{e^+e^-}. \quad (60)$$

Here  $N_0$  is Avogadro's number,  $X_0$  and  $\rho_{\text{sh}}$  are the unit radiation length and density of target material,  $A$  is mass number of target,  $T_{\text{sh}} = L_{\text{sh}}\rho_{\text{sh}}/X_0$ , and  $l_X = \beta\gamma\tau$  is the  $X$  decay length in the lab frame. The exponential terms ensure that  $X$  must decay after the shielding but before or within the detector where  $L_{\text{dec}}$  is the length of the decay region. This term is obtained by integrating the differential decay probability  $dP(l)/dl = e^{-l/l_X}/l_X$  from  $L_{\text{sh}}$  and  $L_{\text{tot}} = L_{\text{sh}} + L_{\text{dec}}$ . A detailed explanation of computing this integral is provided in the appendix of [217]. Constraints are placed by excluding regions of the  $\{m_X, g_X\}$  parameter space that result in excess events over the 95% C.L. upper limit of the number of observed events in each experiment. Using this framework, we derive constraints from Orsay [218], KEK [219], NA64 [220, 221], E137 [215], E141 [222], and E774 [223].

In proton beam dumps,  $X$  can be produced either via bremsstrahlung or through the decays of mesons ( $\pi^0, \eta, \eta'$ ) produced in the target. The bremsstrahlung process is analogous to the electron beam dump case, with the effective cross section for proton collision determined experimentally [224]. Constraints on a dark photon have been derived in [225–227] on U70 [228], NOMAD [229], PS191 [230], CHARM [231], LSND [2],  $\nu\text{Cal}$  [231], and FASER [37, 38]. In our analysis, we recast these dark photon constraints to our model using Eq. (30) and the methodology developed in [1]. The same procedure is applied to fixed target experiments: APEX [232], A1/MAMI [233, 234], HPS [235, 236], and NA48/2 [237]. These experiments probe  $m_X < 1$  GeV and rely on  $X \rightarrow e^+e^-$  decay as their signal channel. In this mass range, the RGE induced electron charge in the chargephobic limit is at most  $x_e \sim \mathcal{O}(10^{-3})$ , so both the bremsstrahlung production channel and  $e^+e^-$  decay are suppressed by  $x_e^2$ . As a result, the expected event yields in the chargephobic case are negligible and so the constraints vanish.

For the projected SHiP sensitivity, we recast the dark photon reach from Ref. [213] using the LHCb production fractions [1]. In the chargephobic case, the charged lepton decays are negligible and the SHiP sensitivity is effectively determined by the hadronic modes. Therefore, we find that SHiP gains sensitivity starting at  $m_X \simeq 2m_\pi$ , where the  $X \rightarrow \pi^+\pi^-$  channel becomes kinematically accessible. For larger masses, multi-pion and kaon final states also contribute to detection signal, see Fig. 8. Above the pion threshold, a dominant fraction of the production and detection channels remains unsuppressed, so SHiP retains substantial reach in the chargephobic limit. Thus, SHiP is a uniquely powerful probe of the chargephobic case, complementing the  $\text{CE}\nu\text{NS}$  constraints and providing outstanding opportunities for future discovery.

As a final remark, recent studies of neutron initiated production at FASER/FASER2 show that a “neutron beam dump” can enhance sensitivity to the protophobic model [211, 238]. These results still rely on  $X \rightarrow \ell^+\ell^-$  decays for detection and as such do not set constraints on the chargephobic model.

## 5.5 Collider Experiments

In this section, we summarize the constraints obtained from collider searches at LHCb [239], CMS [55], KLOE [39, 240–242], BESIII [243], and BaBar [244]. We recast these bounds to our general  $\varphi$  model using

Eq. (30), following the production, decay, and experimental efficiency rescaling procedures outlined in [1]. Note that there are projections [245, 246] for the improvements in the sensitivity to the dark photon by the LHCb experiment, however we do not anticipate the large improvements in the dark photon parameter space  $m_{A'} \lesssim 500$  MeV to extend to the chargephobic vector boson case given the very small branching fraction to charged leptons.

The LHCb dark photon search [239] considers both prompt and displaced  $X \rightarrow \mu^+\mu^-$  decays in  $pp$  collisions at 13 TeV using  $1.6 \text{ fb}^{-1}$  of data. Because the analysis relies on the dimuon final state, the constraint weakens considerably on the chargephobic case. The constraint does not vanish, however, due to the loop induced charged lepton coupling  $x_e \sim \mathcal{O}(10^{-2})$  at larger masses  $m_X \gtrsim 1$  GeV that is generated by the RGE running as described in App. B. The relevant production modes include meson decays ( $\eta \rightarrow X\gamma$ ,  $\omega \rightarrow X\pi^0$ ), vector meson mixing ( $\omega \rightarrow X$ ,  $\rho \rightarrow X$ ,  $\phi \rightarrow X$ ), and Drell–Yan ( $q\bar{q} \rightarrow X$ ). The dominant production modes vary across the  $m_X$  mass range. Consequently, each  $\varphi$  value can suppress/remove some but not all production mechanisms. For  $m_X \lesssim 0.4$  GeV and  $m_X \gtrsim 1$  GeV, the leading channels are  $\eta \rightarrow X\gamma$  ( $\sim 65\%$ ) and  $u\bar{u} \rightarrow X$  ( $\sim 70\%$ ) which are suppressed/vanish at  $\varphi = \pi - \tan^{-1} 2$ . In the intermediate region  $0.4 - 0.9$  GeV, the leading channels are  $\omega \rightarrow X\pi^0$  ( $\sim 45\%$ ) and  $\rho \rightarrow X$  mixing ( $\sim 65\%$ ) both of which vanish for the  $B - L$  case. A similar analysis is applied to the CMS constraint [55].

The KLOE experiment conducted several searches for dark photon using data taken at DAΦNE with  $\sqrt{s} \simeq 1020$  MeV [39, 240–242]. These analyses considered the process  $e^+e^- \rightarrow \gamma X$  with  $X \rightarrow e^+e^-$ ,  $X \rightarrow \mu^+\mu^-$ , and  $X \rightarrow \pi^+\pi^-$ , as well as the decay chain  $\phi \rightarrow X\eta$  with  $X \rightarrow e^+e^-$ . In both cases, constraints on the chargephobic parameter space are highly suppressed due to the  $x_e^2$  suppression on the production and/or the decay.

Finally, the BaBar dark photon search [244] considered the process  $e^+e^- \rightarrow \gamma X$  with  $X \rightarrow e^+e^-$  and  $X \rightarrow \mu^+\mu^-$  primarily at the  $\Upsilon(4S)$  but also at  $\Upsilon(3S)$  &  $\Upsilon(2S)$  resonances. The reported constraint spans  $0.02 \text{ GeV} < m_X < 10.2 \text{ GeV}$  and has a sensitivity scaling as  $x_e^4$  since both the production and decay proceed through electron coupling. Consequently, the bound vanishes for the chargephobic case even after including small RGE induced couplings. A similar suppression applies to BESIII [243].

## 5.6 Precision Constraints

Precision measurements of SM observables provide powerful probes of new light vectors, since even weak couplings can shift well measured quantities away from their SM predictions. In this section, we discuss the constraints set from the electron/muon anomalous magnetic moments and electroweak precision tests. We also comment on the sensitivity of the proposed REDTOP experiment [247].

We first consider the one-loop contribution of  $X$  to the anomalous magnetic moments  $(g - 2)_\ell$  of the electron and muon,  $a_\ell^X$ , computed following Ref. [248]. The  $(g - 2)_e$  constraint is set such that the effective shift of the fine structure constant,  $\Delta\alpha = 2\pi a_e^X$ , does not exceed 1 ppb in line with the current  $\mathcal{O}(1 \text{ ppb})$  spread among the most precise determinations of  $\alpha$  [249–251]; previous constraints were set at 15 ppb [248] based on older  $\alpha$  determinations including Ref. [252]. For the  $(g - 2)_\mu$ , we use the updated SM prediction and final world average measurement of  $a_\mu$  [253] and require  $a_\mu^X < (a_\mu^{\text{exp}} - a_\mu^{\text{SM}} + 2\sigma)$  where  $\sigma$  is the quoted uncertainty on this difference. These constraints are relevant in the dark photon case where they cover the region of parameter space where collider constraints are not sensitive due to masking out meson resonances. For other  $\varphi$ , these constraints become subdominant to NES and CE $\nu$ NS constraints. In particular, in chargephobic case, the absence of couplings to charged leptons when  $m_X \lesssim 200$  MeV combined with the very small renormalization group induced couplings above this scale imply that both  $(g - 2)_{e,\mu}$  are negligible throughout the parameter space.

At low energies,  $X$  couples to the electromagnetic current, while at electroweak scales, this becomes a

coupling to the hypercharge current. This causes a mass mixing between  $X$  and the  $Z$  boson. This mixing shifts the physical  $Z$  mass and its couplings to fermions, leading to constraints from electroweak precision observables. For a dark photon, constraints were derived in Refs. [254–256] by performing global fits to LEP, SLC, Tevatron, and LHC electroweak precision data. In our analysis, we adopt the 95% C.L. exclusion curve based on the PDG world average value of  $m_W$  (solid blue curve in Fig. 1 of Ref. [256]) in the dark photon limit and recast this constraint for arbitrary  $\varphi$  using the relation  $\epsilon e = g_X \cos \varphi$ . We show this constraint, labeled EWP, in Figs. 3-4.

Finally, REDTOP is a proposed high-intensity  $\eta/\eta'$  factory that aims to collect a data sample of order  $10^{14}$   $\eta$  and  $10^{12}$   $\eta'$  mesons to study very rare decays and to search for BSM physics in the MeV-GeV range [247, 257]. In our case,  $X$  can be produced at REDTOP via  $\eta, \eta' \rightarrow \gamma X$  and the detector is sensitive to the following subsequent decays  $X \rightarrow e^+e^-$ ,  $X \rightarrow \mu^+\mu^-$ , and  $X \rightarrow \pi^+\pi^-$ . In particular, the hadronic channel  $X \rightarrow \pi^+\pi^-$  remains open in the chargephobic limit. In Fig. 4, we show the recasted projected REDTOP sensitivity with  $10^{18}$  protons on target (solid black in Fig. 39 of Ref. [258]).

## 6 Discussion

There is a huge effort exploring the space of possibilities for light vector boson mediators. In this paper, we have demonstrated that when a vector boson  $X^\mu$  couples to a specific “chargephobic” linear combination of the electromagnetic and  $B - L$  currents, there are dramatic changes to the constraints within the  $\{m_X, g_X\}$  parameter space. The changes arise because a chargephobic vector boson does not have (tree-level) couplings to electrons and protons. The resulting sensitivity of most beam dump and collider based experiments is negligible or highly suppressed because they rely on production from proton or electron beams and/or they rely on the decays to leptons that produce an easily visible signal. Two classes of constraints on  $X^\mu$  remain largely unaffected when the couplings to charged leptons and singly-charged baryons are absent: supernova cooling constraints and the constraints on the contributions to  $\Delta N_{\text{eff}}$  in the early universe, due to the nonzero couplings to neutrinos and neutrons.

It is interesting to compare the constraints on the chargephobic case to those on other combinations of currents that are also more weakly constrained. Two specific examples are:  $B - 3L_\tau$  and baryon number by itself. A vector boson coupled to  $B - 3L_\tau$  also has highly suppressed constraints (e.g. [22, 26]) from beam dump experiments and collider experiments due to the absence of interactions with the first two generations of charged leptons. Moreover, because  $B - 3L_\tau$  does not couple to electron or muon neutrinos, it is also unconstrained by COHERENT experiment results on neutrino-nucleus scattering. However, as emphasized in Refs. [22, 25]  $B - 3L_\tau$  is strongly constrained by the neutrino flavor-dependent non-standard interactions (NSI) that affect neutrino oscillations. These turn out to be stronger than the constraints from COHERENT neutrino-nucleus scattering, and so for much of the parameter space we find that the chargephobic limit is *more weakly constrained* than  $B - 3L_\tau$ .

A vector boson coupled to just baryon number is problematic, because baryon number is a non-conserved (anomalous) current in the SM. Refs. [29, 30] examined this case in detail, finding that rare meson decay mediated by the anomalous interaction set several constraints on the parameter space that lead to constraints that are more restrictive than those on the chargephobic case for  $m_X \lesssim 200$  MeV and  $600$  MeV  $\lesssim m_X \lesssim 4$  GeV. In other ranges the two cases are similar, and for larger  $m_X$ , chargephobic is more constrained due to LHCb searches that are (re-)activated due to the small renormalization group-generated couplings to the charged leptons (see App. B) as well as from electroweak precision constraints.

Several open questions remain: one is the prospects for gaining *improved* sensitivity to the chargephobic case. In Fig. 4 we present a rough guide to the increased sensitivities for a handful of experiments, but there are no doubt more possibilities that are worth exploring. One of our primary goals in the paper is to point

out that relying on a charged lepton decay of a light gauge boson can be disastrous for an experiment’s sensitivity. SHiP [207, 209, 213] will be able to probe new regions of the chargephobic parameter space due to the significantly improved detector capabilities that enable it to be sensitive to the hadronic decays of  $X$  when  $m_X \gtrsim 300$  MeV. Also, the proposed REDTOP experiment [247] can gain sensitivity to chargephobic couplings due to rare decays of  $\eta, \eta'$  mesons to vector bosons.

There are also detailed questions one can ask regarding whether there are additional production or decay modes that experiments could be sensitive to. The production of vector bosons in beam dump experiments occurs through bremsstrahlung “coherently” off the proton beam. However, one might expect there is also a rate for incoherent contribution (emission from the quarks)<sup>15</sup>, that is either form-factor suppressed or suppressed by the degree of inelastic scattering. We also anticipate a slightly improved set of constraints on the chargephobic case by considering the absence of high energy neutrino events from SN1987A, as was found for the case of  $L_\mu - L_\tau$  [259].

It is also worth commenting on the very interesting ensemble of bounds on a dark photon arising from its production in supernovae and decay into  $e^+e^-$ , leading to significant observable signals [5]. Most of these constraints do not apply to the chargephobic vector boson because of the dominance of the decay  $X \rightarrow \nu\bar{\nu}$  throughout the mass range that these constraints apply. One needs to be a bit more careful with the low energy supernova constraint (LESNe), since for the dark photon case this extends to  $m_{A'} \sim 500$  MeV. A chargephobic vector boson with mass  $m_X > 2m_\pi$  has an increasing branching fraction to  $\pi^+\pi^-$  (few to 20%), that may or may not affect the low energy supernova dynamics. It would be interesting to determine if a small region of chargephobic parameter space could be constrained, though it requires the convolution of  $X$  decay and  $\pi$  decay to lead to enough energy deposition to disrupt the supernova explosions. This is an interesting question, but beyond the scope of our work.

Finally, while we have focused much of the paper on the specific case of chargephobic,  $\varphi = 3\pi/4$ , our analysis pipeline allows us to consider any angle. As we have pointed out in the paper, some angles have suppressed rates for specific processes where mixing with a particular QCD vector resonance does not occur. We have also pointed out the “nucleophobic” (a related idea to “xenophobic” in Ref. [36]) case where  $\varphi = \pi - \tan^{-1}(Z_{\mathcal{N}}/A_{\mathcal{N}})$ , and the coherent interaction of the vector boson with the nucleus vanishes for a specific isotope. Our interest in this particular case was to explore how much weaker the constraints from COHERENT and other neutrino-nucleus scattering experiments can be. Of course when we consider mixing angle away from the chargephobic limit, constraints from neutrino-electron scattering reappear, as well the ensemble of beam dump and collider experiments, as we show in Fig. 15 (right). Nevertheless, there could be a host of interesting phenomenology when a nucleophobic gauge boson is fused with a model of dark matter – there could be an interesting parameter space where dark matter - electron scattering experiments could have sensitivity in regions of parameter space what would otherwise have been considered ruled out by nuclear recoil (or Migdal) scattering.

## Acknowledgements

We thank Hans-Thomas Janka and Daniel Kresse for providing access to the Garching supernova model data used in this analysis. We thank Andrea Caputo, Ryan Plestid, and Yotam Soreq for helpful discussions. This work is supported in part by the U.S. Department of Energy under grant number DE-SC0011640.

---

<sup>15</sup>We thank Ryan Plestid for pointing this out to us.

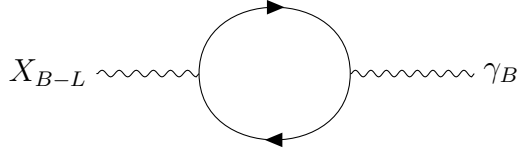


Figure 16: Contributions to the mixing of  $B - L$  with hypercharge.

## A Generating the Dark Mixing Angle

Throughout the paper, we utilized the low energy effective theory of  $X^\mu$  coupled to a linear combination of the electromagnetic current and  $B - L$  current, Eq. 2, that can be written as  $g_X [(\cos \varphi)j_\mu^{\text{EM}} + (\sin \varphi)j_\mu^{B-L}] X^\mu$ . We will not address the strength of the coupling,  $g_X$ . In the case of dark photon, generating a small kinetic mixing has been explored [260]; for  $B - L$ , a small coupling could arise from a gauged (and then spontaneously broken)  $U(1)_{B-L}$  group that simply has a small gauge coupling. The question we wish to address is how a dark mixing angle  $\varphi$  could be generated by UV physics.

Here we consider extending the SM to include a gauged  $U(1)_{B-L}$  at a high scale that is, at lower energies, spontaneously broken to generate a mass for the vector boson that couples to  $B - L$ . It is well known (e.g., [11, 18]) that one-loop corrections arising from matter that transforms under both  $U(1)_{B-L}$  and  $U(1)_Y$  will lead to these gauge bosons mixing with each other, see Fig. 16. In the case that is of most interest to us,  $g_{B-L} \ll g_Y$ , the hypercharge gauge boson remains virtually unchanged due to this mixing. Instead, the gauge boson that (initially) couples to  $B - L$ , however, will have a sizable one-loop induced coupling to the hypercharge current. The contributions to the loop corrections include “threshold” or “matching” finite corrections from heavy fields that transform under both  $U(1)_{B-L}$  and  $U(1)_Y$ , as well as renormalization group generated mixing from light fields (including SM fields).

For example, assuming that  $X^\mu$  couples to just  $B - L$  at a high scale  $\mu_{\text{high}}$ , the leading renormalization group induced contribution to hypercharge (and ultimately electric charge) is

$$\epsilon e = \epsilon g_Y \cos \theta_W \simeq -\frac{b_{\text{SM}} \cos \theta_W}{16\pi^2} g_Y^2 g_{B-L} \ln \frac{\mu_{\text{high}}}{\mu_{\text{low}}}. \quad (61)$$

The coefficient  $b_{\text{SM}} = 32/3$  (26/3) includes (does not include) three right-handed neutrinos. A sizable coupling of  $X^\mu$  to the electromagnetic current is possible even with just the SM field content and a large amount of renormalization group evolution. Moreover, it is interesting that the SM field content leads to  $\varphi$  evolving *towards* the chargephobic limit ( $\varphi > \pi/2$ ). We caution, however, that Eq. (61) is just the leading result; once  $\epsilon g_Y$  is comparable to  $g_{B-L}$  there are significant corrections from additional contributions in the RGE. To achieve an arbitrary angle  $0 < \varphi < \pi$ , additional matter beyond the SM is needed either as threshold corrections or as light(er) fields contributing to the renormalization group evolution.

## B Renormalization Group Equations

In the chargephobic limit,  $X^\mu$  couples the linear combination  $-j_\mu^{\text{EM}} + j_\mu^{B-L}$ , corresponding to the mixing angle  $\varphi = 3\pi/4$ , or equivalently  $\epsilon e = -g_{B-L}$ . The mixing angle is not stable under renormalization group evolution. We can determine the running of  $\varphi$  by first determining the RGEs of the individual couplings.

RGEs have been considered before in similar contexts [261–264]. In our case, the RGEs are given by

$$\mu \frac{de}{d\mu} = \frac{1}{12\pi^2} e^3 \sum_i N_c^i Q_i^2 \quad (62)$$

$$\mu \frac{dg_{B-L}}{d\mu} = \frac{1}{12\pi^2} g_{B-L} \sum_i N_c^i [g_{B-L}^2 q_i^2 + (\varepsilon e)^2 Q_i^2 + 2g_{B-L}(\varepsilon e)Q_i q_i] \quad (63)$$

$$\mu \frac{d\varepsilon e}{d\mu} = \frac{1}{12\pi^2} \sum_i [g_{B-L}^2 (\varepsilon e) q_i^2 + (\varepsilon e)^3 Q_i^2 + 2e^2 (\varepsilon e) Q_i^2 + 2e^2 g_{B-L} Q_i q_i + 2g_{B-L} (\varepsilon e)^2 Q_i q_i], \quad (64)$$

where  $\mu$  is the renormalization scale and the charges of the matter fermions contributing to the RGEs are given by  $Q_i$  (EM) and  $q_i$  ( $B-L$ ) in Sec. 2.1. Below  $\sqrt{s} \sim 2$  GeV, QCD is non-perturbative and it is mesons rather than quarks that determine thresholds in RGEs. For a detailed treatment see for example, [265, 266]. The precision obtained from this full treatment is not necessary to derive our constraints. Instead, we employ the following simplification: In the non-perturbative regime,  $\sqrt{s} < 2$  GeV, quarks are included perturbatively into the RGE at a scale corresponding to lightest meson that “contains” the quarks. Namely, the up and down quark charges are added at the pion mass, the strange quark at the mass of the lightest Kaon, and the charm at the mass of the lightest D meson. The sum of charges at each mass threshold is shown in Fig. 17 for various configurations of charge assignments.

We numerically solve Eqs. (62)–(64) to obtain the running of  $x_e$  in the chargephobic model as shown in Fig. 17. However, one can understand the results more easily by working in the limit  $g_X = \sqrt{(\varepsilon e)^2 + g_{B-L}^2} \ll e$ , and then the RGEs simplify to

$$\mu \frac{de}{d\mu} = \frac{1}{12\pi^2} e^3 \sum_i N_c^i Q_i^2 \quad (65)$$

$$\mu \frac{d\varepsilon e}{d\mu} = \frac{1}{6\pi^2} e^2 \sum_i N_c^i [(\varepsilon e) Q_i^2 + g_{B-L} Q_i q_i] \quad (g_X \ll e \text{ limit}). \quad (66)$$

Here, we have taken  $g_{B-L}$  to be constant since the leading contribution to its running is  $\mathcal{O}(g_X^3)$  as compared with  $\varepsilon e$  that receives its leading contribution at order  $\mathcal{O}(g_X e^2)$ . Interestingly, leptons do not contribute to the running of  $\varepsilon e$ . This is clear because the lepton charges satisfy  $Q_l^2 = Q_l q_l$  (and neutrinos do not contribute  $q_\nu = 0$ ), and so at the chargephobic mixing angle,  $\varepsilon e = -g_{B-L}$ , the contribution of leptons to the term in square brackets in Eq. (66) vanishes.

The main driver of the  $\varepsilon e$  running is the  $e$  running itself. A simple but useful analytic approximation for  $\varepsilon e[\mu]$  can be obtained by running  $e$  starting at the pion threshold then suppressing the solution by  $\varepsilon$ . The result is

$$x_e[\mu] = -\frac{1}{\sqrt{2}} \left( 1 - \frac{1}{\sqrt{1 - \frac{e^2}{6\pi^2} \left(\frac{11}{3}\right) \log\left(\frac{\mu}{m_\pi}\right)}} \right) \approx \frac{\sqrt{2}}{24\pi^2} \frac{11}{3} e^2 \log\left(\frac{\mu}{m_\pi}\right) \quad (\text{analytic approx.}) \quad (67)$$

where the factor of  $11/3$  is the squared charge sum of the electron, muon, up and down quarks all of which contribute to the running of  $e$  above  $\mu = m_\pi$ . The running of  $\varepsilon e$  can be reformulated into the running of  $\varphi$ . The deviation from  $\varphi_0$  is

$$\delta\varphi \approx \frac{e^2}{24\pi^2} \left(\frac{11}{3}\right) \log\left(\frac{\mu}{m_\pi}\right). \quad (68)$$

Notice that mixing angle receives a positive contribution at larger renormalization scales when starting from the chargephobic limit. This means  $X^\mu$  slightly shifts from equal couplings  $g_X = |\varepsilon e|/\sqrt{2} = g_{B-L}/\sqrt{2}$ ,

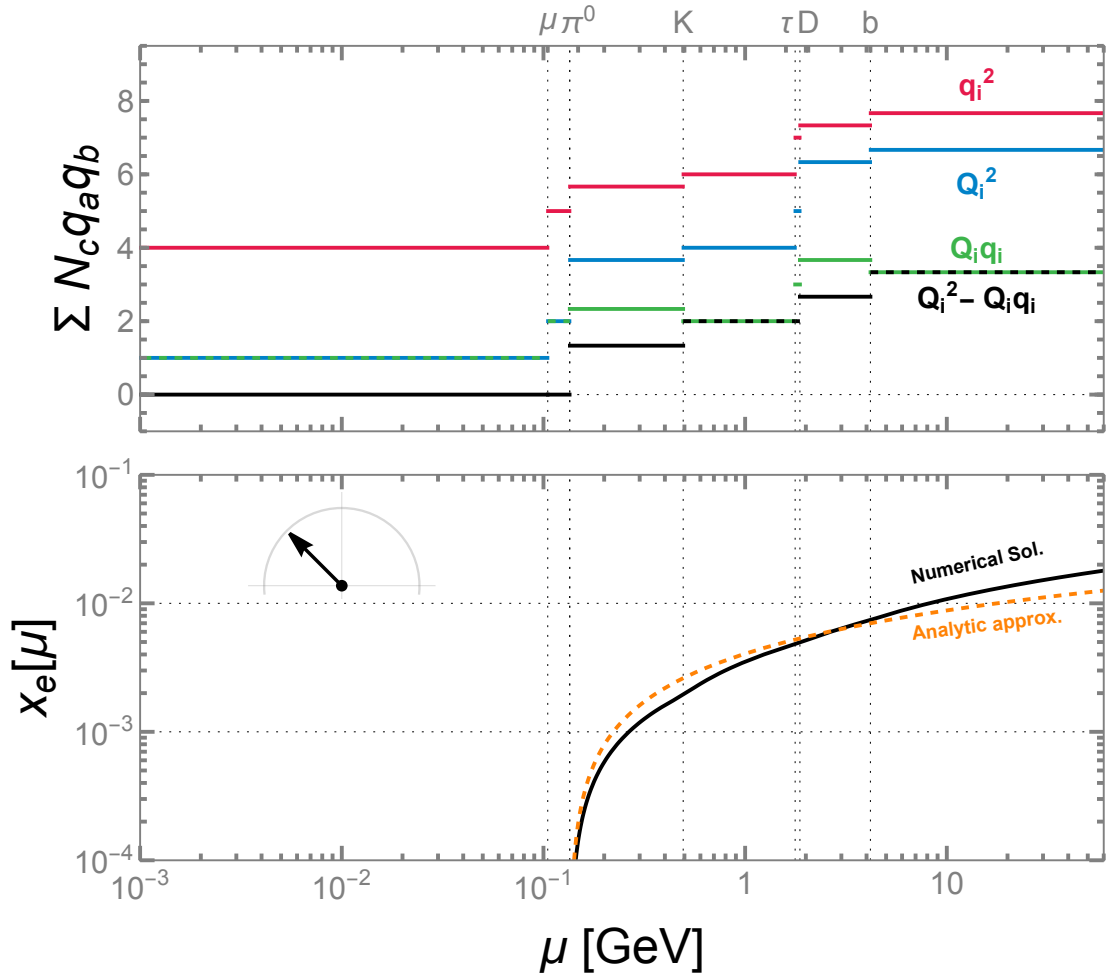


Figure 17: (Top) the squared charge sum of particles contributing to the RGE at threshold and (bottom)  $x_e$  running using the full numerical solution of Eq. 62-64 shown in black for  $g_X = 10^{-2}$  or using the simple analytic approximation ( $g_X \ll e$ ) as discussed in the text (orange dashed).

to one where  $X^\mu$  couples *slightly* more to the electromagnetic current relative to  $B - L$  ( $\varphi$  evolves towards values slightly larger than  $3\pi/4$ .)

Now let's briefly describe the effect of the renormalization group evolution of  $\varphi$  on various observables. For the purposes of this discussion, we take  $\varphi = 3\pi/4$  at low energies, and then consider the effects of the shifts in the couplings of  $X^\mu$  for observables that are sensitive to energies  $\sqrt{s} \gtrsim m_\pi$  where deviations from chargephobic begin to occur, see Fig. 17. The dominant effect is the appearance of a small coupling of  $X^\mu$  to charged leptons, since this is a critically important mode for  $X^\mu$  to be observed. The tail end of current beam dump experiment sensitivity extends into the region  $m_\pi < m_X \lesssim 800$  MeV, however we find that the branching fraction  $Br(X \rightarrow \ell^+ \ell^-)$  remains small enough that these experiments remain insensitive in this region. Most of the supernova constraint region is also below the pion mass threshold, and so is not expected to change. The one region that requires a more careful analysis is the low energy supernova constraints (the region labeled LESNe in Fig. 3 [5]). However, it is likely that the hadronic decay of  $X \rightarrow \pi^+ \pi^-$  is the most important mode at larger chargephobic masses  $m_X \gtrsim 300$  MeV, and this will require a detailed analysis to determine the sensitivity to a chargephobic vector boson.

The most prominent re-appearance of experiments are LHCb constraints (shown in green in Fig. 4) and the neutrino-electron scattering experiments TEXONO and CHARM (shown in pink and orange in Fig. 4). However, these constraints are subdominant to  $CE\nu NS$  and EWP constraints respectively.

## C Bremsstrahlung Interaction in Proto-Neutron Star

The bremsstrahlung channels that contribute to absorption in a general  $\varphi$  model are

$$\begin{array}{cccc}
 \begin{array}{c} K \\ \text{---} \\ P_1 \text{---} P_3 \\ \text{---} \\ P_2 \text{---} P_4 \end{array} &
 \begin{array}{c} K \\ \text{---} \\ P_1 \text{---} P_3 \\ \text{---} \\ P_2 \text{---} P_4 \end{array} &
 \begin{array}{c} P_1 \text{---} P_3 \\ \text{---} \\ P_2 \text{---} P_4 \\ \text{---} \\ K \end{array} &
 \begin{array}{c} P_1 \text{---} P_3 \\ \text{---} \\ P_2 \text{---} P_4 \\ \text{---} \\ K \end{array}, \quad (69)
 \end{array}$$

where  $P_i = \{E_i, \vec{\beta}_i\}$ , and  $K = \{\omega, \vec{v}\}$  are the momenta of nucleons and  $X$  and the shaded circle represents the nucleon-nucleon interaction which takes into account long-distance component arising from pion-exchanges and short-distance components that contribute to nucleon-nucleon scattering [132]. We will designate the charge  $q_1, q_2$  to the upper and lower legs of the diagrams respectively. Following the derivation in [127] with the necessary adjustments, the absorption width

$$\Gamma_{\text{SRA}} \simeq \frac{n_i n_j}{256\pi^5 S_{\mathbf{L}, \mathbf{T}} \omega T^3 m_N^{7/2}} \int d \cos \theta_{\text{CM}} d^3 \vec{p}_+ d^3 \vec{p}_- \overline{(\tilde{\varepsilon} \cdot J)^2} e^{-\frac{|\vec{p}_+|^2 + |\vec{p}_-|^2}{4m_N T}} \sqrt{T_{\text{CM}}} \frac{d\sigma_{ij}}{d \cos \theta_{\text{CM}}}, \quad (70)$$

where  $S_{\mathbf{L}}(S_{\mathbf{T}}) = 1(2)$  is the spin degeneracy of the polarization states,  $n_i$  is the number density of nucleons,  $m_N$  is the nucleon mass,  $T_{\text{CM}} = (\vec{p}_1 - \vec{p}_2)^2 / 4m_N$  is the center of mass kinetic energy,  $\vec{p}_\pm = \vec{p}_1 \pm \vec{p}_2$ ,  $\theta_{\text{CM}}$  is the scattering angle. Furthermore,  $\tilde{\varepsilon}_\mu$  is the  $X$  polarization,

$$J^\mu = \left[ q_1 \left( \frac{P_1}{P_1 \cdot K} - \frac{P_3}{P_3 \cdot K} \right) + q_2 \left( \frac{P_2}{P_2 \cdot K} - \frac{P_4}{P_4 \cdot K} \right) \right]^\mu, \quad (71)$$

is the quadrupole current, and  $\overline{(\tilde{\varepsilon} \cdot J)^2} \equiv \int d\Omega' \Sigma_{\text{pols.}} (\tilde{\varepsilon}_\mu J^\mu)^2$  integrated over the  $X$  scattering angle. To leading order, this integral projected onto the transverse and longitudinal polarizations is

$$\overline{(\tilde{\varepsilon} \cdot J)^2}_{\mathbf{L}, \mathbf{T}} = \frac{8\pi}{15} \frac{T_{\text{CM}}}{m_N \omega^2} \begin{cases} \left[ 10q_-^2 (1 - \cos \theta) + 3v^2 \frac{T_{\text{CM}}}{m_N} q_+^2 (1 - \cos^2 \theta) \right] & (\mathbf{T}) \\ \left[ 5q_-^2 (1 - \cos \theta) + 2v^2 \frac{T_{\text{CM}}}{m_N} q_+^2 (1 - \cos^2 \theta) \right] (1 - v^2) & (\mathbf{L}) \end{cases} \quad (72)$$

where  $q_{\pm} = q_1 \pm q_2$ . The width in Eq. 70 for the transverse mode becomes

$$\Gamma_{\text{SRA}|\mathbf{T}} = \frac{n_i n_j}{30\pi^{1/2}\omega^3 m_N^3 T^{3/2}} \int |\vec{p}_-|^2 d|\vec{p}_-| e^{-|\vec{p}_-|^2/4m_N T} T_{\text{CM}}^{3/2} \left[ 10q_-^2 \sigma_{ij}^{(2)} + 3v^2 \frac{T_{\text{CM}}}{m_N} q_+^2 \sigma_{ij}^{(4)} \right], \quad (73)$$

where the  $p_+$  integral was evaluated to  $\int |\vec{p}_+|^2 e^{-|\vec{p}_+|^2/4m_N T} d|\vec{p}_+| = 2\sqrt{\pi(m_N T)^3}$  and we defined

$$\sigma_{ij}^{(2)}(T_{\text{CM}}) \equiv \int d\cos\theta_{\text{CM}} (1 - \cos\theta_{\text{CM}}) \frac{d\sigma_{ij}}{d\cos\theta_{\text{CM}}} \quad (74)$$

$$\sigma_{ij}^{(4)}(T_{\text{CM}}) \equiv \int d\cos\theta_{\text{CM}} (1 - \cos^2\theta_{\text{CM}}) \frac{d\sigma_{ij}}{d\cos\theta_{\text{CM}}}. \quad (75)$$

Finally, we change to a dimensionless variable  $x = T_{\text{CM}}/T$  and do the  $|p_-|$  integral and go through a similar process for the longitudinal mode to get inverse bremsstrahlung rate

$$\Gamma_{\text{ibr}|\mathbf{L},\mathbf{T}} = \frac{8n_i n_j}{15\pi^2 \omega^3 S_{\mathbf{L},\mathbf{T}}} \left( \frac{\pi T}{m_N} \right)^{3/2} \begin{cases} \left[ 10q_-^2 \langle \sigma_{ij}^{(2)} \rangle + 9q_+^2 \frac{Tv^2}{m_N} \langle \sigma_{ij}^{(4)} \rangle \right] & (\mathbf{T}) \\ \left[ 5q_-^2 \langle \sigma_{ij}^{(2)} \rangle + 6q_+^2 \frac{Tv^2}{m_N} \langle \sigma_{ij}^{(4)} \rangle \right] (1 - v^2) & (\mathbf{L}) \end{cases} \quad (76)$$

where

$$\langle \sigma_{ij}^{(2)}(T) \rangle = \frac{1}{2} \int_0^\infty dx e^{-x} x^2 \sigma_{ij}^{(2)}(xT) \quad (77)$$

$$\langle \sigma_{ij}^{(4)}(T) \rangle = \frac{1}{6} \int_0^\infty dx e^{-x} x^3 \sigma_{ij}^{(4)}(xT) \quad (78)$$

are the energy and angle-averaged nucleon nucleon scattering cross section found in [132]. The calculation for production rate is identical with the restriction that the  $X^\mu$  energy must not exceed the energy of the collision. This takes  $\int_0^\infty \rightarrow \int_{\omega/T}^\infty$ ; for example  $\langle \sigma_{ij}^{(2)}(T) \rangle \rightarrow \langle \sigma_{ij}^{(2)}(T, \omega) \rangle = \frac{1}{2} \int_{\omega/T}^\infty dx e^{-x} x^2 \sigma_{ij}^{(2)}(xT)$ .

## References

- [1] P. Ilten, Y. Soreq, M. Williams, and W. Xue, ‘‘Serendipity in dark photon searches,’’ *JHEP* **06** (2018) 004, [arXiv:1801.04847 \[hep-ph\]](#).
- [2] M. Bauer, P. Foldenauer, and J. Jaeckel, ‘‘Hunting All the Hidden Photons,’’ *JHEP* **07** (2018) 094, [arXiv:1803.05466 \[hep-ph\]](#).
- [3] M. Fabbrichesi, E. Gabrielli, and G. Lanfranchi, ‘‘The Dark Photon,’’ [arXiv:2005.01515 \[hep-ph\]](#).
- [4] A. Caputo, A. J. Millar, C. A. J. O’Hare, and E. Vitagliano, ‘‘Dark photon limits: A handbook,’’ *Phys. Rev. D* **104** no. 9, (2021) 095029, [arXiv:2105.04565 \[hep-ph\]](#).
- [5] A. Caputo, J. Park, and S. Yun, ‘‘The Heavy Dark Photon Handbook: Cosmological and Astrophysical Bounds,’’ [arXiv:2511.15785 \[hep-ph\]](#).
- [6] R. E. Marshak and R. N. Mohapatra, ‘‘Quark - Lepton Symmetry and B-L as the U(1) Generator of the Electroweak Symmetry Group,’’ *Phys. Lett. B* **91** (1980) 222–224.
- [7] R. N. Mohapatra and R. E. Marshak, ‘‘Local B-L Symmetry of Electroweak Interactions, Majorana Neutrinos and Neutron Oscillations,’’ *Phys. Rev. Lett.* **44** (1980) 1316–1319. [Erratum: *Phys.Rev.Lett.* 44, 1643 (1980)].
- [8] C. Wetterich, ‘‘Neutrino Masses and the Scale of B-L Violation,’’ *Nucl. Phys. B* **187** (1981) 343–375.

- [9] P. Langacker, “The Physics of Heavy  $Z'$  Gauge Bosons,” *Rev. Mod. Phys.* **81** (2009) 1199–1228, [arXiv:0801.1345 \[hep-ph\]](#).
- [10] R. Harnik, J. Kopp, and P. A. N. Machado, “Exploring  $\nu$  Signals in Dark Matter Detectors,” *JCAP* **1207** (2012) 026, [arXiv:1202.6073 \[hep-ph\]](#).
- [11] J. Heeck, “Unbroken  $B - L$  symmetry,” *Phys. Lett. B* **739** (2014) 256–262, [arXiv:1408.6845 \[hep-ph\]](#).
- [12] R. Foot, “New Physics From Electric Charge Quantization?,” *Mod. Phys. Lett. A* **6** (1991) 527–530.
- [13] X.-G. He, G. C. Joshi, H. Lew, and R. R. Volkas, “Simplest Z-prime model,” *Phys. Rev. D* **44** (1991) 2118–2132.
- [14] R. Foot, X. G. He, H. Lew, and R. R. Volkas, “Model for a light Z-prime boson,” *Phys. Rev. D* **50** (1994) 4571–4580, [arXiv:hep-ph/9401250](#).
- [15] E. Ma, “Gauged  $B - 3L(\tau)$  and radiative neutrino masses,” *Phys. Lett. B* **433** (1998) 74–81, [arXiv:hep-ph/9709474](#).
- [16] E. Ma and D. P. Roy, “Phenomenology of the  $B - 3L(\tau)$  gauge boson,” *Phys. Rev. D* **58** (1998) 095005, [arXiv:hep-ph/9806210](#).
- [17] T. Appelquist, B. A. Dobrescu, and A. R. Hopper, “Nonexotic Neutral Gauge Bosons,” *Phys. Rev. D* **68** (2003) 035012, [arXiv:hep-ph/0212073](#).
- [18] E. Salvioni, A. Strumia, G. Villadoro, and F. Zwirner, “Non-universal minimal  $Z'$  models: present bounds and early LHC reach,” *JHEP* **03** (2010) 010, [arXiv:0911.1450 \[hep-ph\]](#).
- [19] A. Celis, J. Fuentes-Martin, M. Jung, and H. Serodio, “Family nonuniversal  $Z'$  models with protected flavor-changing interactions,” *Phys. Rev. D* **92** no. 1, (2015) 015007, [arXiv:1505.03079 \[hep-ph\]](#).
- [20] M. Bauer, S. Diefenbacher, T. Plehn, M. Russell, and D. A. Camargo, “Dark Matter in Anomaly-Free Gauge Extensions,” *SciPost Phys.* **5** no. 4, (2018) 036, [arXiv:1805.01904 \[hep-ph\]](#).
- [21] W. Altmannshofer, M. Tamaro, and J. Zupan, “Non-standard neutrino interactions and low energy experiments,” *JHEP* **09** (2019) 083, [arXiv:1812.02778 \[hep-ph\]](#). [Erratum: *JHEP* 11, 113 (2021)].
- [22] J. Heeck, M. Lindner, W. Rodejohann, and S. Vogl, “Non-Standard Neutrino Interactions and Neutral Gauge Bosons,” *SciPost Phys.* **6** no. 3, (2019) 038, [arXiv:1812.04067 \[hep-ph\]](#).
- [23] M. Escudero, D. Hooper, G. Krnjaic, and M. Pierre, “Cosmology with A Very Light  $L_\mu - L_\tau$  Gauge Boson,” *JHEP* **03** (2019) 071, [arXiv:1901.02010 \[hep-ph\]](#).
- [24] T. Han, J. Liao, H. Liu, and D. Marfatia, “Nonstandard neutrino interactions at COHERENT, DUNE, T2HK and LHC,” *JHEP* **11** (2019) 028, [arXiv:1910.03272 \[hep-ph\]](#).
- [25] P. Coloma, M. C. Gonzalez-Garcia, and M. Maltoni, “Neutrino oscillation constraints on  $U(1)'$  models: from non-standard interactions to long-range forces,” *JHEP* **01** (2021) 114, [arXiv:2009.14220 \[hep-ph\]](#). [Erratum: *JHEP* 11, 115 (2022)].
- [26] M. Bauer, P. Foldenauer, and M. Mosny, “Flavor structure of anomaly-free hidden photon models,” *Phys. Rev. D* **103** no. 7, (2021) 075024, [arXiv:2011.12973 \[hep-ph\]](#).
- [27] E. Salvioni, G. Villadoro, and F. Zwirner, “Minimal Z-prime models: Present bounds and early LHC reach,” *JHEP* **11** (2009) 068, [arXiv:0909.1320 \[hep-ph\]](#).
- [28] G. D. Kribs, G. Lee, and A. Martin, “Effective field theory of Stückelberg vector bosons,” *Phys. Rev. D* **106** no. 5, (2022) 055020, [arXiv:2204.01755 \[hep-ph\]](#).

- [29] J. A. Dror, R. Lasenby, and M. Pospelov, “New constraints on light vectors coupled to anomalous currents,” *Phys. Rev. Lett.* **119** no. 14, (2017) 141803, [arXiv:1705.06726 \[hep-ph\]](#).
- [30] J. A. Dror, R. Lasenby, and M. Pospelov, “Dark forces coupled to nonconserved currents,” *Phys. Rev. D* **96** no. 7, (2017) 075036, [arXiv:1707.01503 \[hep-ph\]](#).
- [31] “Garching Core Collapse Supernova Archive.”  
<https://wwwmpa.mpa-garching.mpg.de/ccsnarchive/archive.html>.
- [32] J. A. Dror, R. Lasenby, and M. Pospelov, “Light vectors coupled to bosonic currents,” *Phys. Rev. D* **99** no. 5, (2019) 055016, [arXiv:1811.00595 \[hep-ph\]](#).
- [33] J. A. Dror, “Discovering leptonic forces using nonconserved currents,” *Phys. Rev. D* **101** no. 9, (2020) 095013, [arXiv:2004.04750 \[hep-ph\]](#).
- [34] L. Michaels and F. Yu, “Probing new  $U(1)$  gauge symmetries via exotic  $Z \rightarrow Z'\gamma$  decays,” *JHEP* **03** (2021) 120, [arXiv:2010.00021 \[hep-ph\]](#).
- [35] H. Esseili and G. D. Kribs, “Cosmological implications of gauged  $U(1)_{B-L}$  on  $\Delta N_{eff}$  in the CMB and BBN,” *JCAP* **05** (2024) 110, [arXiv:2308.07955 \[hep-ph\]](#).
- [36] J. L. Feng, J. Kumar, and D. Sanford, “Xenophobic Dark Matter,” *Phys. Rev. D* **88** no. 1, (2013) 015021, [arXiv:1306.2315 \[hep-ph\]](#).
- [37] **FASER** Collaboration, H. Abreu *et al.*, “Search for dark photons with the FASER detector at the LHC,” *Phys. Lett. B* **848** (2024) 138378, [arXiv:2308.05587 \[hep-ex\]](#).
- [38] **FASER** Collaboration, A. Ariga *et al.*, “FASER’s physics reach for long-lived particles,” *Phys. Rev. D* **99** no. 9, (2019) 095011, [arXiv:1811.12522 \[hep-ph\]](#).
- [39] **KLOE-2** Collaboration, F. Archilli *et al.*, “Search for a vector gauge boson in  $\phi$  meson decays with the KLOE detector,” *Phys. Lett. B* **706** (2012) 251–255, [arXiv:1110.0411 \[hep-ex\]](#).
- [40] T. Fujiwara, T. Kugo, H. Terao, S. Uehara, and K. Yamawaki, “Nonabelian Anomaly and Vector Mesons as Dynamical Gauge Bosons of Hidden Local Symmetries,” *Prog. Theor. Phys.* **73** (1985) 926.
- [41] S. Tulin, “New weakly-coupled forces hidden in low-energy QCD,” *Phys. Rev. D* **89** no. 11, (2014) 114008, [arXiv:1404.4370 \[hep-ph\]](#).
- [42] S. Bilmis, I. Turan, T. M. Aliev, M. Deniz, L. Singh, and H. T. Wong, “Constraints on Dark Photon from Neutrino-Electron Scattering Experiments,” *Phys. Rev. D* **92** no. 3, (2015) 033009, [arXiv:1502.07763 \[hep-ph\]](#).
- [43] M. Lindner, F. S. Queiroz, W. Rodejohann, and X.-J. Xu, “Neutrino-electron scattering: general constraints on  $Z'$  and dark photon models,” *JHEP* **05** (2018) 098, [arXiv:1803.00060 \[hep-ph\]](#).
- [44] V. De Romeri, O. G. Miranda, D. K. Papoulias, G. Sanchez Garcia, M. Tórtola, and J. W. F. Valle, “Physics implications of a combined analysis of COHERENT CsI and LAr data,” *JHEP* **04** (2023) 035, [arXiv:2211.11905 \[hep-ph\]](#).
- [45] P. Z. et al. (Particle Data Group), “Review of Particle Physics,” *Progress of Theoretical and Experimental Physics* **2020** no. 8, (08, 2020) ,  
<https://academic.oup.com/ptep/article-pdf/2020/8/083C01/34673722/ptaa104.pdf>.  
<https://doi.org/10.1093/ptep/ptaa104.083C01>.
- [46] V. V. Ezhela, S. B. Lugovsky, and O. V. Zenin, “Hadronic part of the muon  $g-2$  estimated on the  $\sigma^{*2003}(\text{tot})(e^+e^- \rightarrow \text{hadrons})$  evaluated data compilation,” [arXiv:hep-ph/0312114](#).

- [47] **BaBar** Collaboration, J. P. Lees *et al.*, “Precise Measurement of the  $e^+e^- \rightarrow \pi^+\pi^-(\gamma)$  Cross Section with the Initial-State Radiation Method at BABAR,” *Phys. Rev. D* **86** (2012) 032013, [arXiv:1205.2228 \[hep-ex\]](#).
- [48] **BaBar** Collaboration, B. Aubert *et al.*, “Study of  $e^+e^- \rightarrow \pi^+\pi^-\pi^0$  process using initial state radiation with BaBar,” *Phys. Rev. D* **70** (2004) 072004, [arXiv:hep-ex/0408078](#).
- [49] **BaBar** Collaboration, J. P. Lees *et al.*, “Precision measurement of the  $e^+e^- \rightarrow K^+K^-(\gamma)$  cross section with the initial-state radiation method at BABAR,” *Phys. Rev. D* **88** no. 3, (2013) 032013, [arXiv:1306.3600 \[hep-ex\]](#).
- [50] **BaBar** Collaboration, B. Aubert *et al.*, “Measurements of  $e^+e^- \rightarrow K^+K^-\eta$ ,  $K^+K^-\pi^0$  and  $K_s^0K^\pm\pi^\mp$  cross- sections using initial state radiation events,” *Phys. Rev. D* **77** (2008) 092002, [arXiv:0710.4451 \[hep-ex\]](#).
- [51] **BaBar** Collaboration, J. P. Lees *et al.*, “Initial-State Radiation Measurement of the  $e^+e^- \rightarrow \pi^+\pi^-\pi^+\pi^-$  Cross Section,” *Phys. Rev. D* **85** (2012) 112009, [arXiv:1201.5677 \[hep-ex\]](#).
- [52] **BaBar** Collaboration, J. P. Lees *et al.*, “Measurement of the  $e^+e^- \rightarrow \pi^+\pi^-\pi^0\pi^0$  cross section using initial-state radiation at BABAR,” *Phys. Rev. D* **96** no. 9, (2017) 092009, [arXiv:1709.01171 \[hep-ex\]](#).
- [53] M. N. Achasov *et al.*, “Study of the process  $e^+e^- \rightarrow \pi^+\pi^-\pi^0$  in the energy region  $s^{**}(1/2)$  below 0.98-GeV,” *Phys. Rev. D* **68** (2003) 052006, [arXiv:hep-ex/0305049](#).
- [54] M. N. Achasov *et al.*, “Study of the process  $e^+e^- \rightarrow \pi^+\pi^-\pi^0$  in the energy region  $s^{**}(1/2)$  from 0.98-GeV to 1.38-GeV,” *Phys. Rev. D* **66** (2002) 032001, [arXiv:hep-ex/0201040](#).
- [55] **CMS** Collaboration, A. M. Sirunyan *et al.*, “Search for a Narrow Resonance Lighter than 200 GeV Decaying to a Pair of Muons in Proton-Proton Collisions at  $\sqrt{s} = 13$  TeV,” *Phys. Rev. Lett.* **124** no. 13, (2020) 131802, [arXiv:1912.04776 \[hep-ex\]](#).
- [56] **Planck** Collaboration, N. Aghanim *et al.*, “Planck 2018 results. I. Overview and the cosmological legacy of Planck,” *Astron. Astrophys.* **641** (2020) A1, [arXiv:1807.06205 \[astro-ph.CO\]](#).
- [57] **Planck** Collaboration, N. Aghanim *et al.*, “Planck 2018 results. VI. Cosmological parameters,” *Astron. Astrophys.* **641** (2020) A6, [arXiv:1807.06209 \[astro-ph.CO\]](#). [Erratum: *Astron. Astrophys.* 652, C4 (2021)].
- [58] **Atacama Cosmology Telescope** Collaboration, E. Calabrese *et al.*, “The Atacama Cosmology Telescope: DR6 constraints on extended cosmological models,” *JCAP* **11** (2025) 063, [arXiv:2503.14454 \[astro-ph.CO\]](#).
- [59] R. H. Cyburt, B. D. Fields, K. A. Olive, and T.-H. Yeh, “Big Bang Nucleosynthesis: 2015,” *Rev. Mod. Phys.* **88** (2016) 015004, [arXiv:1505.01076 \[astro-ph.CO\]](#).
- [60] T.-H. Yeh, K. A. Olive, and B. D. Fields, “The impact of new  $d(p,\gamma)^3$  rates on Big Bang Nucleosynthesis,” *JCAP* **03** (2021) 046, [arXiv:2011.13874 \[astro-ph.CO\]](#).
- [61] T.-H. Yeh, J. Shelton, K. A. Olive, and B. D. Fields, “Probing physics beyond the standard model: limits from BBN and the CMB independently and combined,” *JCAP* **10** (2022) 046, [arXiv:2207.13133 \[astro-ph.CO\]](#).
- [62] **Particle Data Group** Collaboration, R. L. Workman *et al.*, “Review of Particle Physics,” *PTEP* **2022** (2022) 083C01.
- [63] P. F. de Salas and S. Pastor, “Relic neutrino decoupling with flavour oscillations revisited,” *JCAP* **07** (2016) 051, [arXiv:1606.06986 \[hep-ph\]](#).

- [64] G. Mangano, G. Miele, S. Pastor, T. Pinto, O. Pisanti, and P. D. Serpico, “Relic neutrino decoupling including flavor oscillations,” *Nucl. Phys. B* **729** (2005) 221–234, [arXiv:hep-ph/0506164](#).
- [65] A. D. Dolgov, “Neutrinos in cosmology,” *Phys. Rept.* **370** (2002) 333–535, [arXiv:hep-ph/0202122](#).
- [66] D. A. Dicus, E. W. Kolb, A. M. Gleeson, E. C. G. Sudarshan, V. L. Teplitz, and M. S. Turner, “Primordial Nucleosynthesis Including Radiative, Coulomb, and Finite Temperature Corrections to Weak Rates,” *Phys. Rev. D* **26** (1982) 2694.
- [67] S. Hannestad and J. Madsen, “Neutrino decoupling in the early universe,” *Phys. Rev. D* **52** (1995) 1764–1769, [arXiv:astro-ph/9506015](#).
- [68] S. Dodelson and M. S. Turner, “Nonequilibrium neutrino statistical mechanics in the expanding universe,” *Phys. Rev. D* **46** (1992) 3372–3387.
- [69] A. D. Dolgov, S. H. Hansen, and D. V. Semikoz, “Nonequilibrium corrections to the spectra of massless neutrinos in the early universe,” *Nucl. Phys. B* **503** (1997) 426–444, [arXiv:hep-ph/9703315](#).
- [70] S. Esposito, G. Miele, S. Pastor, M. Peloso, and O. Pisanti, “Nonequilibrium spectra of degenerate relic neutrinos,” *Nucl. Phys. B* **590** (2000) 539–561, [arXiv:astro-ph/0005573](#).
- [71] G. Mangano, G. Miele, S. Pastor, and M. Peloso, “A Precision calculation of the effective number of cosmological neutrinos,” *Phys. Lett. B* **534** (2002) 8–16, [arXiv:astro-ph/0111408](#).
- [72] J. Birrell, C.-T. Yang, and J. Rafelski, “Relic Neutrino Freeze-out: Dependence on Natural Constants,” *Nucl. Phys. B* **890** (2014) 481–517, [arXiv:1406.1759](#) [[nucl-th](#)].
- [73] E. Grohs, G. M. Fuller, C. T. Kishimoto, M. W. Paris, and A. Vlasenko, “Neutrino energy transport in weak decoupling and big bang nucleosynthesis,” *Phys. Rev. D* **93** no. 8, (2016) 083522, [arXiv:1512.02205](#) [[astro-ph.CO](#)].
- [74] M. Cielo, M. Escudero, G. Mangano, and O. Pisanti, “Neff in the Standard Model at NLO is 3.043,” [arXiv:2306.05460](#) [[hep-ph](#)].
- [75] K. Akita and M. Yamaguchi, “A precision calculation of relic neutrino decoupling,” *JCAP* **08** (2020) 012, [arXiv:2005.07047](#) [[hep-ph](#)].
- [76] J. Froustey, C. Pitrou, and M. C. Volpe, “Neutrino decoupling including flavour oscillations and primordial nucleosynthesis,” *JCAP* **12** (2020) 015, [arXiv:2008.01074](#) [[hep-ph](#)].
- [77] J. J. Bennett, G. Buldgen, P. F. De Salas, M. Drewes, S. Gariazzo, S. Pastor, and Y. Y. Y. Wong, “Towards a precision calculation of  $N_{\text{eff}}$  in the Standard Model II: Neutrino decoupling in the presence of flavour oscillations and finite-temperature QED,” *JCAP* **04** (2021) 073, [arXiv:2012.02726](#) [[hep-ph](#)].
- [78] S. Sarkar, “Big bang nucleosynthesis and physics beyond the standard model,” *Rept. Prog. Phys.* **59** (1996) 1493–1610, [arXiv:hep-ph/9602260](#).
- [79] F. Iocco, G. Mangano, G. Miele, O. Pisanti, and P. D. Serpico, “Primordial Nucleosynthesis: from precision cosmology to fundamental physics,” *Phys. Rept.* **472** (2009) 1–76, [arXiv:0809.0631](#) [[astro-ph](#)].
- [80] M. Pospelov and J. Pradler, “Big Bang Nucleosynthesis as a Probe of New Physics,” *Ann. Rev. Nucl. Part. Sci.* **60** (2010) 539–568, [arXiv:1011.1054](#) [[hep-ph](#)].
- [81] M. Blennow, E. Fernandez-Martinez, O. Mena, J. Redondo, and P. Serra, “Asymmetric Dark Matter and Dark Radiation,” *JCAP* **07** (2012) 022, [arXiv:1203.5803](#) [[hep-ph](#)].

- [82] C. Boehm, M. J. Dolan, and C. McCabe, “Increasing  $N_{\text{eff}}$  with particles in thermal equilibrium with neutrinos,” *JCAP* **12** (2012) 027, [arXiv:1207.0497 \[astro-ph.CO\]](#).
- [83] C. Boehm, M. J. Dolan, and C. McCabe, “A Lower Bound on the Mass of Cold Thermal Dark Matter from Planck,” *JCAP* **08** (2013) 041, [arXiv:1303.6270 \[hep-ph\]](#).
- [84] C. Brust, D. E. Kaplan, and M. T. Walters, “New Light Species and the CMB,” *JHEP* **12** (2013) 058, [arXiv:1303.5379 \[hep-ph\]](#).
- [85] H. Vogel and J. Redondo, “Dark Radiation constraints on minicharged particles in models with a hidden photon,” *JCAP* **02** (2014) 029, [arXiv:1311.2600 \[hep-ph\]](#).
- [86] A. Fradette, M. Pospelov, J. Pradler, and A. Ritz, “Cosmological Constraints on Very Dark Photons,” *Phys. Rev. D* **90** no. 3, (2014) 035022, [arXiv:1407.0993 \[hep-ph\]](#).
- [87] K. M. Nollett and G. Steigman, “BBN And The CMB Constrain Neutrino Coupled Light WIMPs,” *Phys. Rev. D* **91** no. 8, (2015) 083505, [arXiv:1411.6005 \[astro-ph.CO\]](#).
- [88] M. A. Buen-Abad, G. Marques-Tavares, and M. Schmaltz, “Non-Abelian dark matter and dark radiation,” *Phys. Rev. D* **92** no. 2, (2015) 023531, [arXiv:1505.03542 \[hep-ph\]](#).
- [89] Z. Chacko, Y. Cui, S. Hong, and T. Okui, “Hidden dark matter sector, dark radiation, and the CMB,” *Phys. Rev. D* **92** (2015) 055033, [arXiv:1505.04192 \[hep-ph\]](#).
- [90] R. J. Wilkinson, A. C. Vincent, C. Boehm, and C. McCabe, “Ruling out the light weakly interacting massive particle explanation of the Galactic 511 keV line,” *Phys. Rev. D* **94** no. 10, (2016) 103525, [arXiv:1602.01114 \[astro-ph.CO\]](#).
- [91] G.-y. Huang, T. Ohlsson, and S. Zhou, “Observational Constraints on Secret Neutrino Interactions from Big Bang Nucleosynthesis,” *Phys. Rev. D* **97** no. 7, (2018) 075009, [arXiv:1712.04792 \[hep-ph\]](#).
- [92] M. Escudero, “Neutrino decoupling beyond the Standard Model: CMB constraints on the Dark Matter mass with a fast and precise  $N_{\text{eff}}$  evaluation,” *JCAP* **02** (2019) 007, [arXiv:1812.05605 \[hep-ph\]](#).
- [93] K. N. Abazajian and J. Heeck, “Observing Dirac neutrinos in the cosmic microwave background,” *Phys. Rev. D* **100** (2019) 075027, [arXiv:1908.03286 \[hep-ph\]](#).
- [94] M. Ibe, S. Kobayashi, Y. Nakayama, and S. Shirai, “Cosmological constraint on dark photon from  $N_{\text{eff}}$ ,” *JHEP* **04** (2020) 009, [arXiv:1912.12152 \[hep-ph\]](#).
- [95] M. Escudero Abenza, “Precision Early Universe Thermodynamics Made Simple:  $N_{\text{eff}}$  and Neutrino Decoupling in the Standard Model and Beyond,” *JCAP* **05** (2020) 048, [arXiv:2001.04466 \[hep-ph\]](#).
- [96] J. Coffey, L. Forestell, D. E. Morrissey, and G. White, “Cosmological Bounds on sub-GeV Dark Vector Bosons from Electromagnetic Energy Injection,” *JHEP* **07** (2020) 179, [arXiv:2003.02273 \[hep-ph\]](#).
- [97] X. Luo, W. Rodejohann, and X.-J. Xu, “Dirac neutrinos and  $N_{\text{eff}}$ ,” *JCAP* **06** (2020) 058, [arXiv:2005.01629 \[hep-ph\]](#).
- [98] X. Luo, W. Rodejohann, and X.-J. Xu, “Dirac neutrinos and  $N_{\text{eff}}$ . Part II. The freeze-in case,” *JCAP* **03** (2021) 082, [arXiv:2011.13059 \[hep-ph\]](#).
- [99] P. Adshead, P. Ralegankar, and J. Shelton, “Dark radiation constraints on portal interactions with hidden sectors,” *JCAP* **09** (2022) 056, [arXiv:2206.13530 \[hep-ph\]](#).

- [100] S. Eijima, O. Seto, and T. Shimomura, “Revisiting sterile neutrino dark matter in gauged U(1)B-L model,” *Phys. Rev. D* **106** no. 10, (2022) 103513, [arXiv:2207.01775 \[hep-ph\]](#).
- [101] S. Sandner, M. Escudero, and S. J. Witte, “Precision CMB constraints on eV-scale bosons coupled to neutrinos,” [arXiv:2305.01692 \[hep-ph\]](#).
- [102] L. J. Hall, K. Jedamzik, J. March-Russell, and S. M. West, “Freeze-In Production of FIMP Dark Matter,” *JHEP* **03** (2010) 080, [arXiv:0911.1120 \[hep-ph\]](#).
- [103] S.-P. Li and X.-J. Xu, “ $N_{\text{eff}}$  constraints on light mediators coupled to neutrinos: the dilution-resistant effect,” [arXiv:2307.13967 \[hep-ph\]](#).
- [104] E. Aver, K. A. Olive, and E. D. Skillman, “The effects of He I  $\lambda$ 10830 on helium abundance determinations,” *JCAP* **07** (2015) 011, [arXiv:1503.08146 \[astro-ph.CO\]](#).
- [105] M. Pettini and R. Cooke, “A new, precise measurement of the primordial abundance of Deuterium,” *Mon. Not. Roy. Astron. Soc.* **425** (2012) 2477–2486, [arXiv:1205.3785 \[astro-ph.CO\]](#).
- [106] R. Cooke, M. Pettini, R. A. Jorgenson, M. T. Murphy, and C. C. Steidel, “Precision measures of the primordial abundance of deuterium,” *Astrophys. J.* **781** no. 1, (2014) 31, [arXiv:1308.3240 \[astro-ph.CO\]](#).
- [107] S. Riemer-Sørensen, J. K. Webb, N. Crighton, V. Dumont, K. Ali, S. Kotuš, M. Bainbridge, M. T. Murphy, and R. Carswell, “A robust deuterium abundance; Re-measurement of the  $z=3.256$  absorption system towards the quasar PKS1937-1009,” *Mon. Not. Roy. Astron. Soc.* **447** (2015) 2925, [arXiv:1412.4043 \[astro-ph.CO\]](#).
- [108] R. J. Cooke, M. Pettini, K. M. Nollett, and R. Jorgenson, “The primordial deuterium abundance of the most metal-poor damped Ly $\alpha$  system,” *Astrophys. J.* **830** no. 2, (2016) 148, [arXiv:1607.03900 \[astro-ph.CO\]](#).
- [109] S. A. Balashev, E. O. Zavarygin, A. V. Ivanchik, K. N. Telikova, and D. A. Varshalovich, “The primordial deuterium abundance: subDLA system at  $z_{\text{abs}} = 2.437$  towards the QSO J 1444+2919,” *Mon. Not. Roy. Astron. Soc.* **458** no. 2, (2016) 2188–2198, [arXiv:1511.01797 \[astro-ph.GA\]](#).
- [110] S. Riemer-Sørensen, S. Kotuš, J. K. Webb, K. Ali, V. Dumont, M. T. Murphy, and R. F. Carswell, “A precise deuterium abundance: remeasurement of the  $z = 3.572$  absorption system towards the quasar PKS1937–101,” *Mon. Not. Roy. Astron. Soc.* **468** no. 3, (2017) 3239–3250, [arXiv:1703.06656 \[astro-ph.CO\]](#).
- [111] E. O. Zavarygin, J. K. Webb, S. Riemer-Sørensen, and V. Dumont, “Primordial deuterium abundance at  $z_{\text{abs}} = 2:504$  towards Q1009+2956,” *J. Phys. Conf. Ser.* **1038** no. 1, (2018) 012012, [arXiv:1801.04704 \[astro-ph.CO\]](#).
- [112] R. J. Cooke, M. Pettini, and C. C. Steidel, “One Percent Determination of the Primordial Deuterium Abundance,” *Astrophys. J.* **855** no. 2, (2018) 102, [arXiv:1710.11129 \[astro-ph.CO\]](#).
- [113] E. Aver, D. A. Berg, K. A. Olive, R. W. Pogge, J. J. Salzer, and E. D. Skillman, “Improving helium abundance determinations with Leo P as a case study,” *JCAP* **03** (2021) 027, [arXiv:2010.04180 \[astro-ph.CO\]](#).
- [114] M. Valerdi, A. Peimbert, M. Peimbert, and A. Sixtos, “Determination of the Primordial Helium Abundance Based on NGC 346, an H ii Region of the Small Magellanic Cloud,” *Astrophys. J.* **876** no. 2, (2019) 98, [arXiv:1904.01594 \[astro-ph.GA\]](#).
- [115] V. Fernández, E. Terlevich, A. I. Díaz, and R. Terlevich, “A Bayesian direct method implementation to fit emission line spectra: Application to the primordial He abundance determination,” *Mon. Not. Roy. Astron. Soc.* **487** no. 3, (2019) 3221–3238, [arXiv:1905.09215 \[astro-ph.GA\]](#).

- [116] O. A. Kurichin, P. A. Kislitsyn, V. V. Klimenko, S. A. Balashev, and A. V. Ivanchik, “A new determination of the primordial helium abundance using the analyses of H II region spectra from SDSS,” *Mon. Not. Roy. Astron. Soc.* **502** no. 2, (2021) 3045–3056, [arXiv:2101.09127](#) [[astro-ph.CO](#)].
- [117] T. Hsyu, R. J. Cooke, J. X. Prochaska, and M. Bolte, “The PHLEK Survey: A New Determination of the Primordial Helium Abundance,” *Astrophys. J.* **896** no. 1, (2020) 77, [arXiv:2005.12290](#) [[astro-ph.GA](#)].
- [118] **Kamiokande-II** Collaboration, K. Hirata *et al.*, “Observation of a Neutrino Burst from the Supernova SN 1987a,” *Phys. Rev. Lett.* **58** (1987) 1490–1493.
- [119] R. M. Bionta *et al.*, “Observation of a Neutrino Burst in Coincidence with Supernova SN 1987a in the Large Magellanic Cloud,” *Phys. Rev. Lett.* **58** (1987) 1494.
- [120] A. Burrows and J. M. Lattimer, “The birth of neutron stars,” *Astrophys. J.* **307** (1986) 178–196.
- [121] A. Burrows and J. M. Lattimer, “Neutrinos from SN 1987A,” *Astrophys. J. Lett.* **318** (1987) L63–L68.
- [122] D. F. G. Fiorillo, M. Heinlein, H.-T. Janka, G. Raffelt, E. Vitagliano, and R. Bollig, “Supernova simulations confront SN 1987A neutrinos,” *Phys. Rev. D* **108** no. 8, (2023) 083040, [arXiv:2308.01403](#) [[astro-ph.HE](#)].
- [123] G. G. Raffelt, “Astrophysical methods to constrain axions and other novel particle phenomena,” *Phys. Rept.* **198** (1990) 1–113.
- [124] G. G. Raffelt, *Stars as laboratories for fundamental physics: The astrophysics of neutrinos, axions, and other weakly interacting particles*. 5, 1996.
- [125] A. Burrows, “A Brief History of the Co-evolution of Supernova Theory with Neutrino Physics,” 12, 2018. [arXiv:1812.05612](#) [[astro-ph.SR](#)].
- [126] H.-T. Janka, K. Langanke, A. Marek, G. Martinez-Pinedo, and B. Mueller, “Theory of Core-Collapse Supernovae,” *Phys. Rept.* **442** (2007) 38–74, [arXiv:astro-ph/0612072](#).
- [127] J. H. Chang, R. Essig, and S. D. McDermott, “Revisiting Supernova 1987A Constraints on Dark Photons,” *JHEP* **01** (2017) 107, [arXiv:1611.03864](#) [[hep-ph](#)].
- [128] E. Hardy and R. Lasenby, “Stellar cooling bounds on new light particles: plasma mixing effects,” *JHEP* **02** (2017) 033, [arXiv:1611.05852](#) [[hep-ph](#)].
- [129] J. D. Bjorken, R. Essig, P. Schuster, and N. Toro, “New Fixed-Target Experiments to Search for Dark Gauge Forces,” *Phys. Rev. D* **80** (2009) 075018, [arXiv:0906.0580](#) [[hep-ph](#)].
- [130] J. B. Dent, F. Ferrer, and L. M. Krauss, “Constraints on Light Hidden Sector Gauge Bosons from Supernova Cooling,” [arXiv:1201.2683](#) [[astro-ph.CO](#)].
- [131] D. Kazanas, R. N. Mohapatra, S. Nussinov, V. L. Teplitz, and Y. Zhang, “Supernova Bounds on the Dark Photon Using its Electromagnetic Decay,” *Nucl. Phys. B* **890** (2014) 17–29, [arXiv:1410.0221](#) [[hep-ph](#)].
- [132] E. Rrapaj and S. Reddy, “Nucleon-nucleon bremsstrahlung of dark gauge bosons and revised supernova constraints,” *Phys. Rev. C* **94** no. 4, (2016) 045805, [arXiv:1511.09136](#) [[nucl-th](#)].
- [133] D. Croon, G. Elor, R. K. Leane, and S. D. McDermott, “Supernova Muons: New Constraints on  $Z'$  Bosons, Axions and ALPs,” *JHEP* **01** (2021) 107, [arXiv:2006.13942](#) [[hep-ph](#)].

- [134] C. S. Shin and S. Yun, “Dark gauge boson production from neutron stars via nucleon-nucleon bremsstrahlung,” *JHEP* **02** (2022) 133, [arXiv:2110.03362 \[hep-ph\]](#).
- [135] A. Caputo, G. Raffelt, and E. Vitagliano, “Muonic boson limits: Supernova redux,” *Phys. Rev. D* **105** no. 3, (2022) 035022, [arXiv:2109.03244 \[hep-ph\]](#).
- [136] A. W. Steiner, M. Hempel, and T. Fischer, “Core-collapse supernova equations of state based on neutron star observations,” *Astrophys. J.* **774** (2013) 17, [arXiv:1207.2184 \[astro-ph.SR\]](#).
- [137] J. M. Lattimer and F. D. Swesty, “A Generalized equation of state for hot, dense matter,” *Nucl. Phys. A* **535** (1991) 331–376.
- [138] S. E. Woosley, A. Heger, and T. A. Weaver, “The evolution and explosion of massive stars,” *Rev. Mod. Phys.* **74** (2002) 1015–1071.
- [139] T. Sukhbold, S. Woosley, and A. Heger, “A High-resolution Study of Presupernova Core Structure,” *Astrophys. J.* **860** no. 2, (2018) 93, [arXiv:1710.03243 \[astro-ph.HE\]](#).
- [140] S. E. Woosley and A. Heger, “Nucleosynthesis and Remnants in Massive Stars of Solar Metallicity,” *Phys. Rept.* **442** (2007) 269–283, [arXiv:astro-ph/0702176](#).
- [141] R. Bollig, W. DeRocco, P. W. Graham, and H.-T. Janka, “Muons in Supernovae: Implications for the Axion-Muon Coupling,” *Phys. Rev. Lett.* **125** no. 5, (2020) 051104, [arXiv:2005.07141 \[hep-ph\]](#). [Erratum: *Phys.Rev.Lett.* 126, 189901 (2021)].
- [142] E. Braaten and D. Segel, “Neutrino energy loss from the plasma process at all temperatures and densities,” *Phys. Rev. D* **48** (1993) 1478–1491, [arXiv:hep-ph/9302213](#).
- [143] H. An, M. Pospelov, and J. Pradler, “New stellar constraints on dark photons,” *Phys. Lett. B* **725** (2013) 190–195, [arXiv:1302.3884 \[hep-ph\]](#).
- [144] H. A. Weldon, “Simple Rules for Discontinuities in Finite Temperature Field Theory,” *Phys. Rev. D* **28** (1983) 2007.
- [145] E. Braaten, “Neutrino emissivity of an ultrarelativistic plasma from positron and plasmino annihilation,”.
- [146] E. Hardy, A. Sokolov, and H. Stubbs, “Supernova bounds on new scalars from resonant and soft emission,” [arXiv:2410.17347 \[hep-ph\]](#).
- [147] A. Pastorello *et al.*, “Low luminosity type II supernovae: spectroscopic and photometric evolution,” *Mon. Not. Roy. Astron. Soc.* **347** (2004) 74, [arXiv:astro-ph/0309264](#).
- [148] S. e. a. Spiro, “Low luminosity type ii supernovae – ii. pointing towards moderate mass precursors,” *Monthly Notices of the Royal Astronomical Society* **439** no. 3, (Feb., 2014) 2873–2892. <http://dx.doi.org/10.1093/mnras/stu156>.
- [149] L. Oberauer, C. Hagner, G. Raffelt, and E. Rieger, “Supernova bounds on neutrino radiative decays,” *Astropart. Phys.* **1** (1993) 377–386.
- [150] T. Piran, “Gamma-ray bursts and the fireball model,” *Phys. Rept.* **314** (1999) 575–667, [arXiv:astro-ph/9810256](#).
- [151] M. Diamond, D. F. G. Fiorillo, G. Marques-Tavares, and E. Vitagliano, “Axion-sourced fireballs from supernovae,” *Phys. Rev. D* **107** no. 10, (2023) 103029, [arXiv:2303.11395 \[hep-ph\]](#). [Erratum: *Phys.Rev.D* 108, 049902 (2023)].
- [152] W. DeRocco, P. W. Graham, D. Kasen, G. Marques-Tavares, and S. Rajendran, “Observable signatures of dark photons from supernovae,” *JHEP* **02** (2019) 171, [arXiv:1901.08596 \[hep-ph\]](#).

- [153] **LIGO Scientific, Virgo** Collaboration, B. P. Abbott *et al.*, “GW170817: Observation of Gravitational Waves from a Binary Neutron Star Inspiral,” *Phys. Rev. Lett.* **119** no. 16, (2017) 161101, [arXiv:1710.05832 \[gr-qc\]](#).
- [154] A. Murguia-Berthier, E. Ramirez-Ruiz, F. De Colle, A. Janiuk, S. Rosswog, and W. H. Lee, “The Fate of the Merger Remnant in GW170817 and its Imprint on the Jet Structure,” *Astrophys. J.* **908** no. 2, (2021) 152, [arXiv:2007.12245 \[astro-ph.HE\]](#).
- [155] M. Diamond, D. F. G. Fiorillo, G. Marques-Tavares, I. Tamborra, and E. Vitagliano, “Multimessenger Constraints on Radiatively Decaying Axions from GW170817,” *Phys. Rev. Lett.* **132** no. 10, (2024) 101004, [arXiv:2305.10327 \[hep-ph\]](#).
- [156] N. Prantzos *et al.*, “The 511 keV emission from positron annihilation in the Galaxy,” *Rev. Mod. Phys.* **83** (2011) 1001–1056, [arXiv:1009.4620 \[astro-ph.HE\]](#).
- [157] J. Liao and D. Marfatia, “Coherent constraints on nonstandard neutrino interactions,” *Physics Letters B* **775** (Dec, 2017) 54–57. <http://dx.doi.org/10.1016/j.physletb.2017.10.046>.
- [158] **COHERENT** Collaboration, D. Akimov *et al.*, “Observation of Coherent Elastic Neutrino-Nucleus Scattering,” *Science* **357** no. 6356, (2017) 1123–1126, [arXiv:1708.01294 \[nucl-ex\]](#).
- [159] M. Abdullah *et al.*, “Coherent elastic neutrino-nucleus scattering: Terrestrial and astrophysical applications,” [arXiv:2203.07361 \[hep-ph\]](#).
- [160] J. B. Dent, B. Dutta, S. Liao, J. L. Newstead, L. E. Strigari, and J. W. Walker, “Probing light mediators at ultralow threshold energies with coherent elastic neutrino-nucleus scattering,” *Phys. Rev. D* **96** no. 9, (2017) 095007, [arXiv:1612.06350 \[hep-ph\]](#).
- [161] I. M. Shoemaker, “COHERENT search strategy for beyond standard model neutrino interactions,” *Phys. Rev. D* **95** no. 11, (2017) 115028, [arXiv:1703.05774 \[hep-ph\]](#).
- [162] D. K. Papoulias and T. S. Kosmas, “COHERENT constraints to conventional and exotic neutrino physics,” *Phys. Rev. D* **97** no. 3, (2018) 033003, [arXiv:1711.09773 \[hep-ph\]](#).
- [163] M. Abdullah, J. B. Dent, B. Dutta, G. L. Kane, S. Liao, and L. E. Strigari, “Coherent elastic neutrino nucleus scattering as a probe of a  $Z'$  through kinetic and mass mixing effects,” *Phys. Rev. D* **98** no. 1, (2018) 015005, [arXiv:1803.01224 \[hep-ph\]](#).
- [164] P. B. Denton, Y. Farzan, and I. M. Shoemaker, “Testing large non-standard neutrino interactions with arbitrary mediator mass after COHERENT data,” *JHEP* **07** (2018) 037, [arXiv:1804.03660 \[hep-ph\]](#).
- [165] **CONNIE** Collaboration, A. Aguilar-Arevalo *et al.*, “Search for light mediators in the low-energy data of the CONNIE reactor neutrino experiment,” *JHEP* **04** (2020) 054, [arXiv:1910.04951 \[hep-ex\]](#).
- [166] M. Cadeddu, N. Cargioli, F. Dordei, C. Giunti, Y. F. Li, E. Picciau, and Y. Y. Zhang, “Constraints on light vector mediators through coherent elastic neutrino nucleus scattering data from COHERENT,” *JHEP* **01** (2021) 116, [arXiv:2008.05022 \[hep-ph\]](#).
- [167] O. G. Miranda, D. K. Papoulias, G. Sanchez Garcia, O. Sanders, M. Tórtola, and J. W. F. Valle, “Implications of the first detection of coherent elastic neutrino-nucleus scattering (CEvNS) with Liquid Argon,” *JHEP* **05** (2020) 130, [arXiv:2003.12050 \[hep-ph\]](#). [Erratum: *JHEP* 01, 067 (2021)].
- [168] **CONUS** Collaboration, H. Bonet *et al.*, “Novel constraints on neutrino physics beyond the standard model from the CONUS experiment,” *JHEP* **05** (2022) 085, [arXiv:2110.02174 \[hep-ph\]](#).

- [169] L. M. G. de la Vega, L. J. Flores, N. Nath, and E. Peinado, “Complementarity between dark matter direct searches and CE $\nu$ NS experiments in U(1)’ models,” *JHEP* **09** (2021) 146, [arXiv:2107.04037 \[hep-ph\]](#).
- [170] P. Coloma, I. Esteban, M. C. Gonzalez-Garcia, L. Larizgoitia, F. Monrabal, and S. Palomares-Ruiz, “Bounds on new physics with data of the Dresden-II reactor experiment and COHERENT,” *JHEP* **05** (2022) 037, [arXiv:2202.10829 \[hep-ph\]](#).
- [171] M. Atzori Corona, M. Cadeddu, N. Cargioli, F. Dordei, C. Giunti, Y. F. Li, E. Picciau, C. A. Ternes, and Y. Y. Zhang, “Probing light mediators and  $(g - 2)_\mu$  through detection of coherent elastic neutrino nucleus scattering at COHERENT,” *JHEP* **05** (2022) 109, [arXiv:2202.11002 \[hep-ph\]](#).
- [172] V. De Romeri, D. K. Papoulias, and G. Sanchez Garcia, “Implications of the first CONUS+ measurement of coherent elastic neutrino-nucleus scattering,” *Phys. Rev. D* **111** no. 7, (2025) 075025, [arXiv:2501.17843 \[hep-ph\]](#).
- [173] A. Chattaraj, A. Majumdar, and R. Srivastava, “Probing standard model and beyond with reactor CE $\nu$ NS data of CONUS+ experiment,” *Phys. Lett. B* **864** (2025) 139438, [arXiv:2501.12441 \[hep-ph\]](#).
- [174] **TEXONO** Collaboration, S. Karadağ *et al.*, “Constraints on new physics with light mediators and generalized neutrino interactions via coherent elastic neutrino nucleus scattering,” *Phys. Rev. D* **112** no. 3, (2025) 035038, [arXiv:2502.20007 \[hep-ex\]](#).
- [175] **COHERENT** Collaboration, D. Akimov *et al.*, “Measurement of the Coherent Elastic Neutrino-Nucleus Scattering Cross Section on CsI by COHERENT,” *Phys. Rev. Lett.* **129** no. 8, (2022) 081801, [arXiv:2110.07730 \[hep-ex\]](#).
- [176] **COHERENT** Collaboration, D. Akimov *et al.*, “First Measurement of Coherent Elastic Neutrino-Nucleus Scattering on Argon,” *Phys. Rev. Lett.* **126** no. 1, (2021) 012002, [arXiv:2003.10630 \[nucl-ex\]](#).
- [177] N. Ackermann *et al.*, “Direct observation of coherent elastic antineutrino–nucleus scattering,” *Nature* **643** no. 8074, (2025) 1229–1233, [arXiv:2501.05206 \[hep-ex\]](#).
- [178] A. M. Konovalov, “Status of the COHERENT Experiment and New Physics Opportunities at the SNS Facility,” *Moscow Univ. Phys. Bull.* **79** no. Suppl 1, (2024) 220–226.
- [179] E. Picciau, *Low-energy signatures in DarkSide-50 experiment and neutrino scattering processes*. PhD thesis, Università degli Studi di Cagliari, Italy, Cagliari U., 2022.
- [180] J. Colaresi, J. I. Collar, T. W. Hossbach, C. M. Lewis, and K. M. Yocum, “Measurement of Coherent Elastic Neutrino-Nucleus Scattering from Reactor Antineutrinos,” *Phys. Rev. Lett.* **129** no. 21, (2022) 211802, [arXiv:2202.09672 \[hep-ex\]](#).
- [181] **TEXONO** Collaboration, S. Karmakar *et al.*, “New Limits on the Coherent Neutrino-Nucleus Elastic Scattering Cross Section at the Kuo-Sheng Reactor-Neutrino Laboratory,” *Phys. Rev. Lett.* **134** no. 12, (2025) 121802, [arXiv:2411.18812 \[nucl-ex\]](#).
- [182] **NUCLEUS** Collaboration, C. Goupy *et al.*, “Exploring coherent elastic neutrino-nucleus scattering of reactor neutrinos with the NUCLEUS experiment,” *SciPost Phys. Proc.* **12** (2023) 053, [arXiv:2211.04189 \[physics.ins-det\]](#).
- [183] **Ricochet** Collaboration, C. Augier *et al.*, “Fast neutron background characterization of the future Ricochet experiment at the ILL research nuclear reactor,” *Eur. Phys. J. C* **83** no. 1, (2023) 20, [arXiv:2208.01760 \[astro-ph.IM\]](#).

- [184] **CONNIE** Collaboration, A. A. Aguilar-Arevalo *et al.*, “Searches for CE $\nu$ NS and Physics beyond the Standard Model using Skipper-CCDs at CONNIE,” [arXiv:2403.15976 \[hep-ex\]](#).
- [185] M. Atzori Corona, M. Cadeddu, N. Cargioli, F. Dordei, and C. Giunti, “Reactor antineutrinos CE $\nu$ NS on germanium: CONUS+ and TEXONO as a new gateway to SM and BSM physics,” *Phys. Rev. D* **112** no. 1, (2025) 015007, [arXiv:2501.18550 \[hep-ph\]](#).
- [186] M. Atzori Corona, M. Cadeddu, N. Cargioli, F. Dordei, C. Giunti, and R. Pavarani, “Toward precision physics tests with future COHERENT detectors,” [arXiv:2509.04205 \[physics.ins-det\]](#).
- [187] G. Bellini *et al.*, “Precision measurement of the  $^7\text{Be}$  solar neutrino interaction rate in Borexino,” *Phys. Rev. Lett.* **107** (2011) 141302, [arXiv:1104.1816 \[hep-ex\]](#).
- [188] **Borexino** Collaboration, G. Bellini *et al.*, “Final results of Borexino Phase-I on low energy solar neutrino spectroscopy,” *Phys. Rev. D* **89** no. 11, (2014) 112007, [arXiv:1308.0443 \[hep-ex\]](#).
- [189] **BOREXINO** Collaboration, G. Bellini *et al.*, “Neutrinos from the primary proton–proton fusion process in the Sun,” *Nature* **512** no. 7515, (2014) 383–386.
- [190] **Borexino** Collaboration, M. Agostini *et al.*, “First Simultaneous Precision Spectroscopy of  $pp$ ,  $^7\text{Be}$ , and  $pep$  Solar Neutrinos with Borexino Phase-II,” *Phys. Rev. D* **100** no. 8, (2019) 082004, [arXiv:1707.09279 \[hep-ex\]](#).
- [191] **BOREXINO** Collaboration, M. Agostini *et al.*, “Comprehensive measurement of  $pp$ -chain solar neutrinos,” *Nature* **562** no. 7728, (2018) 505–510.
- [192] **BOREXINO** Collaboration, M. Agostini *et al.*, “Experimental evidence of neutrinos produced in the CNO fusion cycle in the Sun,” *Nature* **587** (2020) 577–582, [arXiv:2006.15115 \[hep-ex\]](#).
- [193] **TEXONO** Collaboration, M. Deniz *et al.*, “Measurement of  $\text{Nu}(e)\text{-bar}$ -Electron Scattering Cross-Section with a CsI(Tl) Scintillating Crystal Array at the Kuo-Sheng Nuclear Power Reactor,” *Phys. Rev. D* **81** (2010) 072001, [arXiv:0911.1597 \[hep-ex\]](#).
- [194] P. V. et al., “Precision measurement of electroweak parameters from the scattering of muon-neutrinos on electrons,” *Physics Letters B* **335** no. 2, (1994) 246–252. <https://www.sciencedirect.com/science/article/pii/0370269394914214>.
- [195] **CHARM-II** Collaboration, P. Vilain *et al.*, “Measurement of differential cross-sections for muon-neutrino electron scattering,” *Phys. Lett. B* **302** (1993) 351–355.
- [196] P. Vogel and J. Engel, “Neutrino Electromagnetic Form-Factors,” *Phys. Rev. D* **39** (1989) 3378.
- [197] P. Coloma, M. C. Gonzalez-Garcia, M. Maltoni, J. a. P. Pinheiro, and S. Urrea, “Constraining new physics with Borexino Phase-II spectral data,” *JHEP* **07** (2022) 138, [arXiv:2204.03011 \[hep-ph\]](#). [Erratum: *JHEP* 11, 138 (2022)].
- [198] P. J. Fox, R. Harnik, J. Kopp, and Y. Tsai, “LEP Shines Light on Dark Matter,” *Phys. Rev. D* **84** (2011) 014028, [arXiv:1103.0240 \[hep-ph\]](#).
- [199] **NA64** Collaboration, D. Banerjee *et al.*, “Search for vector mediator of Dark Matter production in invisible decay mode,” *Phys. Rev. D* **97** no. 7, (2018) 072002, [arXiv:1710.00971 \[hep-ex\]](#).
- [200] **BaBar** Collaboration, J. P. Lees *et al.*, “Search for Invisible Decays of a Dark Photon Produced in  $e^+e^-$  Collisions at BaBar,” *Phys. Rev. Lett.* **119** no. 13, (2017) 131804, [arXiv:1702.03327 \[hep-ex\]](#).

- [201] **Belle-II** Collaboration, I. Adachi *et al.*, “Search for an Invisibly Decaying  $Z'$  Boson at Belle II in  $e^+e^- \rightarrow \mu^+\mu^- (e^\pm\mu^\mp)$  Plus Missing Energy Final States,” *Phys. Rev. Lett.* **124** no. 14, (2020) 141801, [arXiv:1912.11276 \[hep-ex\]](#).
- [202] **NA62** Collaboration, E. Cortina Gil *et al.*, “Search for production of an invisible dark photon in  $\pi^0$  decays,” *JHEP* **05** (2019) 182, [arXiv:1903.08767 \[hep-ex\]](#).
- [203] **NA64** Collaboration, Y. M. Andreev *et al.*, “Constraints on New Physics in Electron  $g - 2$  from a Search for Invisible Decays of a Scalar, Pseudoscalar, Vector, and Axial Vector,” *Phys. Rev. Lett.* **126** no. 21, (2021) 211802, [arXiv:2102.01885 \[hep-ex\]](#).
- [204] **NA64** Collaboration, Y. M. Andreev *et al.*, “Search for a New B-L  $Z'$  Gauge Boson with the NA64 Experiment at CERN,” *Phys. Rev. Lett.* **129** no. 16, (2022) 161801, [arXiv:2207.09979 \[hep-ex\]](#).
- [205] **NA64** Collaboration, Y. M. Andreev *et al.*, “Search for Light Dark Matter with NA64 at CERN,” *Phys. Rev. Lett.* **131** no. 16, (2023) 161801, [arXiv:2307.02404 \[hep-ex\]](#).
- [206] **DONuT** Collaboration, K. Kodama *et al.*, “Final tau-neutrino results from the DONuT experiment,” *Phys. Rev. D* **78** (2008) 052002, [arXiv:0711.0728 \[hep-ex\]](#).
- [207] **SHiP** Collaboration, M. Anelli *et al.*, “A facility to Search for Hidden Particles (SHiP) at the CERN SPS,” [arXiv:1504.04956 \[physics.ins-det\]](#).
- [208] **FASER** Collaboration, H. Abreu *et al.*, “Detecting and Studying High-Energy Collider Neutrinos with FASER at the LHC,” *Eur. Phys. J. C* **80** no. 1, (2020) 61, [arXiv:1908.02310 \[hep-ex\]](#).
- [209] **SHiP** Collaboration, C. Ahdida *et al.*, “SND@LHC,” [arXiv:2002.08722 \[physics.ins-det\]](#).
- [210] F. Kling, “Probing light gauge bosons in tau neutrino experiments,” *Phys. Rev. D* **102** no. 1, (2020) 015007, [arXiv:2005.03594 \[hep-ph\]](#).
- [211] F. Kling, P. Reimitz, and A. Ritz, “Dark Vector Boson Bremsstrahlung: New Form Factors for a Broader Class of Models,” [arXiv:2509.09437 \[hep-ph\]](#).
- [212] S. Alekhin *et al.*, “A facility to Search for Hidden Particles at the CERN SPS: the SHiP physics case,” *Rept. Prog. Phys.* **79** no. 12, (2016) 124201, [arXiv:1504.04855 \[hep-ph\]](#).
- [213] **SHiP** Collaboration, C. Ahdida *et al.*, “Sensitivity of the SHiP experiment to dark photons decaying to a pair of charged particles,” *Eur. Phys. J. C* **81** no. 5, (2021) 451, [arXiv:2011.05115 \[hep-ex\]](#).
- [214] T. Zhou, R. Plestid, K. J. Kelly, N. Blinov, and P. J. Fox, “Long-lived vectors from electromagnetic cascades at SHiP,” *JHEP* **02** (2025) 107, [arXiv:2412.01880 \[hep-ph\]](#).
- [215] J. D. Bjorken, S. Ecklund, W. R. Nelson, A. Abashian, C. Church, B. Lu, L. W. Mo, T. A. Nunamaker, and P. Rassmann, “Search for Neutral Metastable Penetrating Particles Produced in the SLAC Beam Dump,” *Phys. Rev. D* **38** (1988) 3375.
- [216] Y.-S. Tsai, “AXION BREMSSTRAHLUNG BY AN ELECTRON BEAM,” *Phys. Rev. D* **34** (1986) 1326.
- [217] S. Andreas, *Light Weakly Interacting Particles: Constraints and Connection to Dark Matter*. PhD thesis, Hamburg U., 2013.
- [218] M. Davier and H. Nguyen Ngoc, “An Unambiguous Search for a Light Higgs Boson,” *Phys. Lett. B* **229** (1989) 150–155.
- [219] A. Konaka *et al.*, “Search for Neutral Particles in Electron Beam Dump Experiment,” *Phys. Rev. Lett.* **57** (1986) 659.

- [220] **NA64** Collaboration, D. Banerjee *et al.*, “Search for a Hypothetical 16.7 MeV Gauge Boson and Dark Photons in the NA64 Experiment at CERN,” *Phys. Rev. Lett.* **120** no. 23, (2018) 231802, [arXiv:1803.07748 \[hep-ex\]](#).
- [221] **NA64** Collaboration, D. Banerjee *et al.*, “Improved limits on a hypothetical X(16.7) boson and a dark photon decaying into  $e^+e^-$  pairs,” *Phys. Rev. D* **101** no. 7, (2020) 071101, [arXiv:1912.11389 \[hep-ex\]](#).
- [222] E. M. Riordan *et al.*, “A Search for Short Lived Axions in an Electron Beam Dump Experiment,” *Phys. Rev. Lett.* **59** (1987) 755.
- [223] A. Bross, M. Crisler, S. H. Pordes, J. Volk, S. Errede, and J. Wrbanek, “A Search for Shortlived Particles Produced in an Electron Beam Dump,” *Phys. Rev. Lett.* **67** (1991) 2942–2945.
- [224] J. R. Cudell, V. Ezhela, P. Gauron, K. Kang, Y. V. Kuyanov, S. Lugovsky, B. Nicolescu, and N. Tkachenko, “Hadronic scattering amplitudes: Medium-energy constraints on asymptotic behavior,” *Phys. Rev. D* **65** (2002) 074024, [arXiv:hep-ph/0107219](#).
- [225] J. Blumlein and J. Brunner, “New Exclusion Limits for Dark Gauge Forces from Beam-Dump Data,” *Phys. Lett. B* **701** (2011) 155–159, [arXiv:1104.2747 \[hep-ex\]](#).
- [226] S. N. Gninenko, “Stringent limits on the  $\pi^0 \rightarrow \gamma X, X \rightarrow e^+e^-$  decay from neutrino experiments and constraints on new light gauge bosons,” *Phys. Rev. D* **85** (2012) 055027, [arXiv:1112.5438 \[hep-ph\]](#).
- [227] S. N. Gninenko, “Constraints on sub-GeV hidden sector gauge bosons from a search for heavy neutrino decays,” *Phys. Lett. B* **713** (2012) 244–248, [arXiv:1204.3583 \[hep-ph\]](#).
- [228] J. Blümlein and J. Brunner, “New Exclusion Limits on Dark Gauge Forces from Proton Bremsstrahlung in Beam-Dump Data,” *Phys. Lett. B* **731** (2014) 320–326, [arXiv:1311.3870 \[hep-ph\]](#).
- [229] **NOMAD** Collaboration, P. Astier *et al.*, “Search for heavy neutrinos mixing with tau neutrinos,” *Phys. Lett. B* **506** (2001) 27–38, [arXiv:hep-ex/0101041](#).
- [230] G. Bernardi *et al.*, “Search for Neutrino Decay,” *Phys. Lett. B* **166** (1986) 479–483.
- [231] Y.-D. Tsai, P. deNiverville, and M. X. Liu, “Dark Photon and Muon  $g - 2$  Inspired Inelastic Dark Matter Models at the High-Energy Intensity Frontier,” *Phys. Rev. Lett.* **126** no. 18, (2021) 181801, [arXiv:1908.07525 \[hep-ph\]](#).
- [232] **APEX** Collaboration, S. Abrahamyan *et al.*, “Search for a New Gauge Boson in Electron-Nucleus Fixed-Target Scattering by the APEX Experiment,” *Phys. Rev. Lett.* **107** (2011) 191804, [arXiv:1108.2750 \[hep-ex\]](#).
- [233] **A1** Collaboration, H. Merkel *et al.*, “Search for Light Gauge Bosons of the Dark Sector at the Mainz Microtron,” *Phys. Rev. Lett.* **106** (2011) 251802, [arXiv:1101.4091 \[nucl-ex\]](#).
- [234] H. Merkel *et al.*, “Search at the Mainz Microtron for Light Massive Gauge Bosons Relevant for the Muon  $g-2$  Anomaly,” *Phys. Rev. Lett.* **112** no. 22, (2014) 221802, [arXiv:1404.5502 \[hep-ex\]](#).
- [235] M. Battaglieri *et al.*, “The Heavy Photon Search Test Detector,” *Nucl. Instrum. Meth. A* **777** (2015) 91–101, [arXiv:1406.6115 \[physics.ins-det\]](#).
- [236] P. H. Adrian *et al.*, “Searching for prompt and long-lived dark photons in electroproduced  $e^+e^-$  pairs with the heavy photon search experiment at JLab,” *Phys. Rev. D* **108** no. 1, (2023) 012015, [arXiv:2212.10629 \[hep-ex\]](#).

- [237] **NA48/2** Collaboration, J. R. Batley *et al.*, “Search for the dark photon in  $\pi^0$  decays,” *Phys. Lett. B* **746** (2015) 178–185, [arXiv:1504.00607 \[hep-ex\]](#).
- [238] P. S. B. Dev, B. Dutta, T. Han, A. Karthikeyan, D. Kim, and H. Kim, “New physics at a neutron beam dump,” *Phys. Rev. D* **110** no. 5, (2024) L051703, [arXiv:2311.10078 \[hep-ph\]](#).
- [239] **LHCb** Collaboration, R. Aaij *et al.*, “Search for Dark Photons Produced in 13 TeV  $pp$  Collisions,” *Phys. Rev. Lett.* **120** no. 6, (2018) 061801, [arXiv:1710.02867 \[hep-ex\]](#).
- [240] **KLOE-2** Collaboration, D. Babusci *et al.*, “Limit on the production of a light vector gauge boson in phi meson decays with the KLOE detector,” *Phys. Lett. B* **720** (2013) 111–115, [arXiv:1210.3927 \[hep-ex\]](#).
- [241] A. Anastasi *et al.*, “Limit on the production of a low-mass vector boson in  $e^+e^- \rightarrow U\gamma$ ,  $U \rightarrow e^+e^-$  with the KLOE experiment,” *Phys. Lett. B* **750** (2015) 633–637, [arXiv:1509.00740 \[hep-ex\]](#).
- [242] **KLOE-2** Collaboration, A. Anastasi *et al.*, “Combined limit on the production of a light gauge boson decaying into  $\mu^+\mu^-$  and  $\pi^+\pi^-$ ,” *Phys. Lett. B* **784** (2018) 336–341, [arXiv:1807.02691 \[hep-ex\]](#).
- [243] **BESIII** Collaboration, M. Ablikim *et al.*, “Dark Photon Search in the Mass Range Between 1.5 and 3.4 GeV/ $c^2$ ,” *Phys. Lett. B* **774** (2017) 252–257, [arXiv:1705.04265 \[hep-ex\]](#).
- [244] **BaBar** Collaboration, J. P. Lees *et al.*, “Search for a Dark Photon in  $e^+e^-$  Collisions at BaBar,” *Phys. Rev. Lett.* **113** no. 20, (2014) 201801, [arXiv:1406.2980 \[hep-ex\]](#).
- [245] M. Graham, C. Hearty, and M. Williams, “Searches for Dark Photons at Accelerators,” *Ann. Rev. Nucl. Part. Sci.* **71** (2021) 37–58, [arXiv:2104.10280 \[hep-ph\]](#).
- [246] D. Craik, P. Ilten, D. Johnson, and M. Williams, “LHCb future dark-sector sensitivity projections for Snowmass 2021,” in *Snowmass 2021*. 3, 2022. [arXiv:2203.07048 \[hep-ph\]](#).
- [247] **REDTOP** Collaboration, J. Elam *et al.*, “The REDTOP experiment: Rare  $\eta/\eta'$  Decays To Probe New Physics,” [arXiv:2203.07651 \[hep-ex\]](#).
- [248] M. Pospelov, “Secluded U(1) below the weak scale,” *Phys. Rev. D* **80** (2009) 095002, [arXiv:0811.1030 \[hep-ph\]](#).
- [249] R. H. Parker, C. Yu, W. Zhong, B. Estey, and H. Müller, “Measurement of the fine-structure constant as a test of the Standard Model,” *Science* **360** (2018) 191, [arXiv:1812.04130 \[physics.atom-ph\]](#).
- [250] L. Morel, Z. Yao, P. Cladé, and S. Guellati-Khélifa, “Determination of the fine-structure constant with an accuracy of 81 parts per trillion,” *Nature* **588** no. 7836, (2020) 61–65.
- [251] X. Fan, T. G. Myers, B. A. D. Sukra, and G. Gabrielse, “Measurement of the Electron Magnetic Moment,” *Phys. Rev. Lett.* **130** no. 7, (2023) 071801, [arXiv:2209.13084 \[physics.atom-ph\]](#).
- [252] P. Clade, E. de Mirandes, M. Cadoret, S. Guellati-Khelifa, C. Schwob, F. Nez, L. Julien, and F. Biraben, “Determination of the Fine Structure Constant Based on Bloch Oscillations of Ultracold Atoms in a Vertical Optical Lattice,” *Phys. Rev. Lett.* **96** (2006) 033001, [arXiv:physics/0510101](#).
- [253] R. Aliberti *et al.*, “The anomalous magnetic moment of the muon in the Standard Model: an update,” *Phys. Rept.* **1143** (2025) 1–158, [arXiv:2505.21476 \[hep-ph\]](#).
- [254] A. Hook, E. Izaguirre, and J. G. Wacker, “Model Independent Bounds on Kinetic Mixing,” *Adv. High Energy Phys.* **2011** (2011) 859762, [arXiv:1006.0973 \[hep-ph\]](#).
- [255] D. Curtin, R. Essig, S. Gori, and J. Shelton, “Illuminating Dark Photons with High-Energy Colliders,” *JHEP* **02** (2015) 157, [arXiv:1412.0018 \[hep-ph\]](#).

- [256] B. M. Loizos, X. G. Wang, A. W. Thomas, M. J. White, and A. G. Williams, “Constraints on the dark sector from electroweak precision observables,” *J. Phys. G* **51** no. 7, (2024) 075002, [arXiv:2306.13408 \[hep-ph\]](#).
- [257] M. Zieliński and C. Gatto, “The REDTOP Experiment: an  $\eta/\eta'$  Factory to Explore Dark Matter and Physics Beyond the Standard Model,” *Acta Phys. Polon. Supp.* **18** no. 4, (2025) 4–A5, [arXiv:2509.26552 \[hep-ex\]](#).
- [258] L. Gan, B. Kubis, E. Passemar, and S. Tulin, “Precision tests of fundamental physics with  $\eta$  and  $\eta'$  mesons,” *Phys. Rept.* **945** (2022) 1–105, [arXiv:2007.00664 \[hep-ph\]](#).
- [259] N. Blinov, P. J. Fox, K. J. Kelly, R. Plestid, and T. Zhou, “ $L_\mu - L_\tau$  gauge bosons in beam dumps and supernovae,” [arXiv:2511.09619 \[hep-ph\]](#).
- [260] T. Gherghetta, J. Kersten, K. Olive, and M. Pospelov, “Evaluating the price of tiny kinetic mixing,” *Phys. Rev. D* **100** no. 9, (2019) 095001, [arXiv:1909.00696 \[hep-ph\]](#).
- [261] F. del Aguila, G. D. Coughlan, and M. Quiros, “Gauge Coupling Renormalization With Several U(1) Factors,” *Nucl. Phys. B* **307** (1988) 633. [Erratum: Nucl.Phys.B 312, 751 (1989)].
- [262] F. del Aguila, M. Masip, and M. Perez-Victoria, “Physical parameters and renormalization of  $U(1)_a \times U(1)_b$  models,” *Nucl. Phys. B* **456** (1995) 531–549, [arXiv:hep-ph/9507455](#).
- [263] K. S. Babu, C. F. Kolda, and J. March-Russell, “Leptophobic U(1)  $s$  and the R( $b$ ) - R( $c$ ) crisis,” *Phys. Rev. D* **54** (1996) 4635–4647, [arXiv:hep-ph/9603212](#).
- [264] K. R. Dienes, C. F. Kolda, and J. March-Russell, “Kinetic mixing and the supersymmetric gauge hierarchy,” *Nucl. Phys. B* **492** (1997) 104–118, [arXiv:hep-ph/9610479](#).
- [265] S. Eidelman and F. Jegerlehner, “Hadronic contributions to  $g - 2$  of the leptons and to the effective fine structure constant  $\alpha(M_Z^2)$ ,” *Z. Phys. C* **67** (1995) 585–602, [arXiv:hep-ph/9502298](#).
- [266] F. Jegerlehner, “Precision measurements of  $\sigma(\text{hadronic})$  for  $\alpha(\text{eff})(E)$  at ILC energies and  $(g-2)(\mu)$ ,” *Nucl. Phys. B Proc. Suppl.* **162** (2006) 22–32, [arXiv:hep-ph/0608329](#).